Spring 2010

Solid-state reactions in co-crystals: applications in synthetic chemistry and materials science

Saikat Dutta
University of Iowa

SOLID-STATE REACTIONS IN CO-CRYSTALS: APPLICATIONS IN SYNTHETIC CHEMISTRY AND MATERIALS SCIENCE

by

Saikat Dutta

An Abstract

Of a thesis submitted in partial fulfillment
of the requirements for the Doctor of
Philosophy degree in Chemistry
in the Graduate College of
The University of Iowa

May 2010

Thesis Supervisor: Associate Professor Leonard R. MacGillivray

ABSTRACT

Chemistry is on the verge of a new era where the attention of chemists has shifted from covalent bonds to noncovalent interactions and their use as a reliable tool to design functional materials and to control the outcome of organic reactions. Although covalent synthesis in fluidic medium *via* supramolecular control has been achieved with limited success, the organic solid state has been of particular interest since it is not affected by solvent effects, thus enabling the formation of unique materials with remarkable stereoselectivity under environment-friendly conditions. Although reactions in solids have resulted in a number of remarkable discoveries in chemistry and materials science, solid-state synthesis is generally not considered as a mainstream synthetic medium and solid-state reactions are seldom appreciated as an efficient way to access molecular targets. Owing to the limited number of solid-state reactions and the uncontrollable nature of crystal packing, the solid state has not been utilized readily as a primary synthetic medium. In this context, reactions conducted in multi-component molecular assemblies or co-crystals have been recently recognized as a general way of controlling reactivity in the solid state. In recent years, our group has demonstrated that small organic molecules can be incorporated into organic solids to alter the crystal packing of olefins and semiconducting molecules, thereby controlling their physicochemical properties. The [2+2]photodimerization of olefins is a successful demonstration how templated solid state synthesis can efficiently synthesize complex targets that are synthetically challenging *via* conventional routes. In this dissertation, the generality and synthetic applicability of the templated synthetic approach in solid state will be described. How supramolecular interactions in molecular co-crystals precisely guide covalent bond formation in order to construct complex molecular targets will be

demonstrated. Finally, co-crystallization will be shown as a general way to control chromic properties in crystals.

Abstract Approved: _____
Thesis Supervisor

_____
Title and Department

_____
Date

SOLID-STATE REACTIONS IN CO-CRYSTALS: APPLICATIONS IN SYNTHETIC CHEMISTRY AND MATERIALS SCIENCE

by

Saikat Dutta

A thesis submitted in partial fulfillment
of the requirements for the Doctor of
Philosophy degree in Chemistry
in the Graduate College of
The University of Iowa

May 2010

Thesis Supervisor: Associate Professor Leonard R. MacGillivray

Graduate College
The University of Iowa
Iowa City, Iowa

CERTIFICATE OF APPROVAL

_____

PH.D. THESIS

_____

This is to certify that the Ph.D. thesis of

Saikat Dutta

has been approved by the Examining Committee
for the thesis requirement for the Doctor of Philosophy
degree in Chemistry at the May 2010 graduation.

Thesis Committee: _____
Leonard R. MacGillivray, Thesis Supervisor

_____
Christopher Pigge

_____
Ned B. Bowden

_____
Christopher M. Cheatum

_____
Horacio F. Olivo

To my parents

"There are pearls in the deep sea, but one must hazard all to find them. If diving once does not bring you pearls, you need not therefore conclude that the sea is without them. Dive again and again. You are sure to be rewarded in the end. So is it with the finding of the Lord in this world. If your first attempt proves fruitless, do not lose heart. Persevere in your efforts. You are sure to realize Him at last."

Sri RamaKrishna

ACKNOWLEDGMENTS

In the University of Iowa and Iowa City, I have come across several interesting and friendly people that helped me to withstand the homesickness and culture shock. Besides chemistry, I have learned a lot of important things in life in the last five years of my graduate student life such as communication skills (in English) and professionalism. I would first like to thank my academic advisor Prof. Leonard R. MacGillivray. I am greatly indebted to him for his kind behaviour, for sharing his great knowledge and experience, and for guiding my work with enthusiasm.

I am thankful to my parents and sister for their support. Thanks to Mala for her understanding and support and also sharing her synthetic chemistry knowledge.

I am like to express gratitude to my colleagues in MacGillivray research group. Thanks to Kreso, Tony, Joe, Beth, John, Jelena, Poonam, and Manza. Special thanks to Kreso, who was always been a great mentor, as well as a good friend to me. Thanks to my friends Pradeep, Sharavathi, Lokesh, Amninder, and Samrat, who never let me feel lonely.

I would like to thank Dr. Dale Swenson for all his assistance with crystallography.

ABSTRACT

Chemistry is on the verge of a new era where the attention of chemists has shifted from covalent bonds to noncovalent interactions and their use as a reliable tool to design functional materials and to control the outcome of organic reactions. Although covalent synthesis in fluidic medium *via* supramolecular control has been achieved with limited success, the organic solid state has been of particular interest since it is not affected by solvent effects, thus enabling the formation of unique materials with remarkable stereoselectivity under environment-friendly conditions. Although reactions in solids have resulted in a number of remarkable discoveries in chemistry and materials science, solid-state synthesis is generally not considered as a mainstream synthetic medium and solid-state reactions are seldom appreciated as an efficient way to access molecular targets. Owing to the limited number of solid-state reactions and the uncontrollable nature of crystal packing, the solid state has not been utilized readily as a primary synthetic medium. In this context, reactions conducted in multi-component molecular assemblies or co-crystals have been recently recognized as a general way of controlling reactivity in the solid state. In recent years, our group has demonstrated that small organic molecules can be incorporated into organic solids to alter the crystal packing of olefins and semiconducting molecules, thereby controlling their physicochemical properties. The [2+2]photodimerization of olefins is a successful demonstration how templated solid state synthesis can efficiently synthesize complex targets that are synthetically challenging *via* conventional routes. In this dissertation, the generality and synthetic applicability of the templated synthetic approach in solid state will be described. How supramolecular interactions in molecular co-crystals precisely guide covalent bond formation in order to construct complex molecular targets will be

demonstrated. Finally, co-crystallization will be shown as a general way to control chromic properties in crystals.

TABLE OF CONTENTS

LIST OF TABLES

LIST OF FIGURES

CHAPTER 1: INTRODUCTION

1.1 Targeted Synthesis

Advancements in synthetic organic chemistry over the past century have demonstrated an ever increasing mastery over the making and breaking of covalent bonds.[1,2] The synthesis of a complex molecule is a challenging task where every group, every atom must be placed in appropriate position, literally. Thus, it is sometimes said that organic synthesis is at the same time a scientific discipline and a fine art.[1] In its initial phases, the organic syntheses were centered on exploring chemical reactions, mechanisms, and their applications to build molecular libraries. With increase in the wealth of knowledge and the technological advancements, the later phases of organic syntheses were focused on a conceptually more complex strategy known as 'target oriented synthesis' or synthesizing molecules by design.[3] Corey introduced the principles of 'retrosynthetic analysis' (*i.e.,* hypothetical deconstruction of a target molecule alongside into easily accessible starting materials) to incorporate rationality and systematic endeavour into organic synthesis.[4] The analysis of complex target molecules and possible synthetic strategies for their construction can, now, be logically and systematically demonstrated. In the retrosynthetic tree (*i.e.,* a directed acyclic graph of several all retrosyntheses of a single target), various plausible deconstruction sequences are sorted out, where each reverse synthetic step lead to a 'synthon' or an idealized molecular fragment. In the forward synthetic direction, the synthons are converted into readily accessible synthetic equivalents and the target molecule is prepared by stitching the building blocks with covalent bonds in a carefully chosen sequence of chemical reactions. The synthetic viability of this approach is powered by the ease of synthesis in the fluidic matrix, the structure reactivity relationships (*e.g.,* homologous series), and the wealth of knowledge about various bond-forming reactions conducted therein.[1] With the

technological advancements in analytical chemistry, targeted organic synthesis is considered, to a large extent, to be responsible for the relevant and most exciting breakthroughs in chemistry, biology, and medicine.

1.2 Supramolecular Chemistry

Although chemists have succeeded in synthesizing molecules in an elegant and efficient manner,[1-4] they are still thriving to understand how the small molecules (*e.g.,* nucleotides) in biology work cooperatively to build more complex entities (*e.g.,* DNA) with properties and functions beyond the capability of the individual components. Biological structures are usually made from loose aggregates that are held together by weak, noncovalent interactions. Because of their dynamic nature, these interactions are responsible for most of the processes occurring in biological systems.[5] Over the years, noncovalent interactions have been established to play a major role in preorganizing smaller structural units into complex, well-defined entities (*i.e.,* supermolecules) with unique structures, properties, and functions (Figure 1). The use of noncovalent interactions to design supermolecules created a new chemical discipline called supramolecular chemistry, a term that was coined and defined by Jean-Marie-Lehn as "chemistry beyond the molecule" with direct analogy to covalent synthesis as '*supermolecules are to molecules and the intermolecular bond what molecules are to atoms and the covalent bond*'.[6] Clearly, in supramolecular chemistry, the focus has been shifted from the study of individual molecules to molecular aggregates. The structure and properties of the supermolecule are often distinct from the properties of the chemical species or subunits of which it is composed of. Therefore, development of supramolecular chemistry holds promise to discover new supermolecules with exciting properties. It is worth mentioning that supramolecular synthetic strategies do not differ, in their essence, from classical chemical experiments in which molecules are modeled,

synthetic routes devised, products characterized and their properties measured. However, in supramolecular chemistry this two step process has to be repeated twice: first to synthesize the building blocks (*e.g.,* molecules, ions) and then, to arrange the building blocks in a desired way to attain and/or control crystal properties.[7] Over the last few decades, supramolecular chemistry has been one of the most popular and fastest growing areas of experimental chemistry and developed into a highly interdisciplinary subject. Comparable to conventional organic synthesis, the first few years of this field were invested in discovering and understanding the rules and regulations that determine how small molecules self-assemble and function as a supermolecule.[6] As the wealth of knowledge about the noncovalent interactions and their impacts on self-assembly processes increased, a substantial amount of recent research has converged on applications of designed supermolecules with tailored properties.[8] Though noncovalent interactions are relatively weak (hydrogen bonds are only about 1-30 kcal/mol compared to carbon-carbon single bond (C-C) dissociation energy of 88 kcal/mol), their presence in large number statistically adds up to play a significant role, determining, for example, the identity and the geometry of the supermolecule.[6, 8]

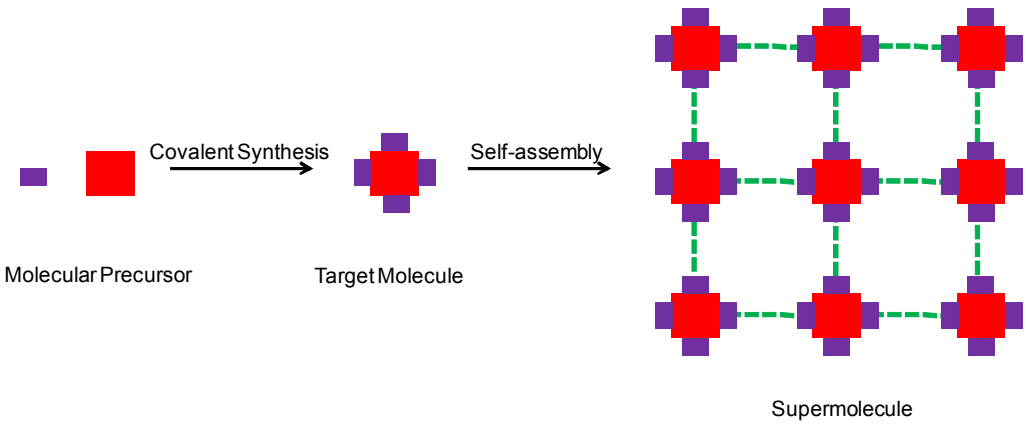

Figure 1. Stepwise synthesis of supermolecules.

1.2.1 Crystal Engineering

A crystal of an organic compound is the ultimate supermolecule, and its assembly, governed by chemical and geometrical factors, from individual molecules, is the perfect example of solid-state molecular recognition.[7] The need for rational approaches towards solid-state structures of fundamental and practical importance has led to the emergence and development of crystal engineering, which seeks to understand intermolecular interactions and recognition phenomena in the context of crystal packing. Thus, making crystals by design is the central paradigm of crystal engineering.[9] The goal of this field of research is to establish reliable connections between molecular and supramolecular structures on the basis of noncovalent interactions. Such ‘‘bottom-up’’ process generates collective supramolecular properties from the individual building blocks with the periodicity and symmetry operators of the crystal (Figure 2).[7]

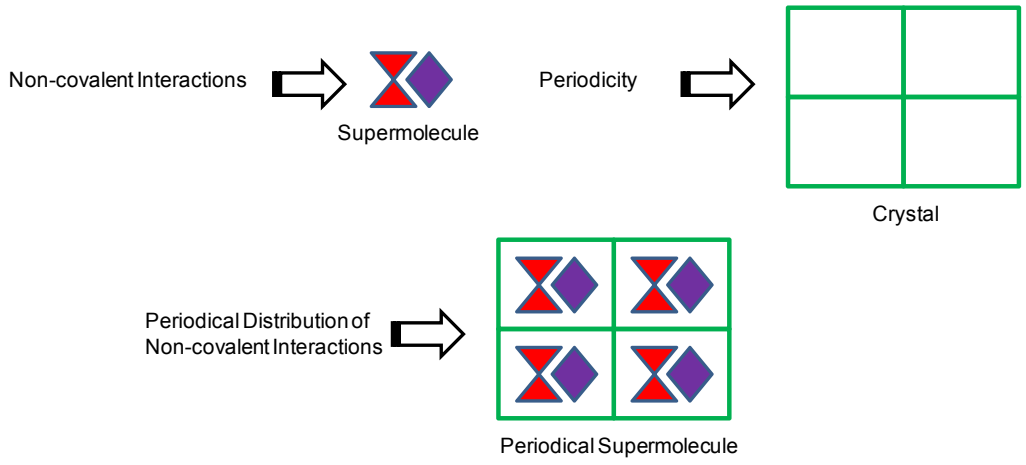

Figure 2. From molecules to periodical supermolecules.

The components of a molecular crystal are held together by intermolecular links that are weaker than the covalent bonds within the individual components. After metal-

coordination bonds and ionic interactions (*e.g.,* dipole-dipole) the strongest interactions in crystal engineering are hydrogen bonds. Due to the strength, directionality, and ubiquitous presence of hydrogen bonds in organic molecules, it is also termed as the 'key-interaction' in crystal engineering.[10] One of the final frontiers in supramolecular interactions undoubtedly lies in the understanding of closed-shell interactions (*e.g.,* metallophilic, halogen bonding) where the closed valence shell heavy atoms interact with each other *via* electron correlation effects or charge anisotropy.[11] Targets in organic synthesis are defined in terms of the connectivity of covalent bonds, whereas at a supramolecular level, targets in crystal engineering are defined in terms of interaction connectivity (*i.e.,* geometrical and topological terms). All crystal structures of organic compounds can be formally depicted as networks with the molecules representing the nodes, while intermolecular interactions acting as the node connections. These interactions can be combined by a designed placement of functional groups in the molecular skeleton to generate supramolecular synthons.[9, 12] Compared to the term 'synthon', originating from the organic synthesis, the concept of supramolecular synthon was described by Desiraju as structural units within supermolecules which can be formed and/or assembled by known or conceivable operations involving intermolecular interactions. Thus, supramolecular synthons are the smallest structural units within which is encoded all the information inherent in the mutual recognition of molecules to yield solid state supermolecules. In effect, the goal of crystal engineering is to recognize and design synthons that are robust enough to be exchanged from one network structure to another ensuring generality and predictability. The carboxylic acid dimer (*e.g.,* benzoic acid dimer) is one of the most extensively studied supramolecular synthon identified in the solid state and in nonpolar solvents.[13] In the crystal structure of benzoic acid, two benzoic acid molecules interact *via* O-H···O hydrogen bonds to form an eight membered cyclic array (Figure 3a). Supramolecular synthons have been divided into two broad categories, namely homosynthon (*i.e.,* interactions between identical functional groups)

and heterosynthon (*i.e.,* interactions between two different functional groups) (Figure 3b). The heterosynthon does not only allow a molecule to self-assemble *via* complementary functionalities on the same molecular structure, but it also allows the formation of multi-component molecular assemblies with complementary functionalities encoded on different molecular components.

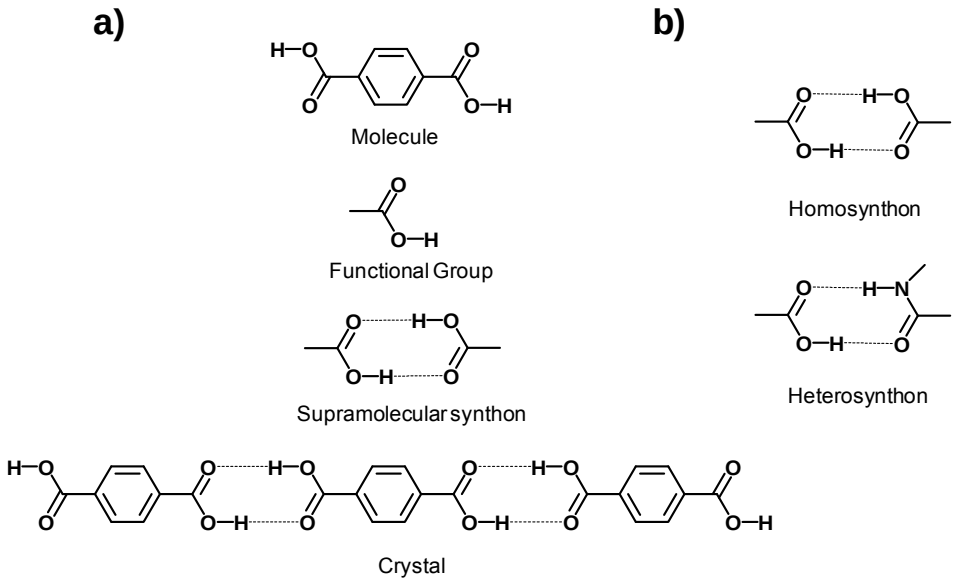

Figure 3. Schematic of a) the relationship between molecules and supermolecules, and b) supramolecular synthons.

1.3 Co-crystal

Co-crystals were originally defined as adducts between two neutral molecular solids at ambient conditions with a definite stoichiometric ratio, held together by hydrogen bonds.[14] With more structural data coming in and the increasing usage of this term, the definition of co-crystal has expanded to accommodate liquids or gases as the second component and to various other intermolecular interactions. Although there are

controversies over the definitions of co-crystals, a co-crystal is, broadly speaking, a multi-component solid-state assembly of two or more molecules mediated by one or multiple types of intermolecular interactions.[15] In co-crystals, different molecules found together in the crystal are distinct, separate, and separable chemical substances. For example, nitro-iodo interactions, shown to be a reliable supramolecular synthon, can be exploited in the design of the co-crystal between p-diiodobenzene and p-dinitrobenzene (Figure 4).[16]

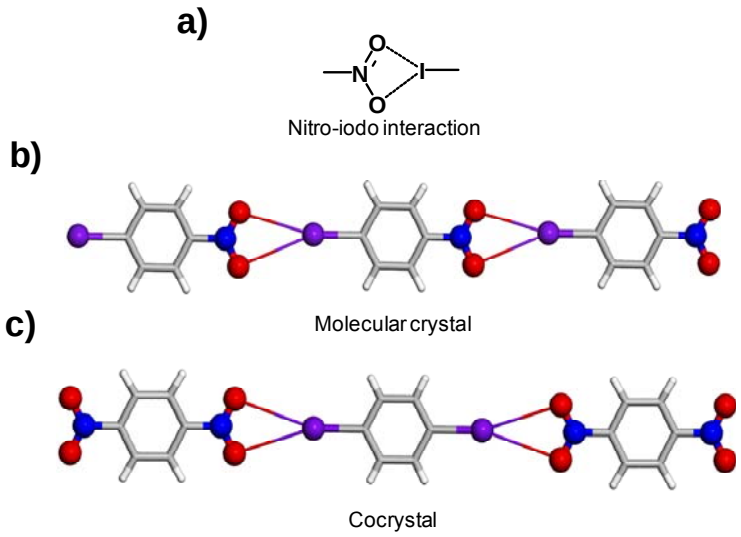

Figure 4. Schematic of nitro-iodo supramolecular synthon, b) single crystal structure of p-iodonitrobenzene, and c) co-crystal of p-diiodobenzene and p-dinitrobenzene. (Colour code: Nitrogen, blue; Oxygen, red; Iodine, violet)

Co-crystals are of particular interest in pharmaceutical industry where formation of co-crystals has been demonstrated as an effective way to favourably modify the properties (*e.g.,* melting point, compressibility, hygroscopicity) of active pharmaceutical ingredients (APIs).[17] The co-crystals are different from the solid solutions wherein the molecules of one of the components are randomly distributed in the crystal matrix of the other

component, as well as from salts wherein atom transfer between one component to the other.[18] MacGillivray *et. al.* have utilized the noncovalent forces as a modular way to control reactivity in co-crystals and will be discussed in section 1.6.

1.4 Molecular Recognition: Self-assembly: Templation

Molecular recognition is the process by which molecules recognize each other and bind in a well defined pattern *via* complementary structural information encoded in their structures.[19] In order to bind, the components of a molecular assembly exhibit both electronic and steric complementarity. Molecular recognition and self-assembly are intimately related and sometimes used interchangeably. Self-assembly is defined as the spontaneous assembly of molecules into structured, stable, noncovalently connected aggregates (Figure 5).[20] An important outcome of employing weak noncovalent forces, is the inherent reversibility of the supramolecular assemblies. While the assembly remains in thermodynamic equilibrium with its components, the molecules can self-correct "mistakes" in any step of the self-assembly process which are common in biological systems. The inherent capacity of supramolecular systems to self-correct is limited to systems that are fully covalently connected.[21]

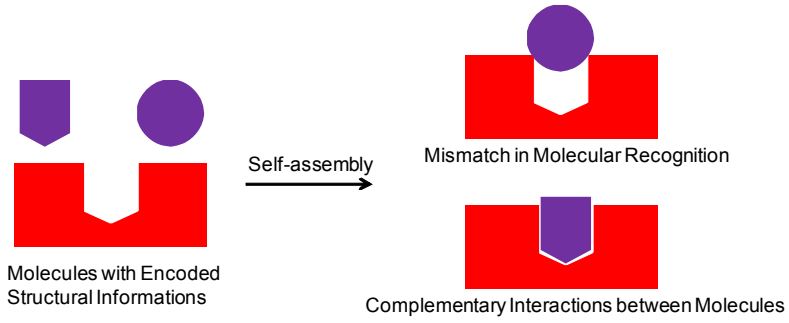

Figure 5. Schematic of a) structural complementarity and molecular recognition, and b) formation of nanostructure by amphiphilic molecules *via* self assembly.

In the manufacture or grafting of macroscopic structures, templates can be described as the support or utensil, those help to fix the independently performed parts of the structure in a relative orientation to each other and be finally connecting them to obtain a desired shape and function.[22] Manufacturing in the microscopic level by transforming and building up molecules, molecular utensils or templates can be used to arrange reactants, direct bond forming processes and to obtain desired molecular architectures. Assistance of noncovalent interactions and self-assembly allow the stereospecific synthesis of biological molecules under mild conditions. During the synthesis of proteins, new peptide (*i.e.,* amide) bond formation with the existing polypeptide chain is template-controlled by ribosomal RNA machinery (Figure 6). The product (*i.e.,* protein) finally self-assembles to form functional entities (*e.g.,* hemoglobin).[5]

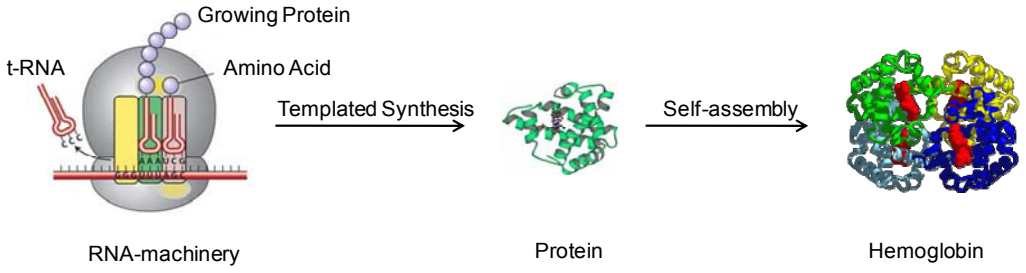

Figure 6. Templated synthesis and self-assembly of proteins in biological environment to form hemoglobin.

Inspired by nature, chemists have been exploring the possibility of templated covalent synthesis *in vitro* by design. The template effect in chemistry was date back to the discovery of crown ethers. The formations of the 18-membered crowns were favoured by the ion-dipole interactions of the oxygen atoms with potassium ions (Figure 7a). The templating effect of the potassium ions has been confirmed by the fact that no crown

ether formed in the absence of potassium ion.[23] The template effect has been demonstrated thereafter for the synthesis of various relevant classes of compounds (*e.g.,* catenane).[24] In addition to the templating effect of various metal ions, the templating roles of organic molecules are also described in the literature. Specifically, a reaction template exhibiting two binding sites has been described. The template was designed to use hydrogen bonding to simultaneously (but transiently) bind two substrates, giving rise to a ternary complex, which positions the substrates in an orientation that facilitates intermolecular nucleophilic substitution reaction (Figure 7b).[25] Templates have also been shown to trigger a [2+2]photodimerization reactions within supramolecular structures (Figure 7c). In particular, a supramolecular hydrogen-bonded assembly based on a cinnamic ester derivative covalently linked to a diaminotriazine moiety was reported to serve as to align the photosensitive cinnamate groups for reaction (Figure 7c).[26]

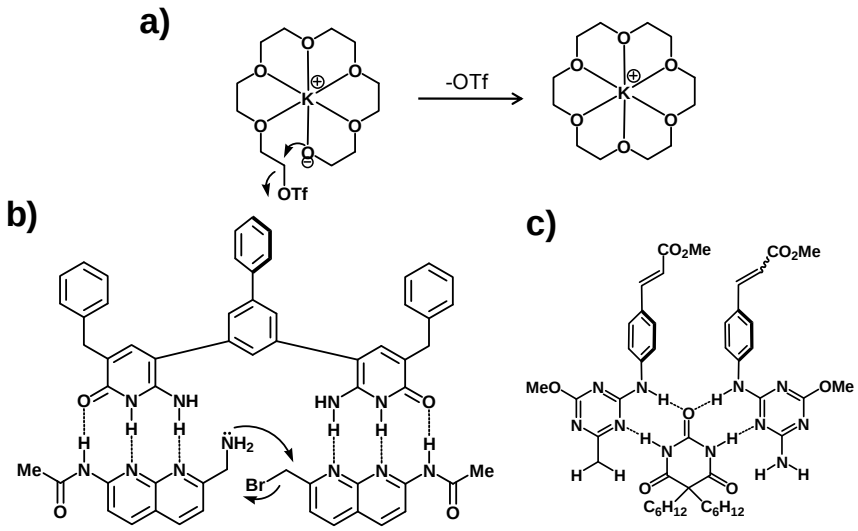

Figure 7. Schematic: a) templated synthesis of 18-crown[6], b) nucleophilic substitution reaction templated by a hydrogen bonded ternary complex, and c) template-directed intermolecular [2+2]photodimerization reaction.

Although the examples described above are successful documentations of templated covalent syntheses, binding of molecules in solution is typically less efficient owing to solvation effects. The solid state, on the other hand, is expected to be a more preferable medium for molecular recognition and template-directed covalent synthesis. The highly constrained and well-organized crystalline solid state could circumvent solvation effect and, thereby, effectively utilize templates as tools to direct the supramolecular construction of molecules.

1.5 Reactivity in Solid State

Although, the fluidic matrices (*e.g.,* solution, melt) are commonly exploited for targeted syntheses, the emergence of the solid state as an alternatively medium for synthesis was evident by some of the most impressive examples of chemical control and mechanistic studies conducted therein.[27] With the accumulated wealth of knowledge about solid state structures and reactions over years, combined with the expense and environmental hazard associated with organic solvents, the solid state is attracting much attention from synthetic chemists in recent years.[28] Solids, in the form of crystals, being highly homogeneous and remarkably ordered, can be an intriguing medium for covalent syntheses. The molecules, being virtually frozen in a particular environment, can favor a reaction path over others to avoid a mixture that often results in solution. The stereoselectivity of the reactions, thus, improves the reaction yield and simplifies the separation procedure.[29] Reactants in the solid state can adopt geometries that may be difficult or impossible to achieve in the liquid phase and, consequently, provide access to molecules upon reaction that are challenging to obtain otherwise. For example, the cinnamic acids undergo [2+2]photodimerization reaction only in the solid state. Most solid-state devices require a degree of order that is only possible in case of crystalline materials. Thus, a single-crystal to single-crystal (SCSC) reaction, where a single crystal

undergoes reaction without loss of crystallinity, has potential applications in functional materials (*e.g.,* molecular electronics).[30] Reactions in the solid state, by definition, avoid the use of expensive and hazardous organic solvents and thus are cost effective and environment friendly. Nevertheless, reactions in crystals have delivered impressive examples of chemical control and provided a useful medium for detailed mechanistic studies.[29] Though remarkable, achievements in organic syntheses in the solid state are not routinely used and seldom appreciated as mainstream organic chemistry; one of the major issues being the limited understanding of the effect of crystal lattice on properties (*e.g.,* reactivity). A continuing challenge in the prediction of the crystal structures of organic molecular solids lies on the fact that the forces determining the crystal structures are weak in nature. A stable crystal structure of most organic compounds is achieved by optimizing a large number of subtle interactions with varying degrees of directionality and electrostatic character. In recent years, the combination of synthetic organic chemistry, computational methods, and X-ray crystallography has proved to be invaluable in establishing structure-reactivity correlations in the organic solid state, specifically in the area of lattice controlled reaction pathways.[31] Apart from X-ray crystallography, high-resolution electron microscopy and solid-state NMR spectroscopy have also contributed to open up a new dimension in organic solid-state synthesis.[32]

Number of possible reactions in the solid state, where crystal packing plays a determining role, is limited due to limited degree of atomic and/or molecular movement. Thus, in crystal-lattice-controlled solid-state reactions, commonly known as 'topochemical reactions', the reactant centers have to be organized in a suitable geometry and in close proximity.[29] Furthermore, bimolecular reactions are expected to undergo between nearest neighbours, which in turn suggests that the molecular structure of the product is dependent on the geometric relations of the reactant molecules in the crystal lattice. Therefore, topochemical reactions hold great potential for the synthesis of molecules with predetermined stereochemistry. Photochemical reactions are probably the

most common reactions carried out in solid state because of simple reaction condition (*i.e.,* UV source), little to no by-products, crystallinity of the material is maintained during reaction, while UV light penetrates through the crystal ensuring homogeneity. In this context, cycloaddition reactions (*e.g.,* [2+2] photodimerization, [2+2]photo-polymerization) are known to take place in solid state for more than hundred years (Figure 8).[29, 33] But, only four decades ago Schmidt established the geometric criteria for molecules to undergo [2+2]photodimerization reactions in solid state, in the form of 'topochemical postulates'.[34]

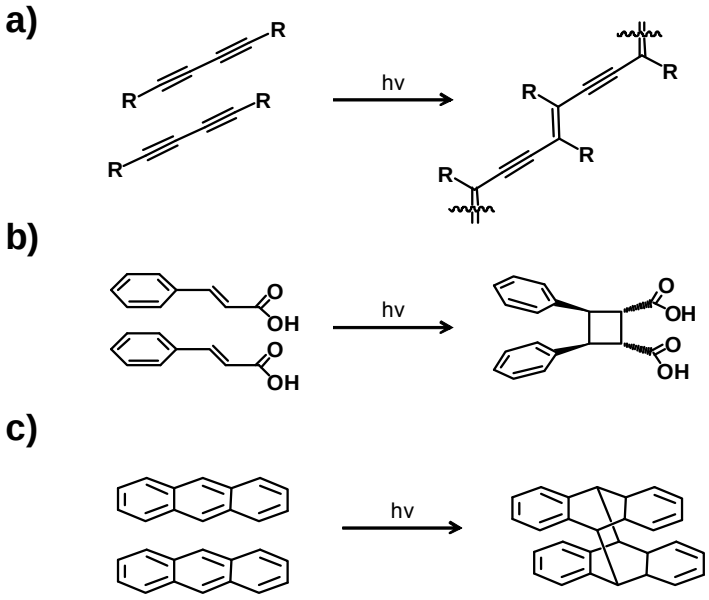

Figure 8. Topochemical reactions in solid state: a) photo-polymerization, and b) [2+2]photodimerization, and c) [4+4]photocycloaddition reaction.

According to the topochemical postulate, olefins have to line up parallel and within a distance of 4.2 Å in the crystal lattice, in order to undergo a [2+2]photodimerization reaction in the solid state. The reactivity of a cinnamic acids was demonstrated to be highly dependent on the polymorphic variations. In particular, the two

known crystal modifications of trans-cinnamic acid comprised identical molecules arranged differently in space, and the stereo-structure of the two photoproducts, α-truxillic and β-truxinic acids, was directly related to the packing geometry of the monomer units in the two crystal structures from which the dimers were derived (Figure 9a). Schmidt showed that the reaction, in contrast to the liquid phase, is generally not maintained among closely related olefins. For example, 4-chlorocinnamic acid reacts in solid state to generate truxillic acid, structurally related 4-methylcinnamc acid form a truxinic acid whereas 4-methoxycinnamic acid remains photostable (Figure 9b). The unpredictability in the subtle, yet pronounced effect of molecular structure on the solid state reactivity was attributed to the sensitivity of crystal packing to molecular structure (*e.g.,* substituent size) that rendered the systematic study of structure-reactivity correlation and chemical generalization for the photoreactivity of cinnamic acids.

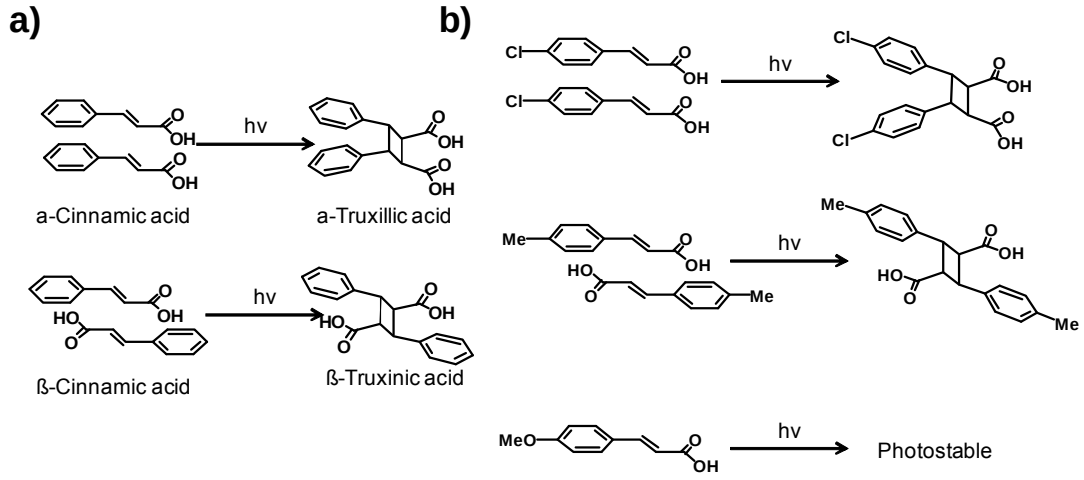

Figure 9. Schematic: a) polymorphic variations, and b) substituent effects on reactivity of cinnamic acids.

Thus, the success of aligning olefinic bonds in a desired orientation in solids was mostly based on discovery.

1.5.1 Crystal Engineering of Photoactive Solids

During the study of the photochemical behaviors of cinnamic acids, it was realized that a particular functionality favors certain geometrical motifs. The systematic and predictive use of such motifs in designing and exploiting crystal structures gave birth to ‘crystal engineering’, a term coined by Schmidt. In order to control the solid-state packing environment of cinnamic acids in a predictable fashion, Schmidt exploited the strength and directionalities of supramolecular forces. It was realized that auxiliary functionalities (*e.g.,* chloro), pendant on aromatic nuclei tend to “steer” the crystal structure to the β-mode, characterized by stacking along the crystallographic short axis of *ca.* 4 Å. Indeed, it was found that dichlorocinnamic acids preferably stack in a head to head geometry to produce truxillic acid *via* [2+2]photodimerization.[34] Aromatic π-π stacking interactions (*e.g.,* phenyl and perfluorophenyl),[35] charge-transfer complexes (*e.g.,* 3,5-dinitrocinnamic acid and 2,5-dimethoxycinnamic acid)[36] and hydrogen bonding[37] have also been utilized to align olefins for a reaction (Figure 10).

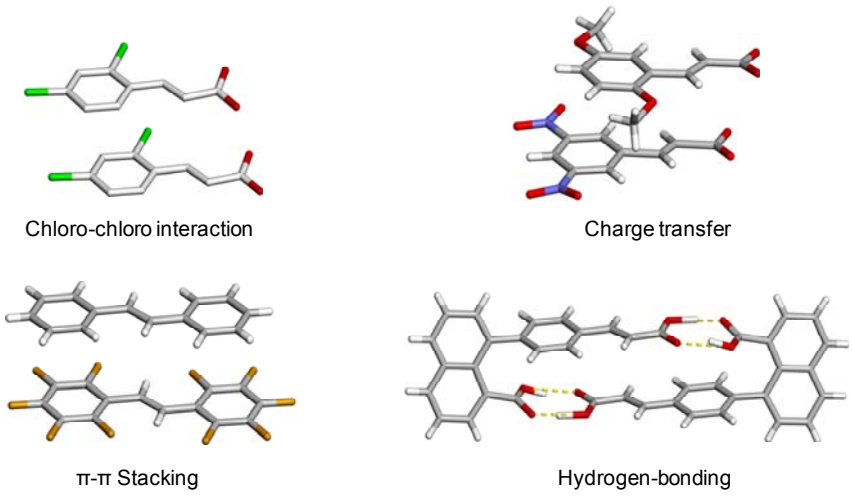

Figure 10. Supramolecular interactions exploited in solid state photoreaction. (Colour code: Chlorine, green; Fluorine,

Although all the above approaches succeeded in carrying out cycloaddition reactions in solids, they had limited control over the solid-state packing with variation of molecular structures as well as product yield and thus, suffered from the lack of synthetic freedom.

1.6 Templated Synthesis in the Solid State

The use of small organic molecules as linear templates to steer the solid-state [2+2] photodimerization reactions of olefins in a two component co-crystal system has been successfully demonstrated by MacGillivray *et. al.*[38] In this approach, the reactants have two parts namely the molecular recognition unit or 'handle' and the reactive group. The handle on the olefinic reactants and the linear template molecule form specific noncovalent interactions by the complementary functional groups encoded on their structures to preorganize the reactants in a suitable geometry for reaction (Figure 11). Formation of the discrete, hydrogen-bonded supermolecule between reactants and the linear template molecules has a structure largely independent of long-range packing interactions. At the same time, the modularity of the templated solid-state synthetic methodology has been demonstrated to accommodate structural variations (*e.g.,* size) in the reactant molecules to access a wide range of products with different levels of complexity. The geometric criteria being well-established, attractive C-C bond forming process, combined with the above mentioned facilities of conducting photochemical reactions in the solid state, [2+2]photodimerization was chosen as a model reaction,

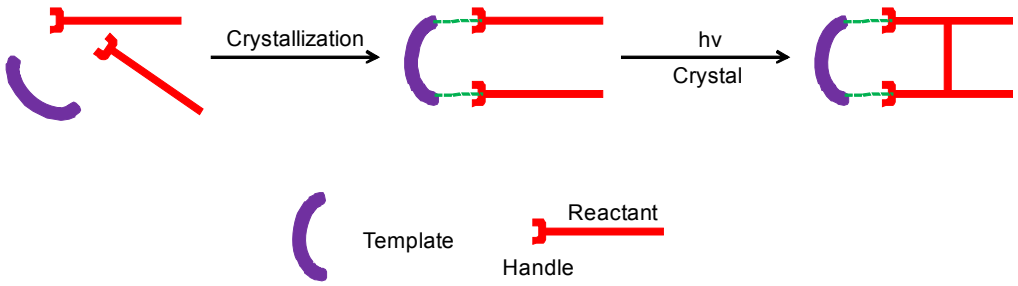

Figure 11. Schematic of templated solid state synthesis.

1.6.1 Organic Template

The pyridine derivatized olefin *trans*-1,2-*bis*(4-pyridyl)ethylene (4,4'-bpe) has been shown to undergo photodimerization in solution providing multiple isomeric cyclobutane products in low yield. The molecule, on the other hand, was determined to be photostable as a pure solid. MacGillivray and co-workers have shown that the use of ditopic molecules in the form of resorcinol, can preorganize 4,4'-bpe, *via* hydrogen bonds for a [2+2] photodimerization in the solid state.[39] An X-ray crystallographic analysis of the solid revealed the formation of the discrete four-component assembly 2(res)·2(4,4'-bpe) held together by four O-H···N Hydrogen bonds (Figure 12). The pyridine moiety is the molecular recognition group that act as a handle to preorganize the reactant olefins suitable for reaction *via* hydrogen-bond formation with resorcinol templates.

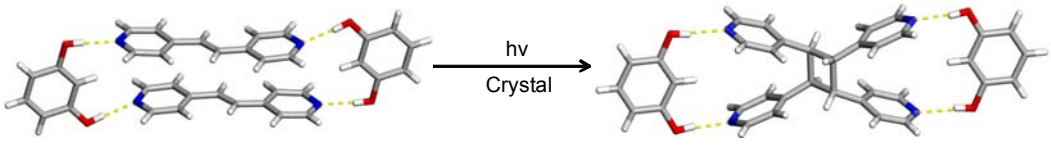

Figure 12. Templated synthesis of 4,4'-tpcb.

Within the assembly, the olefins stacked parallel within a distance of 4.2 Å, satisfying the geometric criteria of [2+2]photodimerization in solid state. UV-irradiation (medium pressure mercury broadband) of the solid resulted in the formation of the cyclobutane product namely, *rctt*-tetrakis(4-pyridyl)cyclobutane (4,4'-tpcb), stereospecifically, quantitatively and even in gram scale. The fact that the linear template assembled the olefins within a discrete supermolecule, made a structure largely independent of long-range packing. Thus, the template could be used to construct molecules of different complexity since the self-assembly process; with the template being located along the exteriors of the olefins could accommodate structural changes (*e.g.,* size) to the reactants.

MacGillivray described that the inherent modularity of this templated synthesis technique can be exploited by incorporating structural change in the template molecules. The structural changes in the template molecules, termed as 'template switching', could potentially change the packing environment of the assemblies to modify the reaction yield as well as the geometry of the products. Reaction yield that can be further improved by the template-switching strategy has been demonstrated during the synthesis of [2.2]paracyclophane.[39] It was observed that use of 5-methoxyresorcinol as the template resulted in only 65% conversion of the desired product whereas switching the template to 4-benzylresorcinol resulted in product formation in quantitative yield (Figure 13).[40]

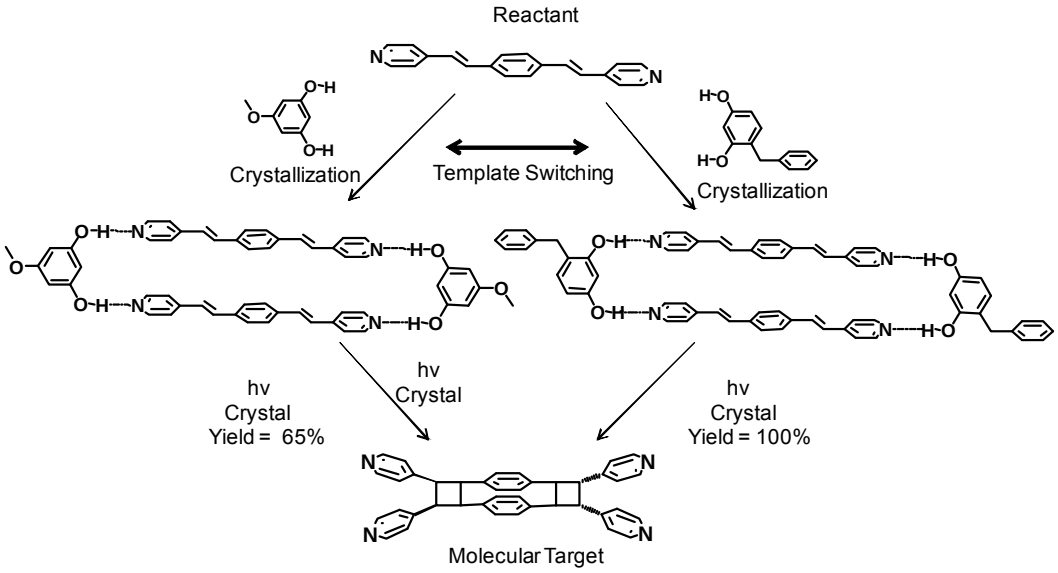

Figure 13. Schematic of the template switching strategy.

MacGillivray and co-workers demonstrated the generality of this approach towards the shape of the reactants by carrying out quantitative and stereospecific reaction of several members of the bpe family. This approach was further extended to more complex and synthetically challenging targets (*i.e.* bigger size) like [2.2]cyclophanes (*e.g.,* ortho, meta, para) and ladderanes (*e.g.,* [3],[5]) (Figure 14).[41]

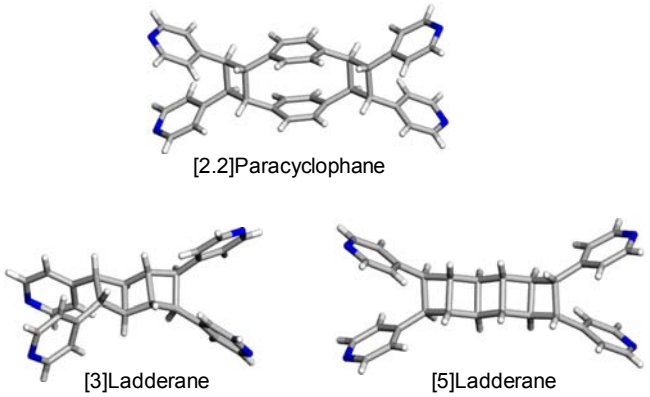

Figure 14. Molecular targets accessed *via* templated solid state synthesis.

MacGillivray *et. al.* also demonstrated that the linear template can be extended to other hydrogen-bond donating functionalities (*e.g.,* carboxylic acid). 1,8-Naphthalenedicarboxylic acid (1,8-nda) has been utilized to direct reactivity of 4,4'-bpe in solids *via* hydrogen-bond formation between pyridine and carboxylic acid functionalities.[42] Spefically, co-crystallization of 4,4'-bpe and 1,8-nda resulted a co-crystal with 1:1 stoichiometry. The X-ray crystal structure analysis revealed the formation of a four component discrete assembly [2(1,8-nda)·2(4,4'-bpe)] (Figure 15). The reactive solid yields 4,4'-tpcb in quantitative yield upon UV-irradiation.

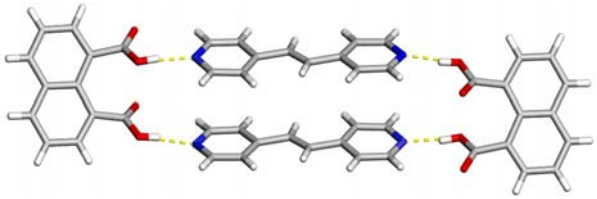

Figure 15. Hydrogen bonded discrete assembly of [2(1,8-nda)·2(4,4'-bpe)].

In order to increase the synthetic versatility of templated synthetic approach, the molecular recognition code has been reversed, where a hydrogen-bond acceptor template has been utilized to align reactant olefins decorated with hydrogen-bond donor functionality. Specifically, 2,3-bis(4-methylenethiopyridyl)naphthalene (mtpn) was used as a template to align fumaric acid (fma) in the solid-state for reaction. Photodimerization of fma resulted in the formation of *rctt*-cyclobutane-1,2,3,4-tetracarboxylic acid, stereospecifically, and up to 70 % yield (Figure 16).[43]

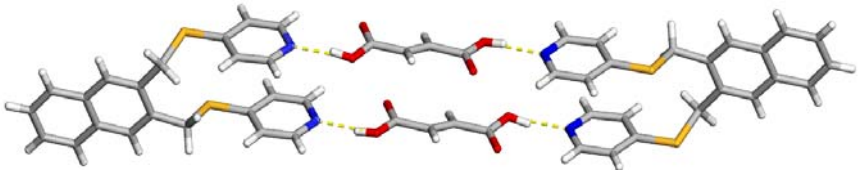

Figure 16. Four component discrete assembly of [2(mtpn)·2(fma)]. (Colour code: Sulfur, yellow)

1.6.2 Metal-organic Complex as Template

Apart from purely organic based systems, metal-organic assembly has also been exploited to align the reacting centers in suitable positions by coordination forces. Praetorius and Korn were the first to report an example of a [2+2] photodimerization mediated by a metal ion in the solid state. Uranyl chloride and *trans*,*trans*-dibenzylideneacetone (dba) resulted a mononuclear complex $[UO_2Cl_2(dba)_2]$.[44] The UV-irradiation of the solid resulted in a stereospecific formation of the "truxillic" (*i.e.,* head-to-tail) dimer *trans*,*trans*-1,3-diphenyl-*cis*,*cis*-2,4-diacetato-cyclobutane both in nonsolvated and acetic acid solvated crystal. X-ray crystal structure of the nonsolvated complex (Figure 17a) revealed that the uranium ions adopted an octahedral geometry where the monocoordinated dba and the chloro groups were in the basal plane and the oxide oxygen atoms satisfying the apical positions. The dba moieties exhibited a *trans*,*trans*-conformation and planar orientation. Later, Lewis *et. al.* demonstrated that [2 + 2] photoreactivity of cinnamic esters can be mediated by metal ions (*e.g.,* $SnCl_4$).[45] Specifically, X-Ray crystal analysis of ethyl cinnamate–$SnCl_4$ complex revealed that ethylcinnamate (etcn) formed $[SnCl_4(etcn)_2]$ (Figure 17b), which upon UV-radiation led exclusively to the formation of ''truxillic'' type dimers. The Sn^{4+} ion adopted an octahedral conformation with four chloro groups in the basal plane whereas axial sites were occupied by keto oxygen atoms of two ester molecules. The reaction occurred

between neighbouring cinnamate ligands. The ligands were planar, stacked in a head-to-tail fashion, and separated by 4.12 Å.

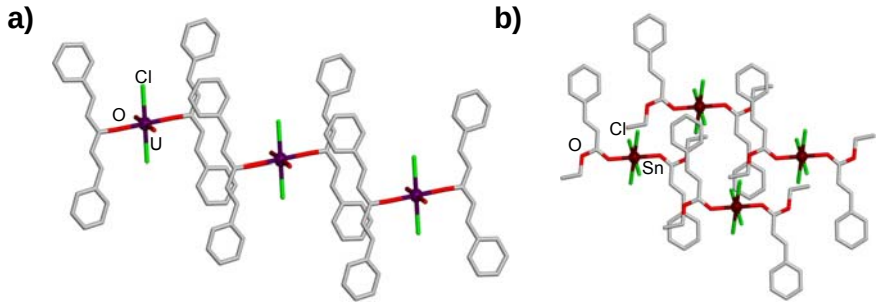

Figure 17. Crystal structure of a) $[UO_2Cl_2(dba)_2]$, and b) $[SnCl_4(etcn)_2]$.

MacGillivray and co-workers have succeeded in using metal-organic complexes as templates in directing [2+2] photodimerization in solids. For example, a binuclear Schiff base Zn^{2+} complex has been utilized to coordinate with 4,4'-bpe and generate discrete complex $[Zn_4L_2(OH)_2(4,4'\text{-bpe})_2](ClO_4)_4.4H_2O$ (where LH = 2,6-bis[*N*-(2-pyridylethyl)formidoyl]-4-methylphenol) wherein the olefinic groups were stacked parallel (Figure 18).[46]

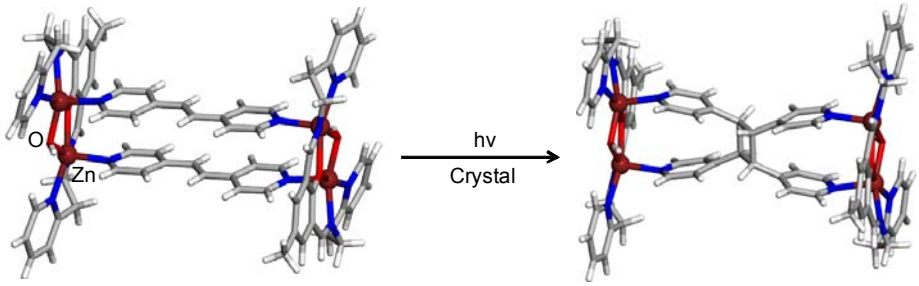

Figure 18. Assembly of $[Zn_4L_2(OH)_2(4,4'\text{-bpe})_2](ClO_4)_4 \cdot 4H_2O$ before and after reaction. Counteranions and the solvent molecules are omitted for clarity.

MacGillivray *et. al.* have also been able to exploit the argentophilic forces to direct reactivity in metal-organic solids. In particular, *trans*-1(4-pyridyl)-2-(phenyl)ethylene (4-stbz) was shown to form the discrete complex $[Ag_2(4\text{-stbz})_4][CO_2CF_3]_2$ which undergoes a [2+2] photodimerization upon UV-irradiation (Figure 19).[47] The X-ray crystal structure revealed that each Ag atom is coordinated to pyridine of two stbz molecules and also monocoordinated to the trifluoroacetate counteranion. Significant argentophilic (*i.e.,* Ag···Ag) forces held the reactant groups in close proximity for reaction. Upon UV-irradiation, the cyclobutane product *rctt*-1,2(4-pyridyl)3,4-(phenyl)cyclobutane formed stereospecifically and in quantitative yield. The silver atoms moved farther from each other breaking the argentophilic interactions.

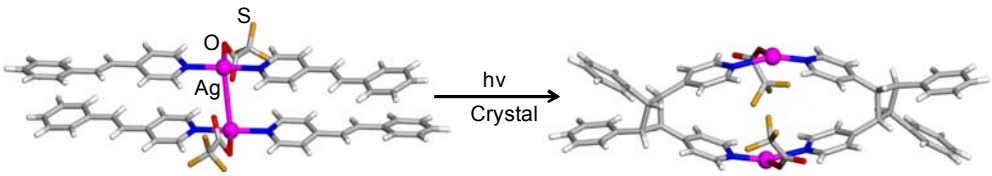

Figure 19. Crystal structure of $[Ag_2(4\text{-stilbz})_4][CO_2CF_3]_2$, before and after photoreaction.

Jin *et. al.* have reported a series of tetranuclear iridium and rhodium supramolecules containing pentamethylcyclopentadienyl (Cp*) ligands in combination with μ-oxalato dinuclear bridging units as short edges. These complexes, when coordinated with pyridines, act as organometallic clip to bring the pyridine-derivatized olefins close to each other *via* π····π interactions.[48] The X-ray crystal structure of $[Cp^*_4Ir_4(4,4'\text{-bpe})_2(C_2O_4)_2](OTf)_4$ (Figure 20) revealed that the complex had a rectangular shape bridged by two oxalate ligands and two molecules of 4,4'-bpe, having inversion center in the middle. Each metal ion adopted a six-coordinate geometry where the pyridyl nitrogen atoms of 4,4'-bpe and oxygen atoms of oxalato ligands occupied the

apical positions, assuming that the Cp* ligand functions as a tridentate ligand. The 4,4'-bpe molecules were placed in close proximity (*ca.* 3.23 Å) within the discrete assembly, suitable for [2+2] photodimerization reaction. When UV-irradiated, 4,4'-tpcb formed stereospecifically and in quantitative yield. The reaction also undergoes in a rare SCSC fashion.

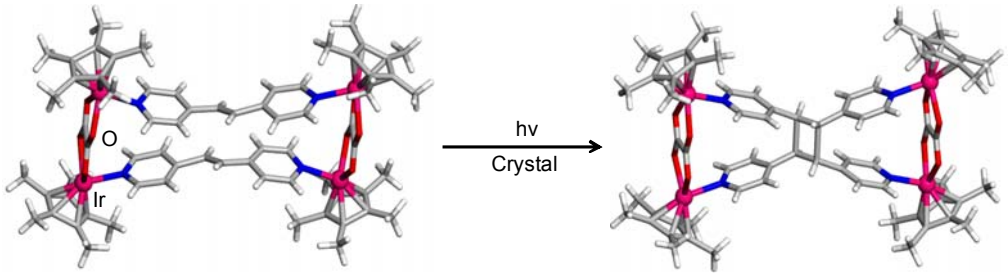

Figure 20. Crystal structure of $[Cp^*_4Ir_4(4,4'\text{-bpe})_2(C_2O_4)_2](OTf)_4$ before and after photoreaction. The counteranions are omitted for clarity.

1.6.3 Reactivity in Metal-organic Solids

Over the last decade, metal-organic frameworks (MOFs) have attracted much attention as promising complements to existing classes of microporous solids.[49] MOFs consist of metal ions or clusters that form vertices of a framework and organic linkers that form bridges. One advantage of MOFs is their easily-modifiable synthesis to control pore connectivity, structure, and dimension by varying the ligands, metals, and/or the counteranions.[50] A wide range of functionality can be incorporated into the pores of MOFs by altering the coordination geometries of the metals and the topicities (*e.g.,* ditopic, tritopic) of the ligands. Developments in the field of coordination-driven supramolecular chemistry and crystal engineering in recent years have led to the synthesis of MOFs with components that undergo reaction in the solid state. The well-

organized environment of the solid state, as well as the geometries adopted by the components of MOFs, can provide useful platforms to assemble molecules into suitable positions to react. It has been demonstrated how reactivity involving the [2+2] photodimerization can be integrated into MOFs.[51] A main motivation to construct MOFs with reactive building units is that the reactions can lead to changes in properties of such porous solids (*e.g.,* pore size). It follows that any changes to the structures of the components can be expected to lead to changes in properties and functions of the pores. For example, it has been shown that the functionalization of mesoporous silica (MCM-41) pore outlets with photoactive groups in form of coumarins leads to controlled access to the pores.[52] Prior to a [2+2] photocycloaddition of the coumarins, the pores are open to appropriate guests (*e.g.,* cholestane). Upon UV-irradiation, the cyclobutane products close the pores, thus, effectively storing guests and limiting access. Upon photocleavage, the pores reopen and release the guests. When considering a MOF, the sizes and shapes, as well as the number of pores, can be tuned using an organic group. Applications in areas such as molecular sensing, controlled guest release, and imaging are envisioned.

A question remains, however, as to whether chemical reactivity can be incorporated into the extended framework of MOFs. Michaelides *et. al*. were the first to describe a photoreaction integrated into a MOF.[53] The structure $[Cd_2(fum)]\cdot 2H_2O$ contained centrosymmetrically related pairs of Cd(II) cations connected to fumarate ligands that result in a planar rectangular-grid network (Figure 21). The coordination sphere at the metal centers contained axially disposed water molecules above and below the grid plane, respectively. The close proximity of olefin groups (3.37 Å) in the adjacent layers of the fumarates allowed the ligands to undergo a [2+2] cycloaddition reaction forming *trans,trans*-1,2,3,4-cyclobutanetetracarboxylic acid in quantitative yield. Although the network did not contain cavities, this example established that photoreactive organic components can be incorporated into a MOF.

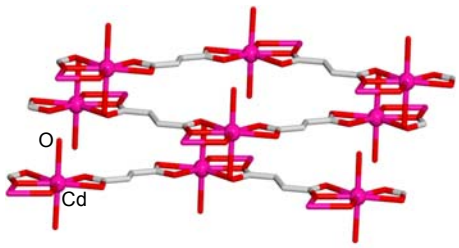

Figure 21. Representation of three adjacent layers of $[Cd_2(fum)]\cdot 2H_2O$.

In related work, Vittal *et al.* reported the photoreactive coordination polymer $[\{CF_3CO_2)(O_2CCH_3)Zn\}_2(4,4'\text{--bpe})_2]_n$ (Figure 22).[54] A single crystal X-ray diffraction analysis revealed the formation of a molecular ladder-like polymer. Each Zn(II) center adopted a distorted octahedral geometry. Two acetate ligands bridged a pair of Zn(II) ions in $[Zn_2(4,4'\text{-bpe})_2]_\infty$ within Zn···Zn distance of 3.85 Å. Each metal center was also chelated by a trifluoroaceate anion to satisfy the coordination geometry. The ethylenic carbons of the bpe ligands of the parallel chains were separated by a distance of 3.75 Å, whereas the closest distance between the alkene groups of the neighbouring ladders was 7.10 Å. UV-irradiation of the solid led to the stereocontrolled formation of 4,4'-tpcb within the ladder framework in quantitative yield. The reaction also underwent a rare SCSC reaction (*i.e.* a reaction where crystallinity of the reactant material is maintained throughout the course of the reaction).

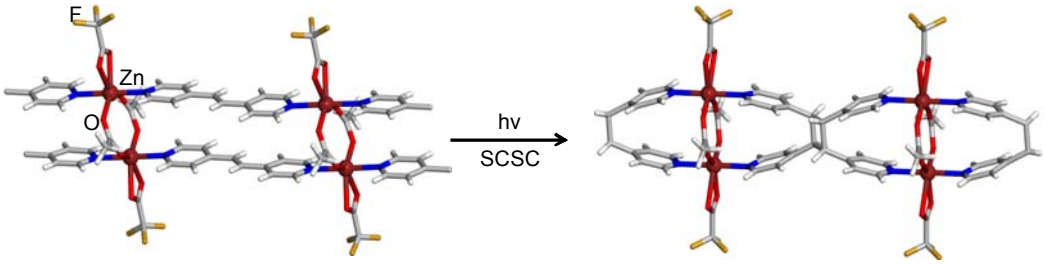

Figure 22. Representation of SCSC [2+2]cycloaddition reaction of $[\{(CF_3CO_2)(O_2CCH_3)Zn\}_2(4,4'\text{-bpe})_2]_n$. Hydrogen atoms are omitted for clarity.

Following the work of Vittal, our group described a dinuclear metal complex that assembled and preorganized two olefins within a 1D MOF to react in the solid state. Specifically, the linear photoreactive coordination polymer $\{[Zn_2L(OH)(4,4'\text{-bpe})_2](ClO_4)_2\}_\infty$ (Figure 23) {where: L = 2,6-bis[*N*-(2-pyridylethyl)formimidoyl]-4-methylphenol} was obtained when reacted with the Schiff-base complex $[Zn_2L(OH)](ClO_4)_2$ with 4,4'-bpe.[55] An X-ray diffraction analysis revealed that each metal ion adopted an octahedral coordination environment. The metals were tetra-coordinated by L in the basal plane while the apical sites were coordinated by pyridyl groups one from two different bpe molecules. The olefins were coordinated to two neighbouring dinuclear complexes while being stacked parallel and separated by 3.71 Å. The formation of 4,4'-tpcb within the assemblies occurred in up to 95% yield upon UV-irradiation. The reaction, however, did not proceed *via* a SCSC transformation. Notably, the assembly included H_2O molecules were liberated from the solid during the course of the photoreaction.

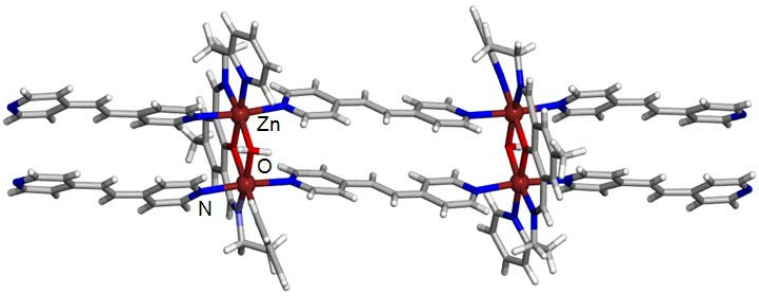

Figure 23. Crystal structure of $[Zn_2L(OH)(4,4'\text{-bpe})_2](ClO_4)_2 \cdot 4H_2O$. Hydrogen atoms and perchlorate counteranions are omitted for clarity.

Whereas argentophilic forces had been used by our group to direct reactivity within a discrete binuclear complex, Vittal *et al.* reported a [2+2] photodimerization within the solvated 1D coordination polymer $[Ag(4,4'\text{-bpe})(H_2O)](CF_3CO_2) \cdot CH_3CN$.[56]

Under UV-irradiation, the solid resulted in an unusual solid-state reorganization and photoreaction that led to the formation of cyclobutane-based polymer, as supported by powder X-ray diffraction studies. Michaelides *et al*. have recently shown that the previous reported 2D layered structure composed of Cd(II) dimers linked by fumarates can be pillared to afford a 3D photoactive MOF.[57] Specifically, the axial water molecules on the Cd(II) metal centers in $[Cd_2(fum)]\cdot 2H_2O$ were substituted by bpe ligands to form a 3D non-cubic octahedral-like net (Figure 24). The fumarate ions played the role of bridging ligands in the 2D grid while the double columns of bpe ligands acted as linkers between the grids. The close proximity between related pairs of Cd(II) ions brought the pillared 4.4'-bpe ligands nearly parallel and within a reactive distance of 3.95 Å. UV-irradiation afforded 4,4'-tpcb stereospecifically and in quantitative yield.

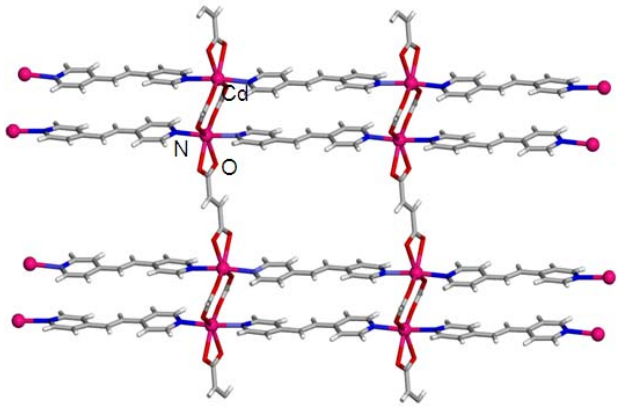

Figure 24. Projection of one 2D network of $[Cd_2(O_2CCH{=}CHCO_2)_2(4,4'\text{-bpe})_2]$ along the crystallographic *a* axis. Hydrogens are omitted for clarity.

Indeed, the above examples are promising in terms of integrating reactivity within the structures of MOFs.

1.7. Downstream Application of Targets

We and others have demonstrated how the molecular targets, obtained *via* templated synthesis in the solid state, can be further utilized in metal-directed self-assemblies. We have shown that 2,2'-tpcb and 4,4'-tpcb, obtained stereospecifically and in quantitative yield *via* templated synthesis in organic solid state, have been further utilized in the formation of 1D and 2D metal-organic assemblies upon binding with $CuSO_4$ and $Co(CH_3CO_2)_2$, respectively.[58] Recently, Schroder *et. al.* have shown the metal mediated synthesis of 4,4'-tpcb in solution and *in-situ* formation of a 3D metal-organic assemblies with $AgBF_4$ (Figure 25).[59]

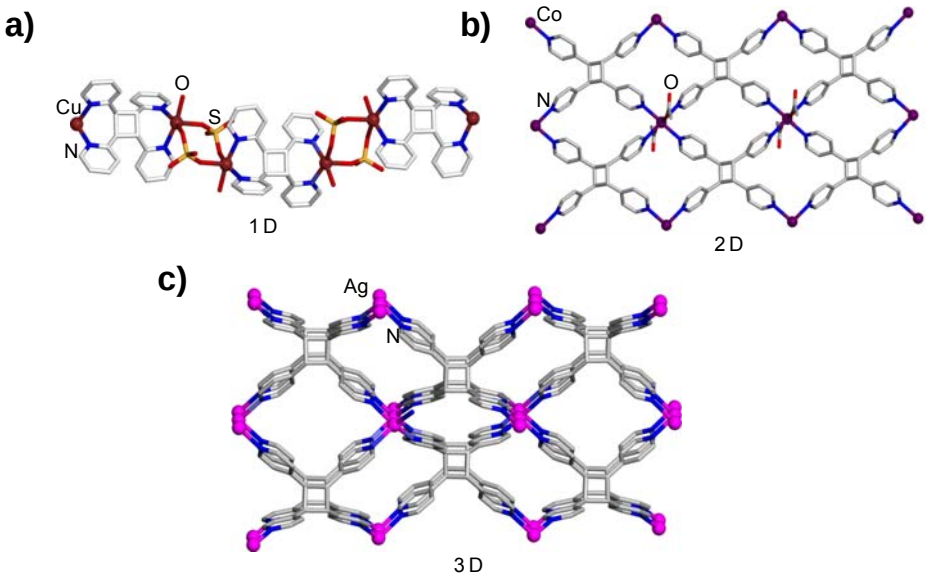

Figure 25. Metal-organic assemblies obtained from molecular products *via* templated synthesis in solid state: a) 1D assembly of $[Cu_2(SO_4)_2(2,2'\text{-tpcb})(H_2O)_2]_\infty$, b) 2D assembly of $[Co(O_2CCH_3)_2(4,4'\text{-tpcb})]_\infty$, and c) 3D framework of $[Ag(4,4'\text{-tpcb})(BF_4)]_\infty$

1.8. Dissertation Overview

The research focus in this dissertation is to increase the synthetic versatility of template-directed synthesis in the solid state. In particular, the aim is to expand the hydrogen-bond directed synthetic strategy in the co-crystals towards the rational design, synthesis and applications of challenging molecular targets.

In chapter 2, the effect of modified pyridine handles towards the self-assembly and photoreactivity of monopyridyl and bipyridyl olefins in the solid state will be demonstrated. Specifically, the effect of *ortho*- and *meta*- substitution by methyl and chloro groups on the pyridyl handle towards the self-assembly and reactivity of olefins within co-crystals will be described. To our knowledge, this is the first systematic study of the generality and synthetic versatility of templated synthesis in the solid state. This study also triggers interests on structure-reactivity correlation in the organic solid state, much appreciated in traditional synthetic organic chemistry.

In chapter 3, rational design, synthesis and application of synthetically challenging cofacial aromatics will be shown. Specifically, we demonstrate the stereospecific, quantitative and gram scale synthesis of an unprecedented cofacial terpyridine and the application of this material in the field of coordination chemistry. To our knowledge, this is also the first study on hydrogen-bond directed self-assembly and photoreactivity involving terpyridine, in general.

In chapter 4, supramolecular construction of heterocyclophanes in the solid state will be demonstrated. The first stereospecific, quantitative and gram scale syntheses of structurally constrained [2.2]pyridinophanes have been successfully accessed *via* template-directed solid-state synthetic approach. We also show the applications of constrained [2.2]pyridinophanes towards coordination-directed self-assemblies.

In chapter 5, we will show how the chromic properties of salicylidineanilines can be modified in the organic solid state *via* co-crystallization. We also show how

thermochromism and photoreactivity, inherent properties of two chemically distinct molecular solids, can be integrated on the same single crystalline solid *via* co-crystallization.

Alltogether, the research described in this dissertation will demonstrate the ability to increase the degree of synthetic freedom in the organic solid state by providing access to elaborate structures with different levels of complexity.

CHAPTER 2: MODIFIED HANDLES IN TEMPLATED SOLID STATE SYNTHESIS

2.1. Introduction

[2+2]Photocycloaddition reaction has been known for more than a hundred years to proceed in the solid state. But only four decades ago, Schmidt outlined the geometric criteria for a cycloaddition reaction to take place in solid state.[34] There have been several attempts to control reactivity in solids since then, but the photoreactive solids dealt with were mostly based on discovery rather than designed. The lack of structure-reactivity correlation mostly lies on the large degree of unpredictability associated to crystal packing with respect to change in molecular structure. As a consequence, the degree of synthetic freedom accomplished in solution phase has never been met in solid state. There have several studies for controlling photoreactivity in solids by employing auxiliary components (*e.g.,* substituents) with limited success. The modularity of those techniques was highly limited in terms of structural complexity incorporated in the reactant structure as well as the yield and stereoselectivity of the products. There is a current surge of interest in employing principles of supramolecular chemistry and self-assembly to simplify the packing issue. Recently, we have shown that small organic molecules in the form of linear templates could circumvent effects of close packing by preorganizing reactant olefins within discrete supermolecules, suitable for [2+2] photocycloaddition. Specifically, linear template based on resorcinols can preorganize pyridine functionalized olefins within a discrete assembly to undergo [2+2]photodimerization reaction, stereospecifically and in quantitative yield. The inherent modularity of this approach is associated to the reversible way of forming hydrogen bonds between the template molecules and the molecular recognition group (*i.e.,* pyridine) attached to the reactant. Formation of a discrete assembly helps to isolate

the reactant molecules from the long range packing forces, thus, simplifying the crystal packing issue. Additionally, the positioning of the template molecules along the exteriors of the assemblies, potentially, allow structural complexities to be incorporated in the reactant structure without significantly affecting the packing motif. We have demonstrated the tolerance of self-assemblies towards structural complexity of reactant olefins as additional olefinic groups and benzene rings. These increasingly complex molecular precursors led to the synthesis of interesting molecular targets such as ladderanes and cyclophanes stereospecifically, quantitatively, and in gram amounts. Since our synthetic approach in solid state is highly dependent on the molecular recognition between pyridine handle and linear templates (*e.g.,* resorcinol), it is of fundamental interest to study the self-assembly process and reactivity of olefins with modified pyridine handles. Successful formation of reactive self-assemblies with chemical control would increase the synthetic applicability of our templated synthetic approach and a step towards much needed synthetic freedom in solid state. Nevertheless, self-assembly and reactivity studies involving olefins with modified pyridine handles would be the first systematic study of the structure-reactivity correlation of reactants towards [2+2]photocycloaddition reaction in solid state. Additionally, substitution of the pyridine ring could, potentially, favor to break open the pyridine ring in order to post-modify the cyclobutane-based molecular targets. We have chosen to modify the pyridine handle by substituting the pyridine ring on the *ortho* and/or *meta* positions. Specifically, pyridine handles has been modified by methyl and chloro substituents (Figure 26). Methyl and chloro groups are not familiar as hydrogen bond donor and/or accepting groups and thus, the steric effects near the hydrogen-bond formation site towards the self-assembly and photoreactivity of pyridine functionalized olefins can be unequivocally demonstrated.[60] Methyl and chloro groups, having different electronic effects, are of importance to study how differing strength of hydrogen-bonds can affect the self-assembly and photoreactivity. Having similar volume (*i.e.,* Me = 24 Å, Cl = 20 Å),

methyl and chloro functionality have a history of being used interchangeably in crystal engineering and thus their use in handle modification would reevaluate their applicability in hydrogen-bonded assemblies. Nevertheless, the synthetic accessibility of olefins with substituted pyridines was also considered given the synthetic challenge of substituted pyridine as well as the scarcity and expense of the commercial starting materials. Even with relatively simple substituents such as methyl and chloro, the number of possible olefins to synthesize and to work with is quite large.

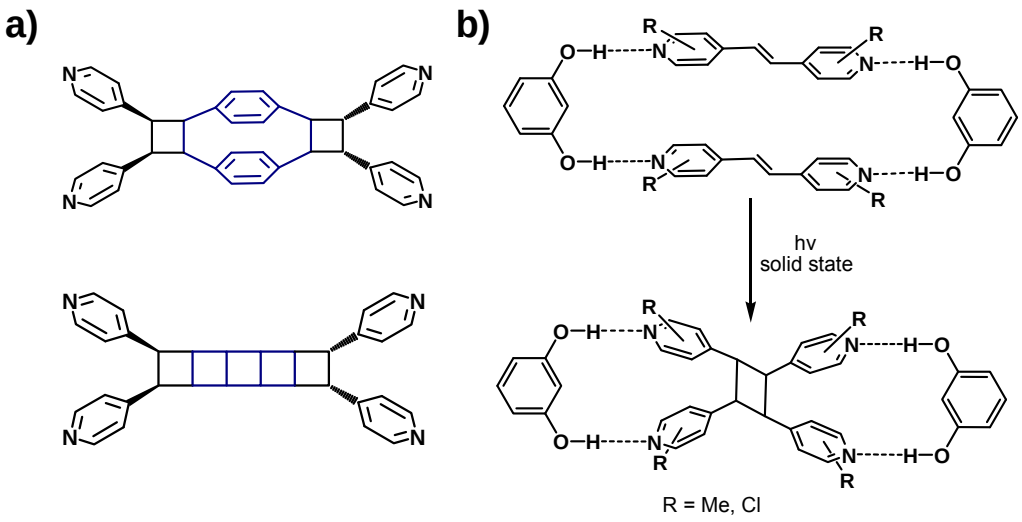

Figure 26. Schematic of a) molecular targets with structural complexity at the reaction site, and b) templated synthesis of targets with structural complexity at the molecular recognition site.

We approached to modify the 4-pyridyl handle by substitution on the *ortho* positions of the aromatic ring considering their closest positioning of hydrogen bonding site. A series of experiments have been undertaken to understand the effect of *ortho* substituents on the pyridine handles in terms of both self-assembly and photoreactivity. In case of methyl and chloro substituents on the *ortho* positions, the number of possible compounds is 86 (Table 1). Methyl and chloro have opposite electronic properties; methyl group acts as

electron donor to increase the basicity of pyridyl group whereas the chloro acts as electron withdrawing group.

Table 1. Total 86 combinations of chloro and methyl substituted olefins.

N-atom position	Monopyridine	N-atom position	Symmetrical bipyridine	N-atom position	Unsymmetrical bipyridine
2	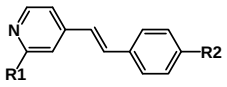	**2,2'**	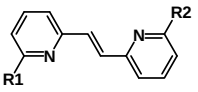	**2,3'**	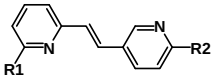
3	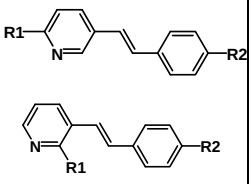	**3,3'**	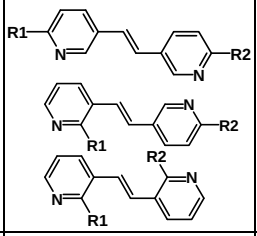	**2,4'**	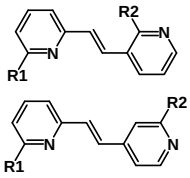
4	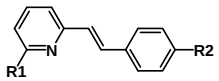	**4,4'**	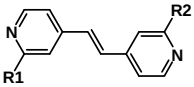	**3,4'**	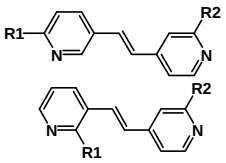
Total combination= 24		Total combination= 25		Total combination= 40	

In this chapter we will discuss the self-assembly and photoreactivity studies of the olefins with methyl and chloro substituents on the *ortho* position of the 4-pyridyl handle (Table 2).

Table 2. Target olefins with methyl and chloro substituents on the pyridine handle.

#	Monosubstituted	#	Disubstituted
1	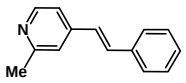 MPyPE	5	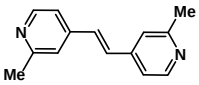 MPyMPyE
2	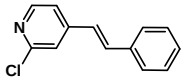 CPyPE		
3	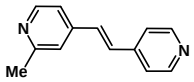 MPyPyE		
4	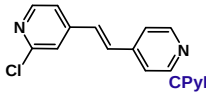 CPyPyE		

[1] **MPyPE:** 1-(3-methyl-4-pyridyl)-2-phenylethylene, **CPyPE:** 1-(3-chloro-4-pyridyl)-2-phenylethylene, **MPyPyE:** 1-(3-methyl-4-pyridyl)-2-(4-pyridyl)ethylene, **CPyPyE:** 1-(3-chloro-4-pyridyl)-2-(4-pyridyl)ethylene, **MPyMPyE:** 1,2-bis(3-methyl-4-pyridyl)ethylene.

2.2 Experimental

2.2.1 Synthesis of 2-methyl-4-pyridinecarboxyaldehyde

2,4-lutidine (2 g, 18.86 mmol) in 40 mL dry THF was cooled down to -78 °C in a dryice-acetone bath under argon atmosphere. nBuLi (8.5 mL, 21.25 mmol) (2.5 M in hexane) was added in the solution slowly *via* syringe not allowing the temperature to rise above -60 °C. The solution was stirred at -78 °C for 30 min. Diethylamine (1.5 g, 20.54 mmol) was added to the solution slowly and the solution was stirred for additional 45 min. DMF (1.5 g, 20.54 mmol) was added to the solution and the solution was stirred for 75 min. The solution was allowed to warm up to room temperature and quenched with saturated solution of ammonium chloride (20 mL). The organic layer was separated in a separating funnel and the aqueous layer was extracted with dichloromethane (3×50 mL). The

organic layers were combined, washed with water (2×100 mL), and dried by $NaSO_4$. The solvent was evaporated in a rotor-evaporator and to yield the product as an orange liquid (3.2 g, 131 %). The product was impure because of the presence of excess DMF. The crude product was used as it is for the next synthetic step.

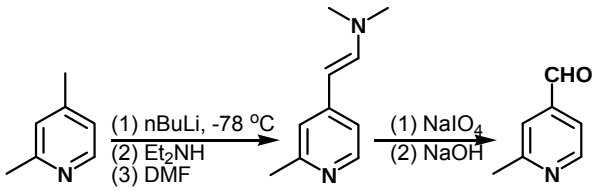

Figure 27. Schematic for the synthesis of 2-mmethyl-4-pyridinecarboxyaldehyde.

2.2.2 Synthesis of benzyl(diethyl)phosphonate

Benzyl bromide (10 g, 58.47 mmol) and triethylphosphite (11.65 g, 70.18 mmol) was refluxed for six hours. The solution was cooled to room temperature and distilled to yield the product (12.5 g, 94%) as a clear liquid.

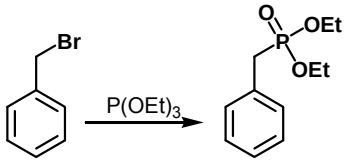

Figure 28. Schematic for the synthesis of benzyl(diethyl)phosphonate.

2.2.3 Synthesis of 1-(3-methyl-4-pyridyl)-2-phenylethylene (MPyPE)

A mixture of crude 2-methyl-4-pyridinecarboxyaldehyde (2 g), benzyl(diethyl)phosphate (3.8 g), and ^{t}BuOH (2 mL) was cooled in an ice bath. ^{t}BuOK (2 g) was added slowly with vigorous stirring. The solution was allowed to warm up to room temperature and allowed to stir for four hours. The reaction mixture was poured in ice cold water (100 mL). The white precipitate of MPyPE (1.2 g, yield = 70%) was filtered under vacuum, washed with excess water, and air-dried. ^{1}H NMR (DMSO-d_6, δ/ppm): 8.40 (1H, d), 7.70 (4H, d), 7.51 (2H, d), 7.45-7.25 (5H, m), 7.20 (2H, d), 2.50 (3H, s). ^{13}C NMR (DMSO-d_6, δ/ppm): δ 158.2, δ 149.2, δ 144.1, δ 135.1, δ 132.8, δ 131.1, δ 128.7, δ 128.6, δ 126.9, δ 120.0, δ 118.0, δ 23.9.

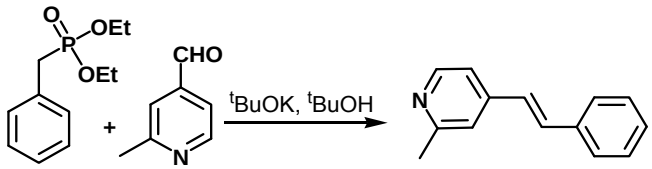

Figure 29. Schematic for the synthesis of 1-(3-methyl-4-pyridyl)-2-phenylethylene.

2.2.4 Synthesis of 1-(3-methyl-4-pyridyl)-2-(4-pyridyl)ethylene (MPyPyE)

2-Methyl-4-bromopyridine (2.0 g, 11.7 mmol) and freshly distilled 4-vinylpyridine (1.3 g, 12.6 mmol) was added to 150 mL of saturated aqueous K_2CO_3 solution. To the solution dichlorobis-(triphenylphosphine)palladium(II) (0.42 g, 5.12 mmol) and triethylamine (1 mL) was added and the solution was refluxed for three days. The solution was cooled down to room temperature and extracted with dichloromethane. The organic layer was washed with water and dried by NaSO4. The solvent was evaporated in

a rotor-evaporator to leave a tan solid. The solid was recrystallized from acetonitrile to yield a white solid of MPyPyE (2 g, 88%). ^{1}H NMR (DMSO-d_6, δ/ppm): 8.59 (2H, d), 8.45 (1H, d), 7.59 (2H, d), 7.50 (1H, s), 7.47 (2H, d), 7.39 (1H, d), 2.49 (3H, s). ^{1}H NMR (DMSO-d_6, δ/ppm): δ 158.4, δ 150.1, δ 149.4, δ 143.4, δ 143.3, δ 130.6, δ 130.1, δ 121.1, δ 120.4, δ 118.3, δ 23.9.

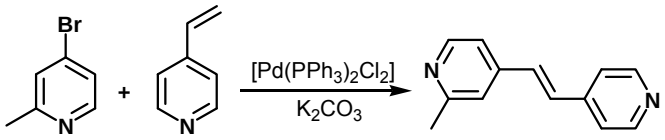

Figure 30. Schematic of the synthesis of 1-(3-methyl-4-pyridyl)-2-(4-pyridyl)ethylene.

2.2.5 Synthesis of 1-(3-methyl-4-pyridyl)-2-(4-pyridyl)ethylene (MPyMPyE)

2-Methyl-4-bromopyridine (2.0 g, 11.7 mmol) and vinyltributyltin (4.0 g, 12.6 mmol) was added to 70 mL of dry toluene and 20 mL of Et_3N. To the solution dichlorobis-(triphenylphosphine)palladium(II) (0.35 g, 5 mmol) was added and the solution was refluxed for 16 hours. The solution was cooled to room temperature and filtered under vacuum. The crude 2-methyl-4-vinylpyridine was used for the second step without further purification. Additional amount of 2-Methyl-4-bromopyridine (2 g, 11.7 mmol) and dichlorobis-(triphenylphosphine)palladium(II) (0.35 g, 5 mmol) were added and the reflux was continued for another two days. The solution was cooled down to room temperature, filtered and evaporated in the rotor-evaporator. The tan precipitate was recrystallized from nitromethane to yield a white solid of MPyMPyE (1.6 g, 66%). ^{1}H NMR (DMSO-d_6, δ/ppm): 8.45 (2H, d), 7.47 (4H, s), 7.39 (2H, d), 2.5 (6H, s, CH_3). ^{13}C NMR (DMSO-d_6, δ/ppm): δ 158.4, δ 149.4, δ 143.5, δ 130.3, δ 120.3, δ 118.3, δ 23.9.

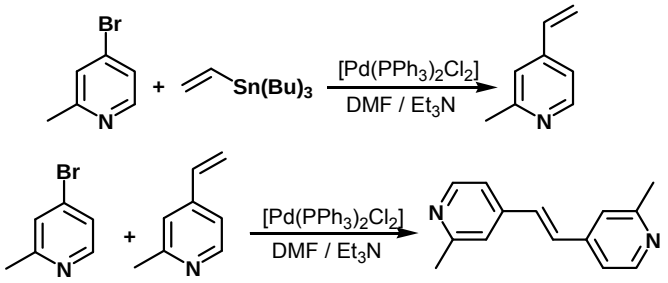

Figure 31. Schematic of the synthesis of MPyMPyE.

2.2.6 Synthesis of 1-(3-chloro-4-pyridyl)-2-phenylethylene (CPyPE)

2-Chloro-4-iodopyridine (2.0 g, 11.7 mmol) and freshly distilled styrene (1.3 g, 12.6 mmol) was added to 150 mL of saturated aqueous K_2CO_3 solution. To the solution dichlorobis-(triphenylphosphine)palladium(II) (0.35 g, 5 mmol) and triethylamine (1 mL) was added and the solution was refluxed for three days. The solution was cooled down to room temperature and extracted with dichloromethane. The organic layer was washed with water and dried by $NaSO_4$. The solvent was evaporated in a rotor-evaporator to leave a tan solid. The solid was recrystallized from acetonitrile to yield a white solid (1.8 g, 81%).

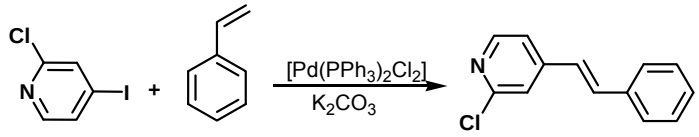

Figure 32. Schematic of the synthesis of CPyPE.

2.2.7 Synthesis of 1-(3-chloro-4-pyridyl)-2-(4-pyridyl)ethylene (CPyPyE)

2-Chloro-4-iodopyridine (2 g, 8.4 mmol) and freshly distilled 4-vinylpyridine (1.3 g, 12.6 mmol) was added to 150 mL of saturated aqueous K_2CO_3 solution. To the solution dichlorobis-(triphenylphosphine)palladium(II) (0.35 g, 5 mmol) and triethylamine (1 mL) was added and the solution was refluxed for three days. The solution was cooled down to room temperature and extracted with dichloromethane. The organic layer was washed with water and dried by $NaSO_4$. The solvent was evaporated in a rotor-evaporator to leave a tan solid. The solid was recrystallized from acetonitrile to yield a white solid (1.5 g, 84%). ^{1}H NMR (DMSO-d_6, δ/ppm): 8.61 (2H, d), 8.43 (1H, d), 7.78 (1H, s), 7.64 (1H, d), 7.61 (1H, s), 7.59 (2H, d), 7.53 (1H, d).

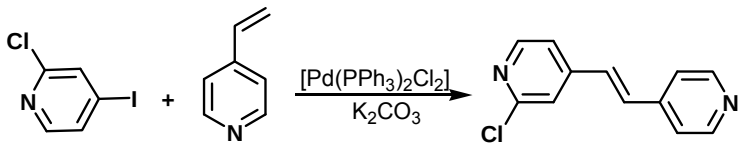

Figure 33. Synthesis of CPyPyE.

2.3. Results and Discussion

In the following section, the co-crystallization, solid-state characterization and photoreactivity of the targeted olefins in Table 2 will be discussed. General and crystallographic parameters for the co-crystals before and after photodimerization are given in Appendix A, Tables A1-A4. The solids which will be discussed are shown in Table 3.

Table 3. Structural formulas of the crystalline solids discussed in first part of Chapter 2.

2(5-CN-res)·(MPyPE)	($AgClO_3$)·2(CPyPE)	(res)·(CPyPyE)
2(4,6-diBr-res)·(MPyPE)	2($AgClO_3$)·2(CPyPE)(ht-CPYPCB)	2(4,6-ditBu-res)·2(CPyPyE).
(4,6-di-^{t}Bu-res)·(MPyPCB)	2(res)·2(MPyMPyE)	2(res)·2(MPyMPyE)
CPyPE	2(4,6-diBr-res)·(MPyPyCB).	
CPyPCB	2(4,4'-bppe)·3(5-iodo-res)	

The white solid of MPyPE was co-crystallized with the templates shown in Table 3. In a typical experiment, one equivalent of resorcinol was co-crystallized with two equivalent amount of MPyPE in nitromethane. Single crystals of 2(resorcinols)·(1-(3-methyl-4-pyridyl)-2-phenylethylene)), suitable for analysis by single crystal X-ray diffraction, were obtained in a period of approximately one day. The resultant co-crystals were powdered and placed between a pair of pyrex glass plates. These samples were then exposed to ultraviolet radiation from a 500 W high pressure mercury lamp. The results of co-crystallization and photoreaction experiments are summarized in Table 4. As shown in the table, the co-crystallization experiments result in co-crystals with 1:2 ratio of template/reactant. Due to the quantitative photoreactions with two templates, only these two samples were chosen to be further studied by single crystal X-ray diffraction studies to investigate the nature of supramolecular architectures formed that result in the reactivity.

Table 4. Results of co-crystallization and photoreactions of MPyPE.

template	stoichiometry (template:reactant)	reaction yield
res	×	×
5-Cl-res	1:2	0%
5-I-res	1:2	12%
5-CN-res	1:2	100%
5-OMe-res	×	×
4-Et-res	×	×
4-Cl-res	1:2	25%
4,6-diCl-res	1:2	38%
4,6-diBr-res	1:2	100%
4,6-dil-res	1:2	25%
4,6-di^{t}Bu-res	1:2	0%

Single crystal structure of 2(5-CN-res)·(MPyPE) showed the formation of a hydrogen-bonded three component discrete assembly (Figure 34). The methyl substituted pyridine group involve in the formation of O-H···N hydrogen bonds with the resorcinol OHs (O···N distance 2.70 Å). The olefins stacked head to head within a distance of 4.01 Å while the double bonds were crossed within the assembly. Interestingly, the methyl groups were pointed in the same direction within a C···C separation of 5.18 Å, contrary to the expectation of being in the opposite direction for steric reasons.

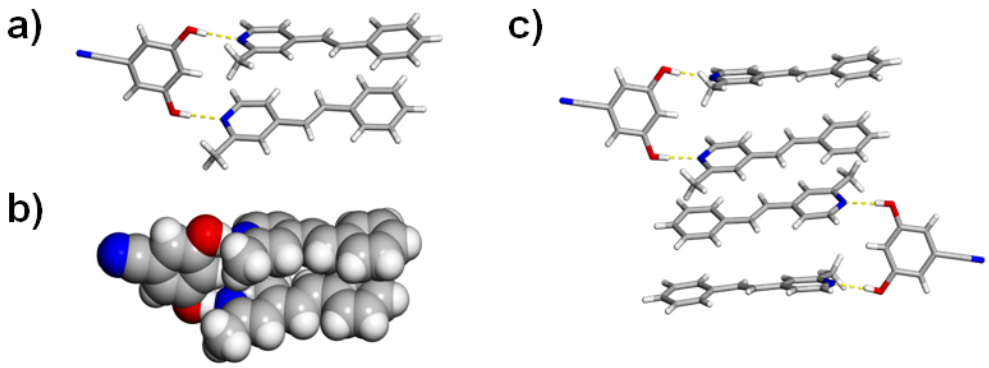

Figure 34. Single crystal structure of 2(5-CN-res)·(MPyPE): a) wireframe view, b) space-filling model and, c) crystal packing environment.

The nearest distance between the olefins in between the assemblies was 4.03 Å where C=C bonds were parallel and the MPyPE molecules were oriented in a head to tail fashion. UV-irradiation of the solid resulted in quantitative formation of a cyclobutane product, namely, *hh-rctt*-1,2-bis-(3-methyl-4-pyridyl)-3,4-diphenylcyclobutane (MPyPCB) as confirmed by the complete disappearance of the olefinic peaks at 7.50 ppm and 7.20 ppm and emergence of cyclobutane peaks at 4.51 ppm. Single crystal structure of 2(4,6-diBr-res)·(MPBE) showed the formation of a hydrogen-bonded three component discrete assembly (Figure 35a). The methyl substituted pyridine group involve in the formation of O-H···N hydrogen bonds with the resorcinol OHs (O···N distances are 2.70 Å, and 2.71 Å). The olefins stacked head to head having parallel olefinic bonds within a distance of 3.90 Å within the assembly. The methyl groups were still oriented in the same direction within a C···C distance of 4.16 Å. The nearest distance between the olefins in between the assemblies was 3.78 Å where C=C bonds were parallel and the MPyPE molecules were oriented in a head to tail fashion (Figure 35b).

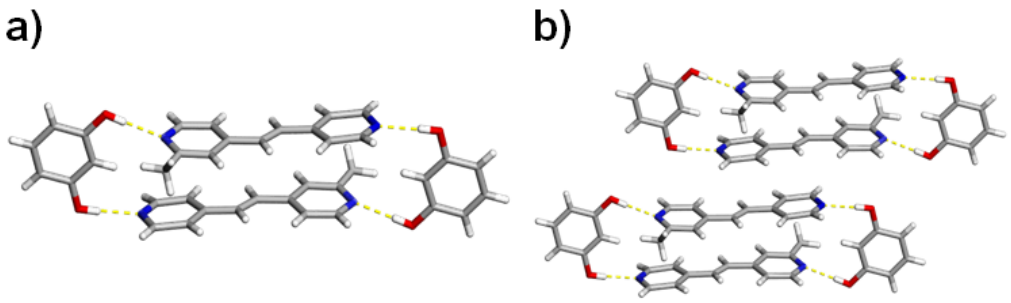

Figure 35. Single crystal structure of 2(4,6-diBr-res)·(MPyPE): a) discrete three component assembly, and b) crystal packing of the neighbouring assemblies.

The photoreacted powdered co-crystals of both 2(5-CN-res)·(MPyPE), and 2(4,6-diBr-res)·(MPyPE) were attempted to recrystallize in order to characterize the photoproduct by single crystal X-ray diffraction. The template molecule was also separated from the co-crystal in order to crystallize the photoproduct as a pure solid. Upon several unsuccessful attempts, we decided to crystallize the product by co-crystallizing it with various resorcinols. There have been several reports on the utilization of co-crystallization as a method to crystallize a molecular target for single crystal X-ray diffraction studies. Co-crystallization of the photoproduct with 4,6-di^{t}Bu-res from nitromethane resulted single crystal of the cyclobutane product with 4,6-di^{t}Bu-res in a 1:1 stoichiometric ratio. The single crystal structure of (4,6-di-^{t}Bu-res)·(MPyPCB) (Figure 36) showed a hydrogen-bonded two-component discrete assembly of expected hh-MPyPCB with 4,6-ditBu-res. The methyl groups are now in the opposite direction because of single bond rotation.

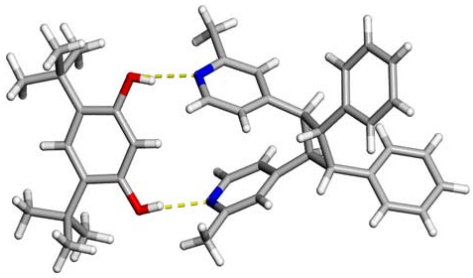

Figure 36. Single crystal structure of (4,6-di-^{t}Bu-res)·(MPyPCB).

The chlorine substituted olefin CPyPE was synthesized and the self-assembly with resorcinols was studied and the photoreactivity was monitored. The molecule, unlike MPyPE, was reluctant to form co-crystals with resorcinols. The lack of hydrogen-bond formation can be explained by the decreased basicity of pyridine nitrogen atom and decreased strength of hydrogen bond. In addition, it was observed that, CPyPE is photoreactive as a pure solid upto quantitative photoconversion. The single crystal structure of CPyPE (Figure 37a) revealed the head-to-tail arrangement of the olefins within a a distance of 3.73 Å. The single crystal structure of the photodimer, namely rctt-1,3-bis-(3-chloro-4-pyridyl)-2,4-diphenylcyclobutane (CPyPCB) (Figure 37b), shows the expected head-to-tail geometry of the cyclobutane product. There are significant chloro-chloro interactions in the crystal structure of CPyPCB. Four neighbouring CPyPCB molecules are held together by chloro-chloro interaction within a distance of 3.45 Å, and 3.48 Å forming a tetramer.

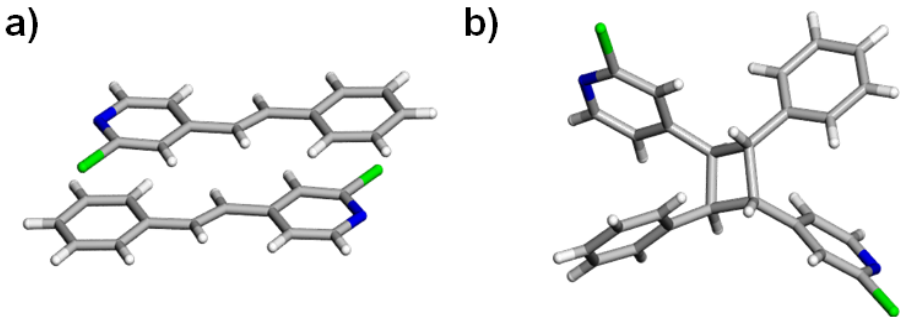

Figure 37. a) Single crystal structure: a) CPyPE, and b) CPyPCB.

As limited numbers of co-crystals were obtained by co-crystallizing with resorcinol templates and they remained photostable, the molecule was co-crystallized with Ag salts in order to exploit the argentophilic interactions to align the CPyPE molecules in a head-to-head geometry and inducing photoreactivity in the solid state. Crystallization of CPyPE with AgOTf from acetonitrile resulted colourless crystals that undergo photodimerization upto 50% yield. The single crystal structure of $(AgClO_3)\cdot 2(CPyPE)$ (Figure 38) shows stacking of olefins in a head-to-tail orientation within a distance of 3.70 Å. Each silver ion is coordinated by pyridines of two CPyPE molecules and the oxygen atom of the triflate anion. There are no argentophilic interactions, instead there is silver-olefinic interactions with the phenyl rings within a distance of 3.45 Å. The complex undergoes photodimerization reaction in the powder form as well as in a single crystalline form to form the cyclobutane product. The single crystal structure of $2(AgClO_3)\cdot 2(CPyPE)$(ht-CPYPCB), obtained *via* SCSC reaction shows the expected formation of the photodimer in a head-to-tail arrangement.

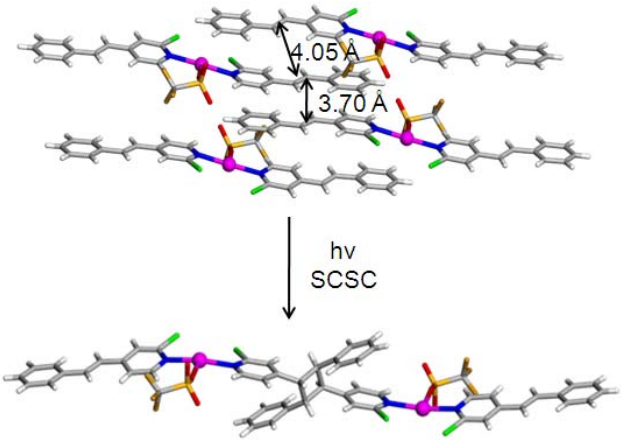

Figure 38. SCSC photoreaction of (AgOTf)·2(CPyPE); a single crystal x-ray crystallographic study.

The olefin 3MPyPyE was synthesized by Heck coupling reaction between 2-methyl-4-bromopyridine and 4-vinylpyridine. The co-crystallization and photoreactivity of the resultant co-crystals were studied as described before. Being an unsymmetrical bipyridyl ethylene, co-crystallization with resorcinol templates would lead to total three possible outcomes (Figure 39). The outcomes involve head-to-head assembly, head-to-tail assembly and a mixture of both in the same crystal.

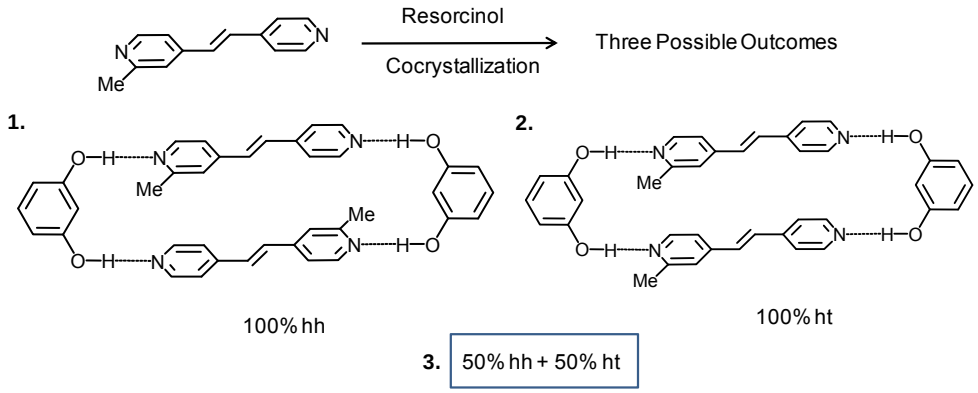

Figure 39. Schematic of the possible outcomes in terms of self-assembly and photoreactivity of MPyPyE.

When MPyPyE was crystallized with resorcinol templates, led to co-crystals with 1:1 stoichiometric ratio. The co-crystals when reacted under broadband UV-irradiation, led to quantitative photoconversion. The ^{1}H NMR spectra of the co-crystals after photoreaction showed a 50:50 mixture of two different products, expected to be a mixture of head-to-head and head-to-tail photodimer. Single crystal structure of 2(res)·2(MPyPyE) (Figure 40) shows the formation a four component discrete assembly consisting of two resorcinol and two MPyPyE molecules. The methyl group is disordered on both sides explaining the formation of both head-to-head (hh) and head-to-tail (ht) products from the same crystal. The distance between the olefins within the assembly is 3.73 Å, whereas the distance between olefinic groups in between two neighbouring assemblies is 5.12 Å.

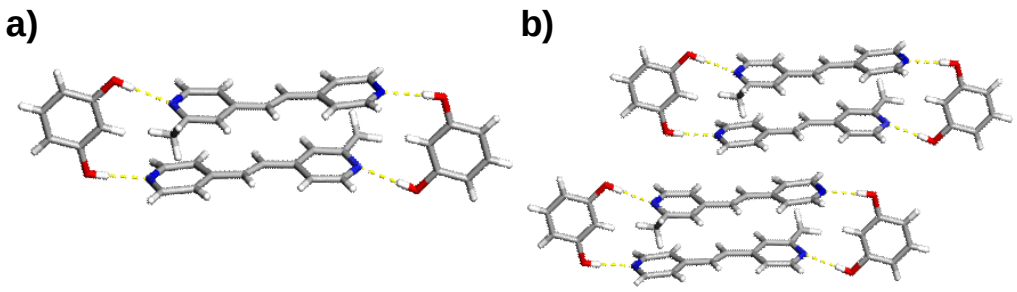

Figure 40. a) Four component discrete assembly of 2(res)·2(MPyMPyE) in head-to-tail orientation, and b) the crystal packing environment.

The photoreacted powder was recrystallized from nitromethane in order to characterize the photodimer by single crystal X-ray diffraction. The template (*i.e.,* resorcinol) was removed from the photoreacted co-crystal, and the pure photoproduct was co-crystallized with substituted resorcinols. When the photodimer was co-crystallized with 4,6-dibromoresorcinol (4,6-diBr-res) from nitromethane, colourless needles appeared by slow cooling of a supersaturated solution. The presence of both components in 2:1 stoichiometry (*i.e.,* 2(4,6-diBr-res)·(MPyPyCB) were confirmed by ^{1}H NMR

spectroscopy (Figure 41). The single crystal structure showed that pyridine groups were involved in O-H···N hydrogen bonds with 4,6-diBr-res on both sides of the cyclobutane rings. Presence of both hh and ht photodimer in the same crystal was supported by two sets of proton signals in the ^{1}H NMR spectroscopy as well as the disordered methyl groups.

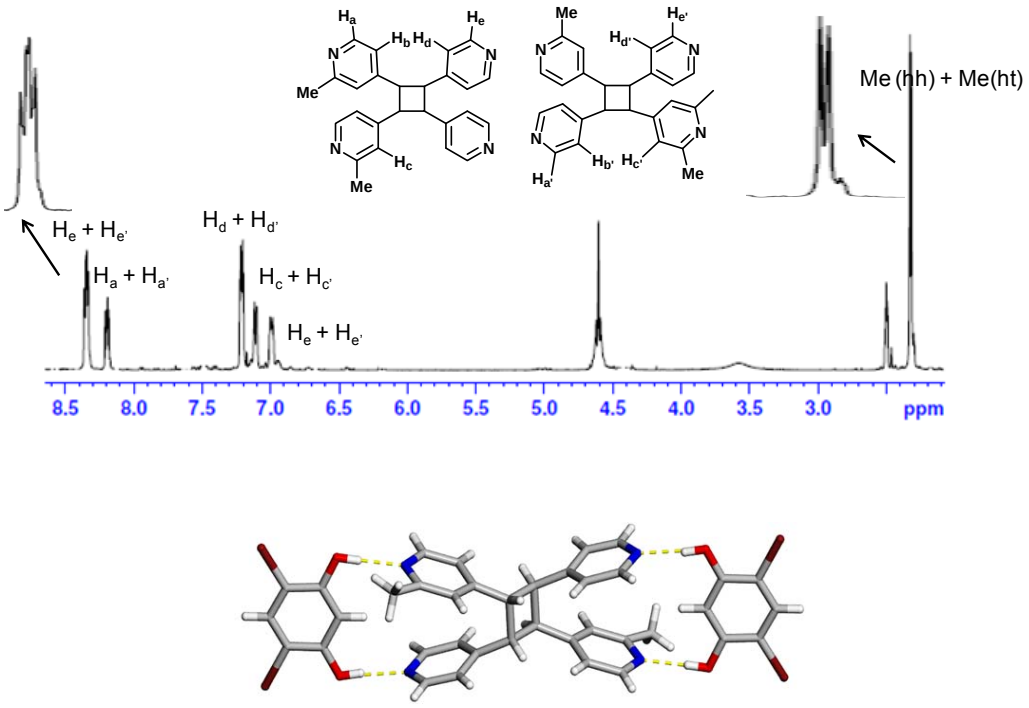

Figure 41. a) ^{1}H NMR spectrum of MPyPyCB, and b) single crystal structure of 2(4,6-diBr-res)·(MPyPyCB).

CPyPyE was synthesized *via* Heck coupling reaction between 2-chloro-4-iodopyridine and 4-vinylpyridine. The molecule was observed to be photoactive as a pure solid with photoconversion upto 80%. When co-crystallized with resorcinol from nitromethane as solvent, colourless needles appeared by slow evaporation. The ^{1}H NMR spectroscopic studies show the presence of both components and their 1:1 stoichiometry in the crystal. When UV-irradiated, however, the co-crystal remained photostable even after prolonged

irradiation (*i.e.,* 72 h). The single crystal structure of (res)·(CPyPyE) (Figure 42) shows the formaton of a 1D hydrogen-bonded polymeric chain consisting of res and CPyPyE sequencially in the chain, unlike discrete assemblies observed for (res)·(4,4'-bpe) and (res)·(MpyPyE). The resorcinol OHs adopted an *anti-anti* conformation to form hydrogen bonds with pyridine nitrogen atoms. The nearest olefinic distance between two neighbouring polymeric chains is 8.05 Å, explaining the photostability of the co-crystal.

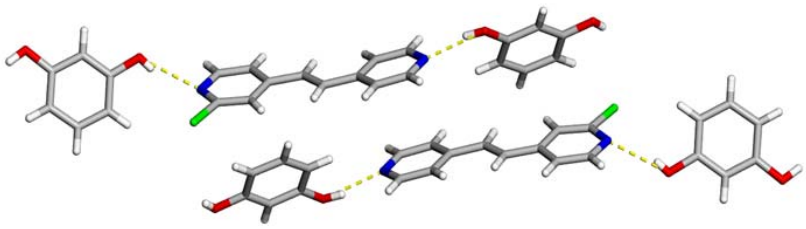

Figure 42. 1D hydrogen-bonded polymer of (res)·(CpyPyE).

Template-switching strategy was exploited in order to obtain photoactive assembly with desired quantitative photoconversion efficiency. When CPyPyE was co-crystallized with 4,6-di^{t}Bu-res from nitromethane, yellow co-crystals of (4,6-ditBu-res)·(CPyPyE) appeared upon slow evaporation of the solvent. The co-crystals, when allowed to react under broadband UV-irradiation, lead to quantitative photoconversion. The single crystal structure analysis showed the formation of a hydrogen-bonded four component discrete assembly 2(4,6-di^{t}Bu-res)·2(CPyPyE) (Figure 43). The resorcinol OHs conform a *syn-syn* geometry to form hydrogen bonds with pyridine nitrogens. The CPyPyE molecules are stacked within the discrete assembly in a head-to-tail geometry within a distance of 4.18 Å.

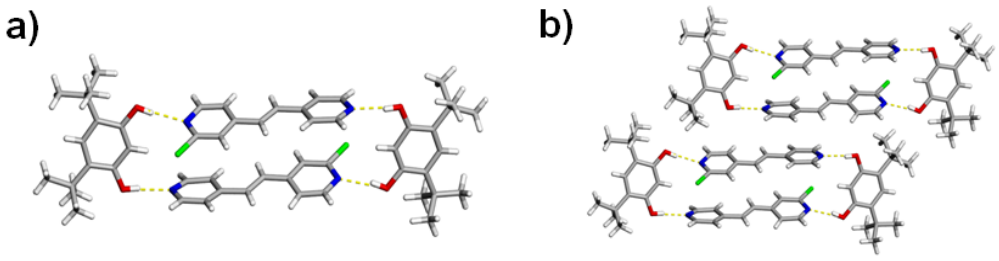

Figure 43. Four-component discrete assembly of 2(4,6-di^{t}Bu-res)·2(CPyPyE).

MPyMPyE, the methyl substituted symmetrical dipyridylethylene was synthesized in three steps. The resultant white solid was co-crystallized with the resorcinol templates using nitromethane as solvent. When co-crystallized with resorcinol, colourless prisms appeared *via* slow cooling of a supersaturated solution. The presence of both components in the crystals in 1:1 stoichiometry was confirmed by ^{1}H NMR speectroscopy. The co-crystals, when allowed to react under broadband UV-irradiation, lead to the formation of a cyclobutane product in quantitative yield as shown by the ^{1}H NMR spectroscopy. Single crystals of (res)·(MPyMPyE), suitable for single crystal X-ray diffraction, were obtained from by slow cooling of a supersaturate nitromethane solution in a period of approximately two hours. The structure showed the formation of a hydrogen-bonded discrete assembly of 2(res)·2(MPyMPyE) (Figure 44).

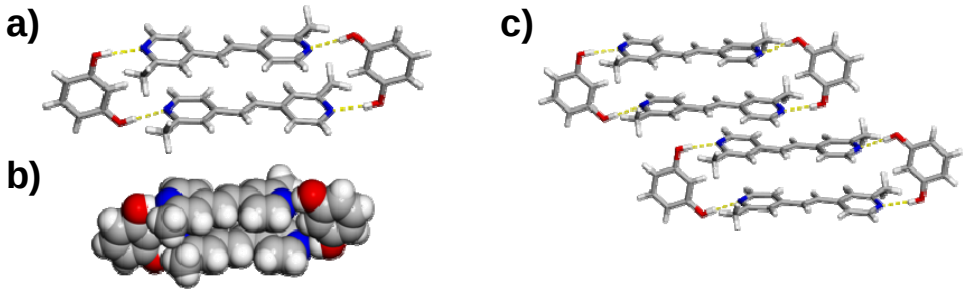

Figure 44. Single crystal structure of 2(res)·2(MPyMPyE): a) discrete assembly, b) space-filling model, and c) packing environment.

2.4 Self-assembly and photoreactivity of unsymmetrical olefins

In this part of the chapter, we will discuss the effect of substitution on the pyridine handle (*e.g.,* 4-,3-,2-) towards the self-assembly and reactivity of selected monopyridyl and bipyridyl olefins from Table 1. We will also show examples of meta substituted pyridine handles and their effect on the self-assembly process.

Table 5. Overview of the synthesized precursors with methyl and chloro substituents on the ortho and meta positions of the 4-pyridyl handle.

Position of N atom	Ortho-substituted	Position of N atom	Meta-substituted
2	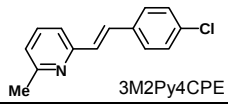 3M2Py4CPE	4	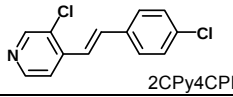 2CPy4CPE
3	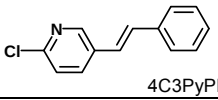 4C3PyPE	4	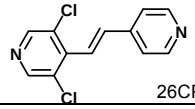 26CPyPyE
4	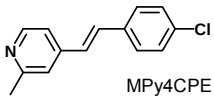 MPy4CPE		
3,4	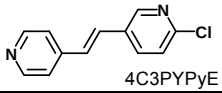 4C3PYPyE		

3M2Py4CPE: 1-(3-methyl-2-pyridyl)-2-(4-chlorophenyl)ethylene, 4**C3PyPE:** 1-(4-chloro-3-pyridyl)-2-phenylethylene, **MPy4CPE:** 1-(3-methyl-4-pyridyl)-2-(4-chlorophenyl)ethylene, 4**C3PyPyE:** 1-(4-chloro-3-pyridyl)-2-(4-pyridyl)ethylene, **2CPy4CPE:** 1-(2-chloro-4-pyridyl)-2-(4-chlorophenyl)ethylene, **26CPyPyE:** 1-(2,6-dichloro-4-pyridyl)-2-(4-pyridyl)ethylene

2.5 Experimental

2.5.1 Synthesis of 3M2Py4CPE

4-chlorobenzylbromide (2.5 g, 12.5 mmol) and triethylphosphite (2 g, 12.5 mmol) was refluxed for 12 hours. The light yellow oil was distilled under vacuum to get 2 g of diethyl(4-chloro-3-pyridinyl)methylphosphonate as a colourless oil (Yield = 78%). A mixture of 6-methyl-2-pyridinecarbaldehyde (2.0 g, 16.67 mmol), diethyl(4-chlorophenyl)methylphosphonate (4.36 g, 16.67 mmol), and ^{t}BuOH (2 mL) was cooled in an ice bath. ^{t}BuOK (2.46 g, 22 mmol) was added slowly with vigorous stirring. The solution was allowed to warm up to room temperature and allowed to stir for another four hours. The reaction mixture was poured in ice cold water (100 mL). The white precipitate of 3M2Py4CPE (3.5 g, yield = 92%) was filtered under vacuum, washed with excess water, and air-dried. ^{1}H NMR (DMSO, δ/ppm): 7.70-7.60 (4H, m), 7.45 (2H, d), 8.64 (2H, d), 7.29 (2H, m), 7.13 (1H, d), 2.50 (3H, s). ^{13}C NMR (DMSO, δ/ppm): δ 157.7, δ 153.9, δ 136.9, δ 135.4, δ 132.5, δ 130.1, δ 129.1, δ 128.7, δ 128.6, δ 121.9, δ 119.6.

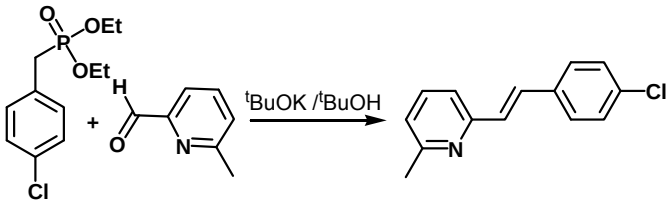

Figure 45. Synthesis of 3M2Py4CPE.

2.5.2 Synthesis of Diethyl (4-chloro-3-pyridinyl)methyl phosphonate

4-chloro-3-pyridinyl)methyl chloride (2 g, 12.5 mmol) and triethylphosphite (2 g, 12.05 mmol) was refluxed for 12 hours. The red oil compound was distilled under vacuum to get 3 g of diethyl(4-chloro-3-pyridinyl)methylphosphonate as a colourless oil (Yield = 91%).

2.5.3 Synthesis of 4C3PyPE

A mixture of benzaldehyde (2 g, 18.86 mmol), diethyl(4-chloro-3-pyridinyl)methylphosphonate (4.9 g, 18.86 mmol), and ^{t}BuOH (2 mL) was cooled in an ice bath. ^{t}BuOK (2.46 g, 22 mmol) was added slowly with vigorous stirring. The solution was allowed to warm up to room temperature and allowed to stir for another four hours. The reaction mixture was poured in ice cold water (100 mL). The white precipitate of 4C3PyPE was filtered under vacuum, washed with excess water, and air-dried (3.5 g, yield = 87%). ^{1}H NMR (DMSO, δ/ppm): 8.60 (1H, d), 8.12 (1H, dd), 7.71 (2H, d), 7.52 (1H, d), 7.46-7.37 (3H, m), 7.31 (1H, t), 7.28 (1H, d). ^{13}C NMR (DMSO, δ/ppm): δ 148.6, δ 148.2, δ 136.4, δ 136.1, δ 132.3, δ 131.3, δ 128.7, δ 128.2, δ 124.2, δ 123.5.

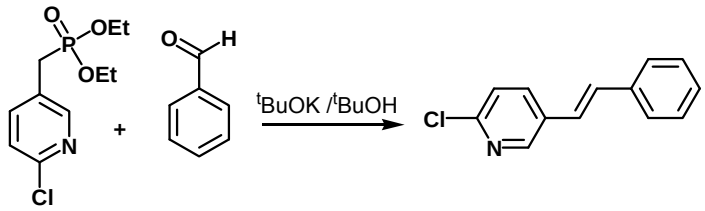

Figure 46. Schematic for the synthesis of 4C3PyPE.

2.5.4 Synthesis of MPy4CPE

A mixture of 2-methyl-4-pyridinecarbaldehyde (2 g, 16.67 mmol), diethyl(4-chlorophenyl)methylphosphonate (4.8 g, 18.34 mmol), and ^{t}BuOH (2 mL) was cooled in an ice bath. ^{t}BuOK (2.46 g, 22 mmol) was added slowly with vigorous stirring. The solution was allowed to warm up to room temperature and allowed to stir for another four hours. The reaction mixture was poured in ice cold water (100 mL). The white precipitate of MPy4CPE (3.5 g, yield = 89%) was filtered under vacuum, washed with excess water, and air-dried. ^{1}H NMR (DMSO-d_6, δ/ppm): 8.41 (1H, d), 7.65 (2H, d), 7.52-7.40 (4H, m), 7.34 (1H, d), 7.21 (1H, d).

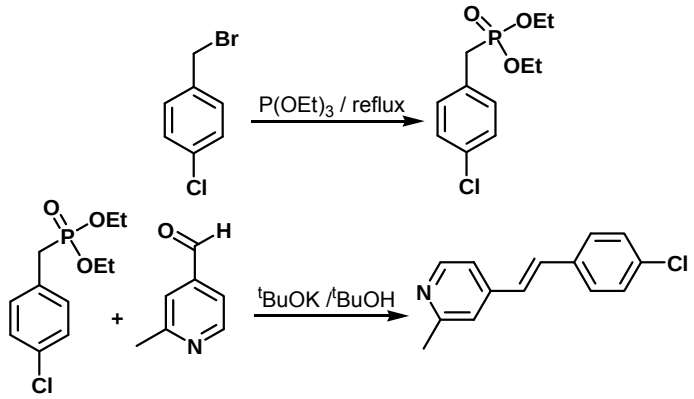

Figure 47. Schematic for the synthesis of MPy4CPE.

2.5.5 Synthesis of 4C3PyPyE

A mixture of 4-pyridinecarbaldehyde (2 g, 18.34 mmol), diethyl(4-chloro-3-pyridinyl)methylphosphonate (4.8 g, 18.34 mmol), and ^{t}BuOH (2 mL) was cooled in an ice bath. ^{t}BuOK (2.46 g, 22 mmol) was added slowly with vigorous stirring. The solution was allowed to warm up to room temperature and allowed to stir for another four

hours. The reaction mixture was poured in ice cold water (100 mL). The turbid solution was allowed to stand for two hours when a white precipitate of 4C3PyPyE appeared. The solid was filtered under vacuum, washed with excess water, and air-dried (3.5 g, yield = 89%). ^{1}H NMR (DMSO, δ/ppm): 8.65 (1H, d), 8.58 (2H, d), 8.64 (2H, d), 8.19 (1H, dd), 7.61-7.55 (4H, m), 7.43 (1H, d). ^{13}C NMR (DMSO, δ/ppm): δ 150.1, δ 149.6, δ 148.7, δ 143.5, δ 136.7, δ 131.5, δ 128.8, δ 128.1, δ 124.4, δ 120.9.

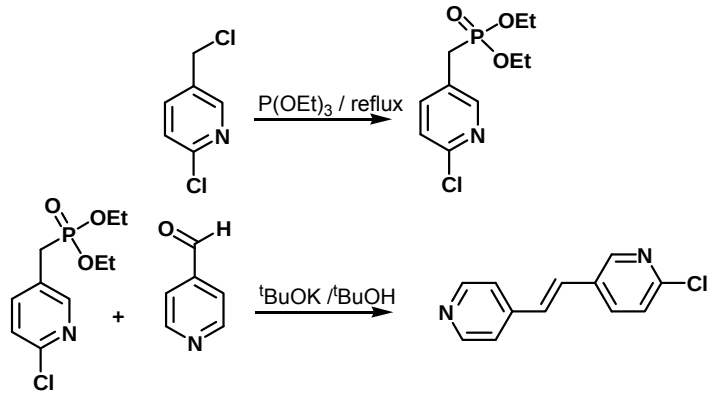

Figure 48. Schematic for the synthesis of 4C3PyPyE.

2.5.6 Synthesis of 2CPyPyE

A mixture of 3-chloro-4-pyridinecarbaldehyde (2.56 g, 18.34 mmol), diethyl(4-chlorophenyl)methylphosphonate (4.8 g, 18.34 mmol), and ^{t}BuOH (2 mL) was cooled in an ice bath. ^{t}BuOK (2.46 g, 22 mmol) was added slowly with vigorous stirring. The solution was allowed to warm up to room temperature and allowed to stir for another four hours. The reaction mixture was poured in ice cold water (100 mL). The white precipitate of 2CPyPyE (3.5 g, yield = 70%) was filtered under vacuum, washed with excess water, and air-dried.

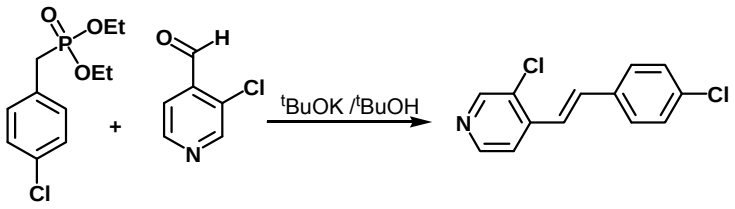

Figure 49. Schematic for the synthesis of 2CPPyPyE.

2.5.7 Synthesis of 26CPyPyE

3,5-dichloro-4-iodopyridine (3.18 g, 11.7 mmol) and freshly distilled 4-vinylpyridine (1.3 g, 12.6 mmol) was added to 150 mL of saturated aqueous K_2CO_3 solution. To the solution dichlorobis-(triphenylphosphine)palladium(II) (0.35 g, 5.12 mmol) and triethylamine (1 mL) was added and the solution was refluxed for three days. The solution was cooled down to room temperature and extracted with dichloromethane. The organic layer was washed with water and dried by Na_2SO_4. The solvent was evaporated in a rotor-evaporator to leave a tan solid. The solid was recrystallized from acetonitrile to yield a white solid of 26CPyPyE (2 g, 88%).

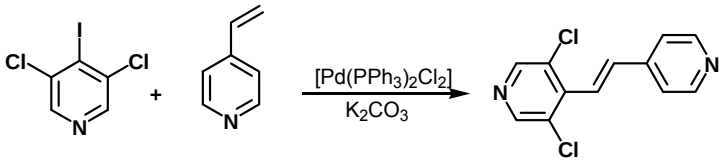

Figure 50. Schematic for the synthesis of 26CPyPyE.

2.6 Results and Discussion

In this section, self-assembly and photoreactivity of olefins of Table 4 with *ortho*- and *meta*- substituted pyridine handle will be described. General and crystallographic parameters for the co-crystals before and after photodimerization are given in Appendix A, Tables A5-A9. The solids which will be described in this part, are shown in Table 6.

Table 6. Structural formulas of the solids discussed in second part of Chapter 2.

(4,6-diI-res)·2(3M2Py4CPE)	(4,6-ditBu-res)(hh-MPy4CPCB)	(res)·(4C3PyPyE)
2(AgClO3)·4(4C3PyPE)	4C3PyPyE	(res)(4C3PyPyCB)
$2(AgClO_3)$· 2(4C3PyPE)· 2(4C3PyPCB)	(res)·(4C3PyPyE),	2(res)·2(MPyMPyE)
(4,6-diI-res)·2(MPy4CPE)	(4-hex-res)·(4C3PyPyE).	(res)·2(2CPy4CPE)
(5-OMe-res)·2(MPy4CPE)	(4-dodec-res)·(4C3PyPyE)	(5-OMe-res)·2(2CPy4CPE)
		(4,6di^{t}Bu-res)·2(26CPyPyE)

When 3M2Py4CPE was co-crystallized with resorcinol templates from nitromethane, co-crystals were formed with 1:2 stoichiometry (template: olefin). When UV-irradiated, photodimerized with quantitative photoconversion. Single crystal structure analysis of (4,6-diI-res)·2(3M2Py4CPE) showed that two 3M2Py4CPE molecules were oriented head-to-head within a distance of 3.93 Å where resorcinol HOs formed hydrogen bond with pyridine. Even with sterically constrained pyridine group, there was no apparent effect on the hydrogen-bonding ability. Surprisingly, the methyl

groups on the pyridine ring pointed at the same direction as observed for other methyl substituted olefins described before.

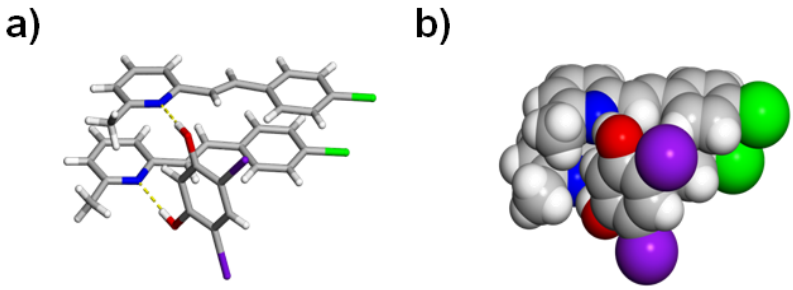

Figure 51. Single crystal structure of (4,6-diI-res)·2(3M2Py4CPE): a) wireframe, and b) space-filling model.

Attempt to co-crystallize 4C3PyPE with resorcinol templates was not successful. Probably the decreased pKa value of pyridine ring disfavour the formation of hydrogen bonds. When co-crystallized with silver salts from acetonitrile, resulted reactive co-crystals. When 4C3PyPE was co-crystallized with $AgClO_3$ in a 1:1 stoichiometric ratio from acetonitrile, colourless block-like crystal appeared after two days *via* slow evaporation of the solvent. When UV-irradiated the complex photodimerized upto 50% yield. Interestingly, the complex photodimerized in both powder and single crystal form. Even when the single crystals of the complex were irradiated seven days, no significant crystal failure was observed. The single crystal structure showed that a dinuclear discrete complex $2(AgClO_3)\cdot4$(4C3PyPE) formed (Figure 52). The chlorate ions coordinated to both silver atoms placed 4.89 Å apart from each other. Each silver atom was tetracocordinated by two chlorate oxygens and two pyridines form 4C3PyPE molecules. Two 4C3PyPE molecules of the discrete complex was planar where as the other two molecules were nonplanar with 48.2° angle of twist. As the distance between the olefins within the complex was 6.50 Å, it was assumed not to undergo reaction within assembly.

The crystal packing showed that the planar 4C3PyPE molecules were stacked head-to-tail with another 4C3PyPE molecule from the neighbouring assembly and this motif is repeated along the crystallographic b-axis. The photodimerization between the planar molecules would result in the cyclobutane product formation upto 50% yield, as seen from the ^{1}H NMR studies. Thus, photodimerization of the complex was expected to yield a 1D coordination polymer with cyclobutane in the main chain.

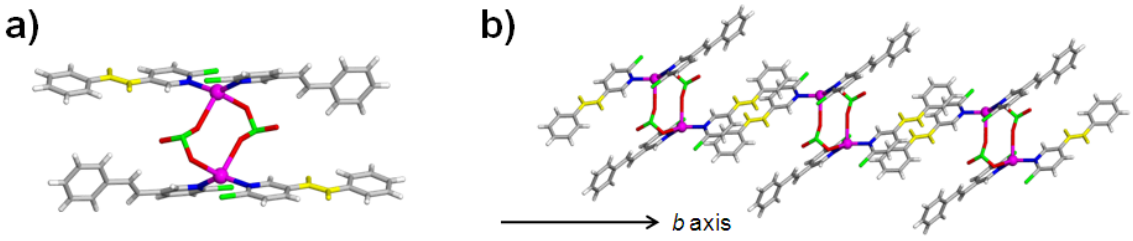

Figure 52. Single crystal structure of 2($AgClO_3$)·4(4C3PyPE): a) discrete assembly, and b) crystal packing environment along crystallographic *b* axis.

[2+2]Photopolymerization in solid state has been a topic of active research for the last few decades.[61] Photopolymerization in solid state often result in highly stereoregular polymer with extensive chemical control.[62] The reaction was also of importance to understand the underlying princicples and mechanisms in topochemical photoreaction conducted in solid state.[35] Photopolymerization of diolefins (*e.g.,* 2,5-distyrylpyrazine) is one of the principal way to conduct photopolymerization in solid state.[63] In summery, photopolymerization has only been studied involving pure organic solids while the photoproduct could not be characterized by single crystal X-ray crystallography. In this context, incorporation of metals in the product is often desirable to incorporate additional important properties (e.g, colour, magnetism, optical).[64] Additionally, the formation of higher dimensional materials is also of importance for materials with high stability. In this case, the formation of a 1D coordination polymer formation was expected from a 0D

metal-organic assembly, where the monoolefin is acting as a potential diolefin *via* coordination bond formation with silver. The single crystal structure of the irradiated crystal showed that a 1D coordination polymer formed with cyclobutanes in the main chain $2(AgClO_3)\cdot 2(4C3PyPE)\cdot 2(4C3PyPCB)$ (Figure 53), as initially expected. The non-planar 4C3PyPE did not undergo photodimerization, where the planar 4C3PyPE molecules formed a head-to-tail photodimer and as a result, the coordination environment of the silver ions did not change.

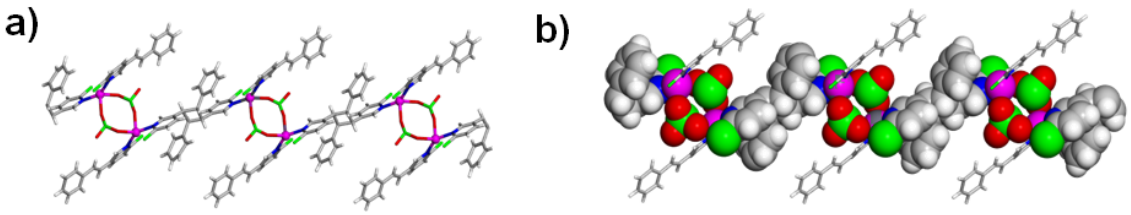

Figure 53. 1D metal-organic polymer of $2(AgClO_3)\cdot 2(4C3PyPE)\cdot 2(4C3PyPCB)$: a) wireframe representation, and b) space-filling model highlighting the silverchlorate and cyclobutanes.

Thus, a SCSC photopolymerization was successfully carried out within a metal-organic complex and the product was characterized by single crystal X-ray diffraction, for the first time.

When co-crystallized with resorcinol templates, MPy4CPE formed co-crystals with 1:2 stoichiometry (template:olefin). When (4,6-diI-res)·2(MPy4CPE), and (5-OMe-res)2(MPy4CPyE) were UV-irradiated as described before, quantitative transformation to cyclobutane products were obtained in 3-5 days. The single crystal structure analysis of (4,6-diI-res)·2(MPy4CPE) (Figure 54a) showed a three component hydrogen-bonded discrete assembly. The olefins were stacked head-to-head within a distance of 3.92 Å. The methyl groups were pointed at the same direction, as observed before, within a

distance of 4.10 Å. The distance of olefinic groups is 4.01 Å, where the MPy4CPE molecules were oriented head-to-tail. The single crystal structure of (5-OMe-res)·2(MPy4CPE) (Figure 54b) showed a three component discrete hydrogen-bonded assembly as before. The MPy4CPE molecules are oriented in a head-to-head fashion where the olefinic double bonds are stacked within a distance of 3.79 Å. The nearest distance of olefins in between assemblies is 3.73 Å, where the molecules are oriented head-to-tail.

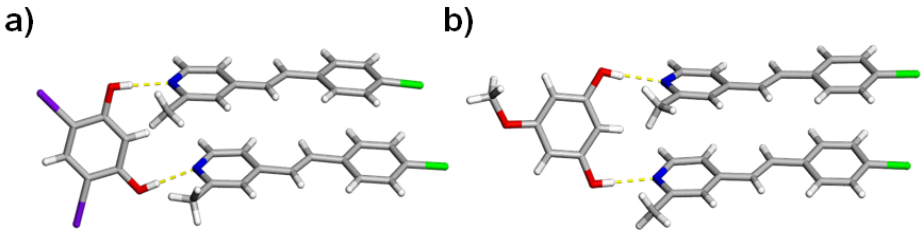

Figure 54. Single crystal structure: a) (4,6-diI-res)·2(MPy4CPE), and b) (5-OMe-res)·2(MPy4CPE).

Although the packing motif suggests the possibility of forming both head-to-head and head-to-tail photodimer, only one product formation was observed in the ^{1}H NMR spectroscopic analysis. In reacting within assembly, the formation of head-to-head photodimer, namely, *rctt*-1,2-bis-(3-methyl-4-pyridyl)-3,4-bis-(4-chlorophenyl)cyclobutane (hh-MPy4CPCB) was expected. The template (*i.e.,* 5-OMe-res) was removed from the photoreacted powder *via* base extraction, and the photodimer was co-crystallized from various other resorcinols in order to characterize the photoproduct *via* single crystal X-ray diffraction in the form of a co-crystal. When co-crystallized with 4,6-di^{t}Bu-res from nitromethane, the photodimer formed colourless prism like co-crystals in a 1:1 stoichiometry, as confirmed by ^{1}H NMR spectroscopy, suitable for single crystal X-ray diffraction. The single crystal structure analysis showed

the formation of (4,6-di^{t}Bu-res)(hh-MPy4CPCB) (Figure 55) as a two component hydrogen-bonded discrete assembly. The head-to-head geometry of the photoproduct supports the possibility of reaction between olefins within the assembly rather than in between.

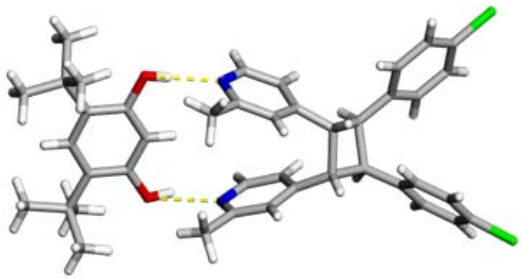

Figure 55. Single crystal structure of (4,6-ditBu-res)(hh-MPy4CPCB.

In order to study the self-assembly and photoreactivity of the unsymmetrically substituted bispyridylethylene, 4C3PyPyE was synthesized. When, UV-irradiated as a pure solid, 4C3PyPyE formed a cyclobutane derivative upto quantitative yield. The single crystal structure analysis of 4C3PyPyE (Figure 56) showed that the nearest olefins are placed head-to-tail within a distance of 3.73 Å, supporting the observed photodimerization reaction in solid state.

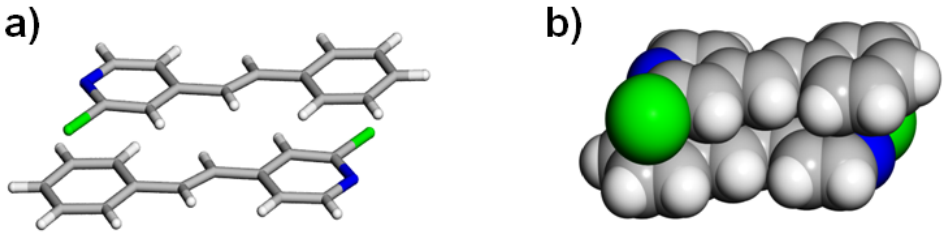

Figure 56. Single crystal structure of 4C3PyPyE: a) wireframe representation, and b) space-filling model.

With the assumption that both pyridines would form hydrogen bonds with resorcinols, 4C3PyPyE was co-crystallized with resorcinols in 1:1 stoichiometric ratio. The co-crystals obtained were also in a 1:1 stoichiometric ratio but remained photostable even after prolonged period UV-irradiation. In order to study the assembly process, the single crystal X-ray diffraction analysis of (res)·(4C3PyPyE) was carried out. The crystal structure showed that only unsubstituted pyridine handle is forming hydrogen bonds with resorcinol OHs, where as the chloro-substituted pyridine handle does not form hydrogen bond (Figure 57a). The preferential formation of hydrogen bond with unsubstituted pyridine can be explained by both sterical accessibility and higher hydrogen-bonding strength. The second OH group the resorcinol molecule is engaged in forming hydrogen bond with the neighbouring resorcinol. The above hydrogen bonding environment led to the formation of a 1D hydrogen bonded staircase-like structure. The hydrogen bonded resorcinols formed the central column, where as the hydrogen bonded 4C3PyPyE molecules formed the stairs on both sides of the column. The nearest distance between the olefins is 4.49 Å, and explains the photostability of the co-crystal. In order to engage the chloro-substituted pyridine in hydrogen-bonding, excess resorcinol was used (*e.g.,* 2 equivalent) during co-crystallization experiments. When co-crystallized with two equivalent of 4-hexyl-resorcinol (4-hex-res) from nitromethane, (4-hex-res)·2(4C3PyPyE) was formed as confirmed by the ^{1}H NMR spectroscopy, but remained photostable. The single crystal structure of (4-hex-res)·2(4C3PyPyE) (Figure 57b) showed that both pyridines are forming hydrogen bond with resorcinol to form a 1D chain. Each resorcinol OH was in a *syn-anti* conformation to form hydrogen bond with unsubstituted pyridine and chloro substituted pyridines of two different 4C3PyPyE molecules. The nearest 4C3PyPyE molecules are oriented in a head-to-tail fashion within a distance of 7.02 Å, explaining the photostability.

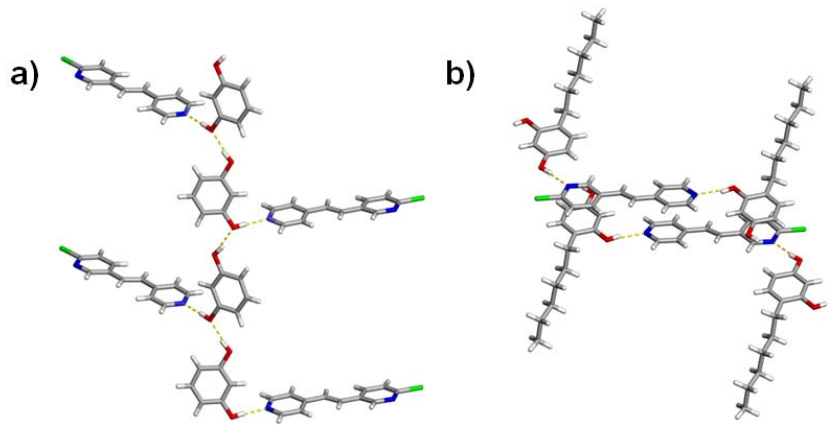

Figure 57. Single crystal structure of: a) (res)·(4C3PyPyE), and b) (4-hex-res)·(4C3PyPyE).

Thus, use of resorcinol in a 1:2 (res: olefin) stoichiometry, would potentially lead to the formation of selective hydrogen bonds between resorcinol and unsubstituted pyridine given the higher pKa value of unsubstituted pyridine ring. When two equivalent 4C3PyPyE was co-crystallized with one equivalent of resorcinols lead to co-crystals with 2:1 stoichiometry. The 2:1 co-crystal of 4C3PyPyE with 4-dodecyl-resorcinol (4-dodec-res) led to partial phtoreaction (ca. 50%) under uv-irradiation. The single crystal of (4-dodec-res)·2(4C3PyPyE) (Figure 58a) shows the formation of a three component hydrogen-bonded discrete assembly where 4C3PyPyE molecules are stacked head-to-head within 3.67 Å. Only unsubstituted pyridines formed hydrogen bonds with resorcinol OHs, as expected.

When 4C3PyPyE was co-crystallized with res in a 2:1 stoichiometric ratio from nitromethane, colourless needles were formed upon slow evaporation of the solvent. The 2:1 stoichiometry of the components was confirmed by ^{1}H NMR spectroscopy. When the powder of the material was UV-irradiated, quantitative formation of cyclobutane was observed. The single crystal structure analysis of (res)·2(4C3PyPyE) (Figure 58b) showed similar discrete three component assembly observed in the case of (4-dodec-

res)·(4C3PyPyE). The distance between the olefinic groups within the assembly is 3.71 Å. The 4C3PyPyE molecules are also oriented head-to-head in between assemblies within a distance of 3.95 Å.

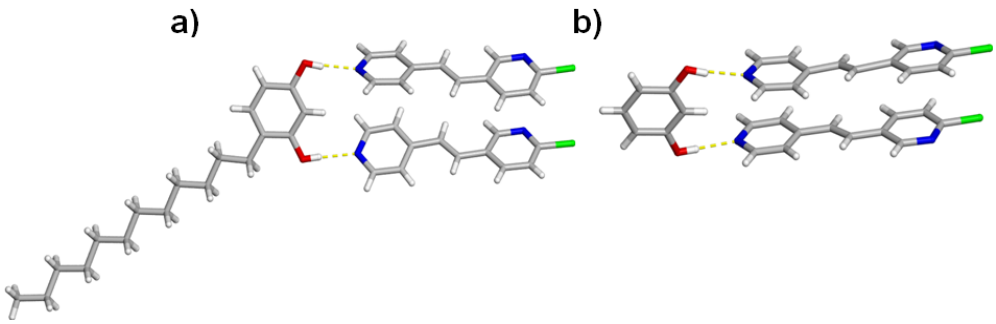

Figure 58. a) Single crystal structure of a) (4-dodec-res)·2(4C3PyPyE), and b) (res)·2(4C3PyPyE) .

The photoreacted material was co-crystallized from nitromethane in order to characterize the geometry of the photodimer. The single crystal structure of the head-to-head photodimer, namely rctt-1,2-bis-(4-chloro-3-pyridyl)-3,4-bis-(4-pyridyl)cyclobutane (4C3PyPyCB) (Figure 59), with res showed that only unsubstituted pyridines were engaged in forming hydrogen bonds. The pyridine nitrogen atoms on the chloro substituted pyridines were oriented on the opposite direction.

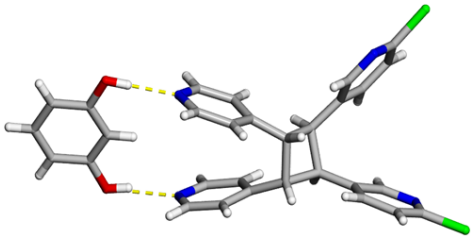

Figure 59. Single crystal structure of (res)(4C3PyPyCB).

In order to study the effect of substituents at the meta- positions of the pyridine handle, 2CPy4CPE, and 26CPyPyE were synthesized. The meta- substitution, by virtue of its position, is not only close to the hydrogen-bonding site, but also close to the reaction site (*i.e.,* double bond). When 2CPy4CPE was co-crystallized with resorcinols, lead to co-crystals with 2:1 stoichiometry (resorcinols: olefin). The photoreaction experiments were carried out as previously described. When co-crystallized with res and 5-OMe-res from nitromethane, colourless co-crystals were obtained by slow evaporation of the solvent. The olefins in the co-crystals reacted to form cyclobutane product upto quantitative yield as confirmed by ^{1}H NMR spectroscopy. Single crystal structure of (res)·2(2CPy4CPE) (Figure 60a) showed the formation of a three component hydrogen-bonded discrete assembly. The olefins form a head-to-head assembly and stacked within a distance of 3.66 Å. The chlorine substituents are pointed at the same direction. In the neighbouring assemblies, 2CPy4CPE molecules are slipped stacked head-to-head within a distance of 4.79 Å. In the single crystal structure of (5-OMe-res)·2(2CPy4CPE) (Figure 60b), the olefins are stacked head-to-head within a distance of 3.92 Å. In the neighbouring assemblies, the olefins are oriented head-to-tail within a distance of 6.52 Å.

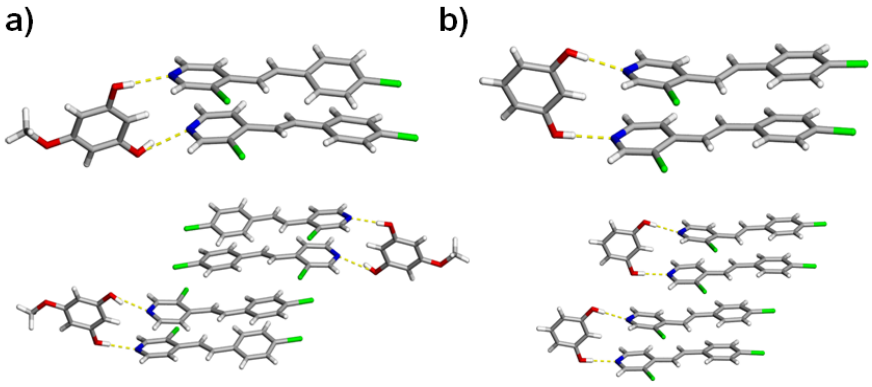

Figure 60. Discrete assembly and crystal packing: a) (res)·2(2CPy4CPE), b) (5-OMe-res)·2(2CPy4CPE).

26CPyPyE was synthesized by Heck coupling reaction between 3,5-dichloro-4-iodopyridine and 4-vinylpyridine using Pd(II) as catalyst. When crystallized with resorcinol templates, co-crystals were formed with 1:1 stoichiometry but remained photostable under UV-irradiation. Single crystal structure analysis of (4,6-diI-res)(26CPyPyE) (Figure 61) showed that a discrete four component hydrogen-bonded assembly was formed consisting of two 4,6-diI-res and two 26CPyPyE molecules. The olefins were oriented head-to-head within a distance of 4.82 Å. It was also observed that, the olefins were nonplanar, where the interplanar angle between the 3,5-dichloro pyridine moiety and the unsubstituted pyridine is 88.4° and 48.3°, respectively. The increased degree of twist of 26CPyPyE in the co-crystal was due to crystal packing environment. In the planar structure, the distance between the chloro substituents and the olefinic protons were 2.49 Å and 2.54 Å, respectively whereas the sum of their van der Waals radius is 2.95 Å. Thus, in order to avoid the steric crowding between them, the olefinic carbons and the unsubstituted pyridine ring are twisted with respect to the plane of dichloro substituted pyridine ring. In fact, structural analysis of the assembly shows that the dichloro substituted pyridine rings within the assembly is coplanar whereas the interplanar angle between the unsubstituted pyridines is 43.1°, and thus responsible for the increased distance between the olefinic double bonds and photostability of the co-crystal.

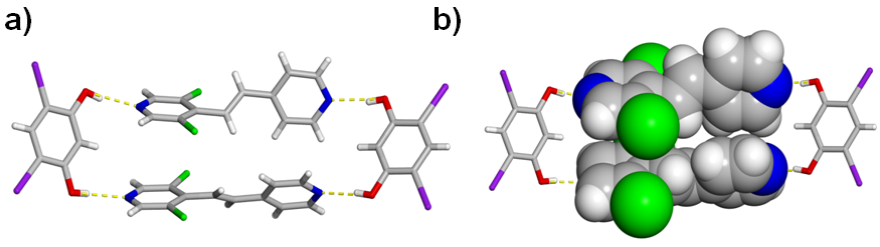

Figure 61. Single crystal structure of (4,6-di^{t}Bu-res)·2(26CPyPyE): a) wireframe representation, and b) space-filling model.

2.7 Conclusion

In conclusion, inherent modularity and synthetic versatility of template-directed solid state synthesis has been successfully demonstrated by self-assembling and reacting olefins with modified pyridine handles. The substituents at the ortho as well as meta position, apparently does not affect the Hydrogen bond formation. Specifically, olefins with both ortho and meta- substituted pyridines have been successfully photodimerized. This is the first systematic study towards the generality of the templated solid state synthesis. Interestingly, dichloro substitution at the meta- position of a pyridine handle did not undergo photodimerization under any experimental condition. The photostability of the olefin was ascribed to the nonplanar geometry of the molecule rather than the lack of suitable self-assembly formation. Thus, this example can be thought as a upper limit of the templated synthesis and [2+2]photodimerization reaction in general, where the geometry of the molecule disfavors the reaction.

CHAPTER 3: SUPRAMOLECULAR CONSTRUCTION OF A COFACIAL TEMPYRIDINE IN SOLID STATE

3.1 Introduction

In multielectron redox enzymes, several metals are generally involved in both substrate binding and the subsequent redox reactions.[65] Thus, functional mimics of multielectron redox enzymes also involve two or more metal centers to be efficacious in terms of increased substrate binding, reactivity and stereoselectivity. Cofacial molecules, because of the control they provide over the geometric and electronic properties of the synthetic reaction center, are ideal bimetallic model complexes. Thus, molecules with π-surfaces in cofacial geometries are of fundamental interest in the chemical sciences.[66] Such molecules are used to assemble metal ions and/or small molecules in close proximity (*i.e. ca* 3 to 7 Å) in order to mimic the behaviors of metals in biological settings, provide geometries for catalysis, and serve as platforms for molecular recognition and coordination-driven self-assembly. Rigid organic spacer molecules are often used to place organic π-surfaces in cofacial geometries (Figure 62).

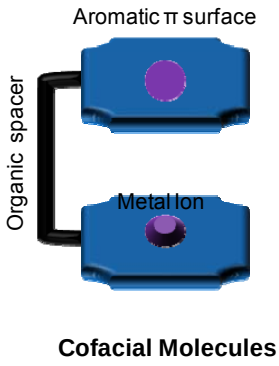

Figure 62. Schematic of cofacial geometry.

Spacers in the form of xylenes, anthracenes, biphenylenes, xanthenes, and amides have all been used as backbones to covalently fix π-surfaces such as porphyrins, pyridines, and other macrocyclic and heteroaromatic functionalities in closed stacked arrangements.[67] Specifically, cofacial diporphyrin with a variety of spacers have been synthesized and studied over the last few decades for their catalytic activities and roles in small molecule activation (*e.g.,* O_2 and N_2 reduction). However, the synthesis of molecules with cofacial geometry is often an arduous task, typically requiring multiple steps that proceed in low overall yields.[68] For example, the cobalt complex of the anthracene pillared cofacial diporphyrin host (Figure 63a), well-known for its electrocatalytic activities, involve a six step synthetic procedure with <10% overall yield. The challenging syntheses often limit the potential applications of cofacial complexes. On the other hand, a cofacial terpyridine has been reported where the terpyridine groups, pillared by an acridine unit (Figure 63b), place two palladium(II)metal ions in cofacial geometry within close compartment (ca. 7Å).[69] The complex has been demonstrated to be a useful building block for supramolecular architectures. For example, the palladium complexes have been shown to form large molecular rectangles with a linear linker such as 4,4'-dipyridyl. Nevertheless, the synthesis of the cofacial terpyridine-based ligand involve ten steps with 10.6% overall yield.

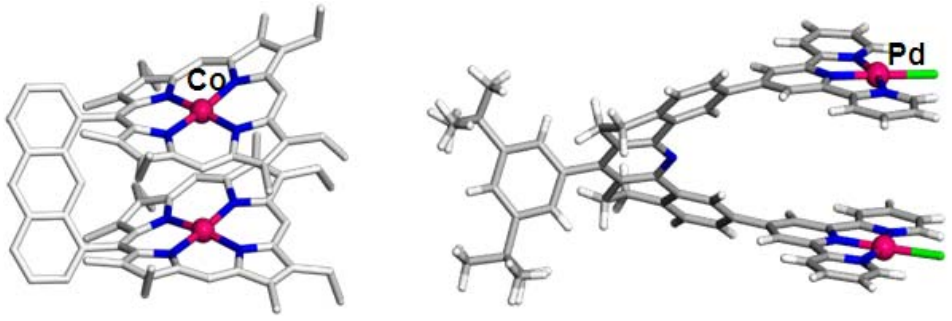

Figure 63. Single crystal structure of a) anthracene pillared cofacial diporphyrin, and b) acridine pillared cofacial terpyridine.

Terpyridine (TP), and its derivatives, has been extensively used as building blocks in the construction of functional metal complexes and supramolecular assemblies (*e.g.,* helicates, dendrimers).[70] The molecule, during the process of binding to metal-ions, rearranges from a *transoid* to *cisoid* conformation to act as a tridentate chelating ligand (Figure 64). Covalently-connected to an organic linker, TP has been exploited to control the positioning of metals in multi-component complexes and materials.[71]

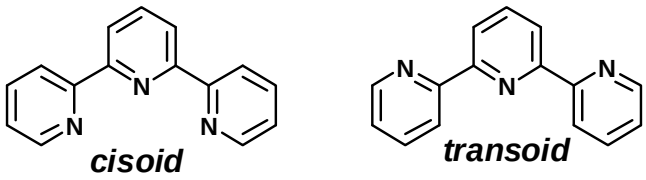

Figure 64. Conformations of terpyridine.

When two TP molecules are coordinated to a single metal ion, often give rise to a discrete, six coordinated cruciform type $[M(TP)_2]$ structure. Up to date, there are 311 $[M(TP)_2]$ cruciform structures reported in Cambridge structural data base (CSD).[72] When TP is derivatized with coordinative functionalities, it can form multidimensional coordination complexes upon binding to metal ions. TP, when derivatized with appropriate organic linkers, can form complex metal-organic assemblies (e.g. macrocycles). Planar and the structurally robust square-planar TP-metal complexes are suitable candidates for DNA intercalation (Figure 65). Thus, TP has been employed in fields ranging from supramolecular chemistry to nanoscience to catalysis.

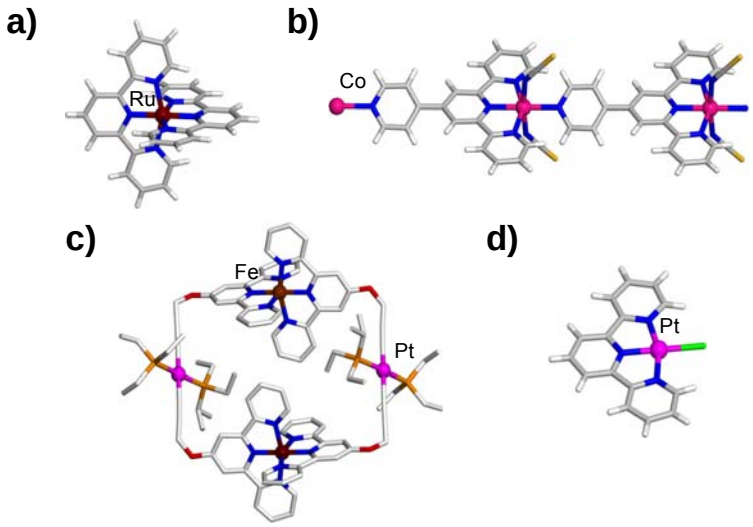

Figure 65. Crystal structures of a) cruciform motif of $[M(TP)_2]$, b) 1D metal-organic complex formed by a TP derivative, c) macrocycle formed by TP-metal complex and d) planar TP-metal complex used in DNA intercalation.

Recently, we demonstrated the supramolecular construction of ladderanes and cyclophanes in the solid state using hydrogen-bond-donor templates (*e.g.,* resorcinol). The templates direct intermolecular [2+2] photodimerizations of olefins lined with pyridyl groups. Given the success of this method to afford the synthesis of molecules from stacked olefins, we were interested to examine whether the approach can be applied to covalently fix large π-surfaces in cofacial arrangements. The cyclobutane that results from the photocycloaddition *de facto* places two pendant aromatic groups parallel and in close proximity while the templated solid-state reaction generates targeted products in a single step, stereospecifically, quantitatively, and in gram amounts.[38] Although TP has three hydrogen bond acceptor pyridine functionalities, hydrogen-bonded assemblies involving TP have never been studied before. The photoreactivity of TP derivatives in solid as well as in liquid state also remains unexplored. We also note that the two atoms that make the double bond represent 7.7% of the total non-hydrogen atoms present in the olefin.[73] From the statistical standpoint it is reasonable to suggest that a crystallization of

such a relatively large molecule, a molecule of increasing size, would likely disfavour the double bond conforming to the strict geometric criteria of Schmidt for reaction. If successful, the application of our templated synthetic approach on TP derivatives will be a triumph of organic synthesis in solid state in general, given the increased complexity of the reactant in terms of both size and conformational flexibility. With this in mind, we targeted the supramolecular construction of a cofacial in the organic solid state. We anticipated that co-crystallization of 1-([2,2':6',2'']terpyridyl)-2-phenylethylene (TPE) with a resorcinol template would afford a three-component crystalline assembly wherein two TPE molecules will be stacked in a hh geometry and *cisoid* conformation *via* two trifurcated O-H···N hydrogen bonds (Figure 66).[74] UV-irradiation of the solid would generate the corresponding cofacial head-to-head cyclobutane product, namely 1,2-bis-([2,2':6',2'']terpyridyl)-3,4-bis-(phenyl)cyclobutane (hh-TPC) stereospecifically and in up to quantitative yield.

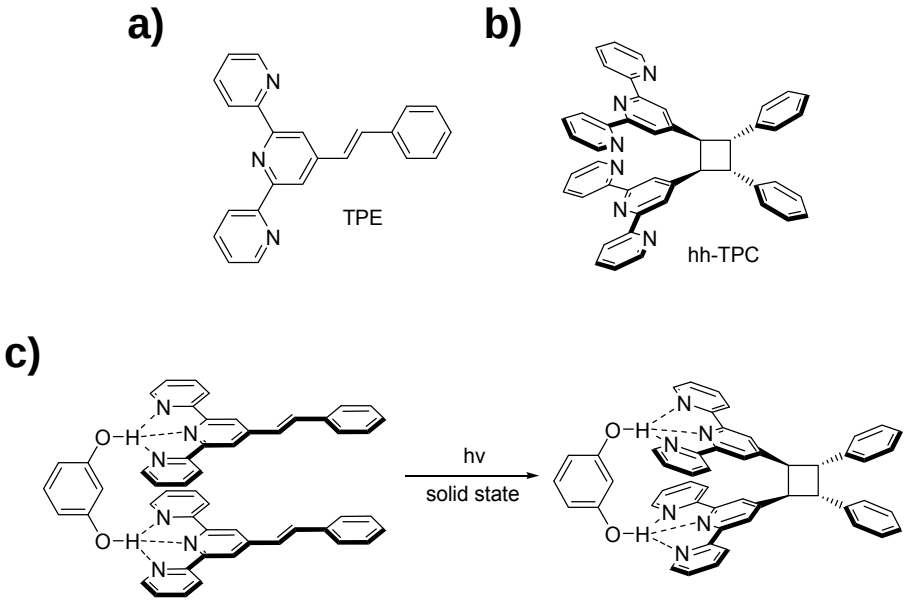

Figure 66. Schematic of (a) TPE, (b) hh-TPC, and (c) planned templated solid-state synthesis of hh-TPC.

3.2 Experimental

All reagents and solvents used were reagent grade and commercially available. methanol, nitromethane, acetonitrile, chloroform were purchased from Fisher Scientific Co. *trans*-cinnamaldehyde, iodine, 4-acetylpyridine and resorcinol were purchased from Sigma-Aldrich Chemical Company. Templates used for co-crystallization experiments (4,6-diiodoresorcinol, 4,6-dibromoresorcinol, 4-chlororesorcinol, 5-iodoresorcinol, 5-methoxyresorcinol) were made available by the synthesizing those using standard procedures reported in literature.

Single crystal X-ray diffraction experiments were performed on a Bruker-Nonius Kappa CCD diffractometer using MoKα radiation (λ = 0.7107 Å). The structures were solved using direct methods and refined by full-matrix least-squares based on F2. All non-hydrogen atoms were refined using the anisotropic model. Hydrogen atoms bonded to carbon atoms were placed in idealized positions defined by the hybridization of the belonging carbon atom. The positions of hydrogen atoms bonded to oxygen atoms were calculated so as to establish the best possible hydrogen bonds to a nearest neighbour hydrogen bond acceptor. All crystallographic calculations were performed using the set of crystallographic programs WinGX, along with SHELX-97 locally implemented on a Pentium-based PC.

3.2.1 1-(4-pyridylketo)-2-phenyl-*trans*-1,3-butadiene (**A**)

The synthesis of A was accomplished by the aldol reaction between 2-acetylpyridine and *trans*-cinnamaldehyde using NaOH as base. In a typical experiment, *trans*-cinnamaldehyde (2.0 g, 15.15 mmol) of and NaOH (2 g, 50 mmol) was dissolved in 80 ml MeOH. 4-Acetylpyridine (1.82 g, 15.15 mmol) was added to the mixture slowly and the mixture was allowed to stir at room temperature. After about 15 minutes, an yellow precipitate appeared. The solution was filtered in vacuum and the yellow

precipitate was washed with cold methanol (15 ml) to remove extra base. The resultant yellow solid (2.83 g, 80 %) was dried in air. ^{1}H NMR (DMSO-d_6, δ/ppm): 8.77 (1H, s), 8.09–8.01 (m, 2H), 7.83 (d, 2H), 7.70-7.60 (m, 4H), 7.45-7.32 (m, 4H), 7.25 (1H, d).

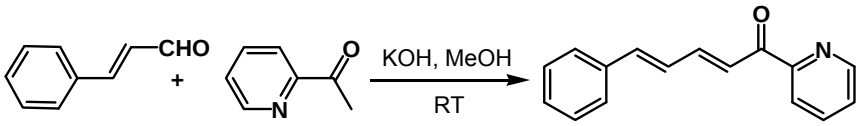

Figure 67. Schematic of the synthesis of A.

3.2.2 1-(-2-pyridinylcarbonyl)pyridinium iodide (B)

The pyridinium salt of 4-acetylpyridine (B) was synthesized by refluxing 4-acetylpyridine and iodine in pyridine. In a typical experiment, 4-acetylpyridine (10 g, 75.15 mmol) and iodine (22.9 g, 90.18 mmol) was refluxed in 50 ml pyridine for 12 hours. The solution was cooled to room temperature and the precipitate was filtered under vacuum. The black precipitate was dissolved in boiling methanol (100 mL) and activated charcoal was added. The solution was refluxed for 15 minutes and filtered while hot. Yellow crystals of B separated from the methanol solution upon standing. The crystals (27 g, quantitative) were collected by filtration and dried in air.

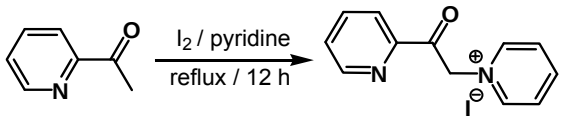

Figure 68. Schematic of the synthesis of B.

3.2.3 Synthesis of TPE

Compound A (5 g, 21.25 mmol), compound B (8.07 g, 25 mmol) and ammonium acetate (3.28 g, 42.5 mmol) were refluxed in methanol (100 ml) overnight. The solvent was rotor-evaporated, the residue was dissolved in $CHCl_3$, and washed with water. The aqueous layer was extracted with fresh $CHCl_3$. The combined organic layers were dried over Na_2SO_4 and filtered. The $CHCl_3$ solution was passed through a silica gel column and evaporated in a rotor-evaporator to give TPE (4.96 g, 70%) as light yellow solid.[75] ^{1}H NMR (DMSO, δ/ppm): 8.76 (2H, d), 8.65 (2H, d), 8.64 (2H, d), 8.03 (2H, d), 7.80 (2H, d), 7.72 (1H, d), 7.57 (1H, d), 7.53 (2H, dd), 7.44 (2H, t), 7.35 (1H, t). ^{13}C NMR (DMSO, δ/ppm): δ 155.4, δ 155.0, δ 149.2, δ 146.6, δ 137.3, δ 136.2, δ 128.7, δ 128.6, δ 127.2, 126.3, δ 124.3, δ 120.8, δ 117.6.

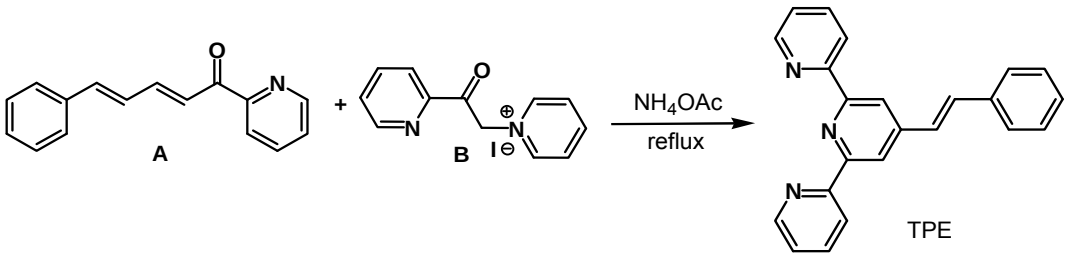

Figure 69. Schematic of the synthesis of TPE.

3.2.4 Synthesis of (triphenylphosphoranylidene)acetaldehyde

To a stirred suspension of 2-oxoethyl(triphenylphosphonium)chloride (3 g, 8.82 mmol) in 100 mL water, 1N NaOH solution (50 mL) was added slowly. The solution was stirred for two hours and filtered under vacuum. The yellow solid of

(triphenylphosphoranylidene)acetaldehyde (2.5 g, yield = 93 %) was washed with plenty of water until the pH of water becomes neutral and then air-dried.

3.2.5 Synthesis of *trans*-4-bromocinnamaldehyde

(triphenylphosphoranylidene)acetaldehyde (3.0 g g, 14.7 mmol) and 4-bromobenzaldehyde (2.72 g, 14.7 mmol) in benzene (70 mL) was refluxed overnight. The solvent was evaporated in vacuum and the yellow precipitate was recrystallized from hexane to yield yellow crystalline solid of trans-4-bromocinnamaldehyde (2.0 g) in 64 % yield.

3.2.6 1-(2-pyridylketo)-4-(4-bromophenyl)-*trans*-1,3-butadiene (pbpb)

The synthesis of pbpb was accomplished by the aldol reaction between 2-acetylpyridine and *trans*-4-bromocinnamaldehyde using NaOH as base. In a typical experiment, *trans*-cinnamaldehyde (2.0 g, 15.15 mmol) of and NaOH (2 g, 50 mmol) was dissolved in 80 ml MeOH. 4-Acetylpyridine (1.82 g, 15.15 mmol) was added to the mixture slowly and the mixture was allowed to stir at room temperature. After about 15 minutes, a yellow precipitate appeared. The solution was filtered in vacuum and the yellow precipitate was washed with cold methanol (15 ml) to remove extra base. The resultant yellow solid (2.83 g, 80 %) was dried in air. ^{1}H NMR ($CDCl_3$, 300 MHz): δ 7.00–7.18 (m, 2H), 7.27–7.46 (m, 6H), 7.64–7.78 (m, 2H), 7.70 (d, 2H), 7.65 (d, 2H), 7.56 (d, 2H).

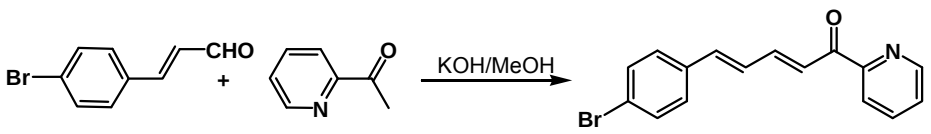

Figure 70. Schematic of the synthesis of pbpb.

3.2.7 1-([2,2':6',2'']terpyridyl)-2-(4-bromophenyl)ethylene (4BrTPE)

4BrTPE was synthesized by Krohnke reaction between B and bpeb in presence of ammonium. In a typical experiment, pbpb (2 g, 15.15 mmol) and B (2 g, 50 mmol), and excess ammonium aceate (4 g) was dissolved in 80 ml MeOH and refluxed overnight. After the solvent was evaporated in a rotor-evaporator, water was added (100 mL) and the mixture was extracted with CH_2Cl_2. The organic layer was washed with water and the solvent was dried, and evaporated to yield a yellow solid of 4-BrTPE (2.83 g, 80 %). ^{1}H NMR (DMSO, δ/ppm): 8.76 (2H, d), 8.65 (2H, d), 8.64 (2H, d), 8.03 (2H, dt), 7.75 (2H, d), 7.66 (2H, d), 7.62 (2H, dd). ^{13}C NMR (DMSO, δ/ppm): δ 155.4, δ 155.0, δ 149.1, δ 146.3, δ 137.3, 135.5, δ 131.9, δ 131.6, δ 129.1, δ 127.2, δ 124.3, δ 121.7, δ 120.8, δ 117.6.

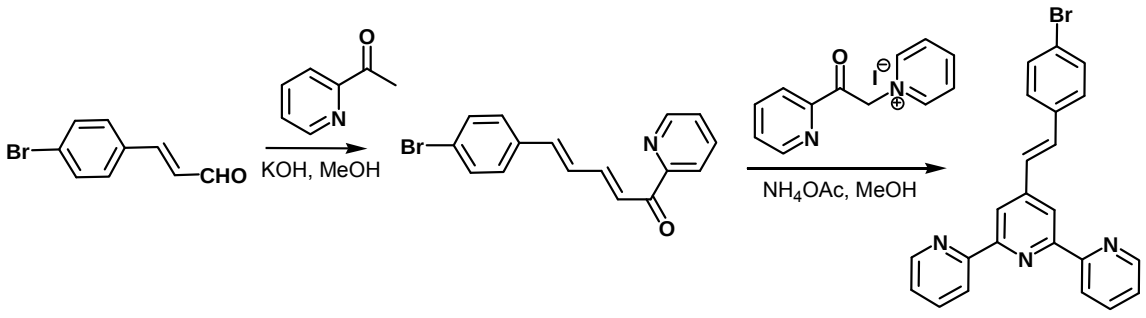

Figure 71. Synthetic Scheme of 4BrTPE.

3.2.8 Synthesis of di-2-pyridylpentane-1,3,6-trione

A solution of acetone (1.8 mL, 25 mmol) and ethyl 2-pyridinecarboxylate (10.1 mL, 75 mmol) in dry THF (50 mL) was added to a suspension of sodium hydride (95%, 1.9 g, 75 mmol) in dry THF **(**50 mL) in a nitrogen atmosphere with vigorous stirring. After about 20 minutes, a violent reaction occurred and a yellow precipitate formed. The solution was refluxed for six hours. The solvent was removed in vacuo and the remaining orange paste carefully treated with water (100 mL). The resultant orange solution was filtered through celite and the pH of the fdtrate adjusted to pH 7 by the dropwise addition of 5% acetic acid. The resultant yellow solid was collected, washed with water, and dried. After recrystallization from 95% ethanol, the triketone was obtained as small, yellow needles: 5.4 g (65%).

3.2.9 Synthesis of 2,6-di-2-pyridyl-4(1H)-pyridone

A solution of Di-2-pyridylpentane-1,3,6-trione (1.8 g, 6.76 mmol) and NH_4OAc (2 g, excess) in absolute ethanol (50 mL) was refluxed overnight. The solution was rotor-evaporated to the half of its original volume and stored at -20 °C overnight. The white crystals of 2,6-di-2-pyridyl-4(1H)-pyridone 5.4 g (yield = 65%) were filtered under vacuum, washed with ice-cold methanol, and air-dried.

3.2.10 4’-[[(trifluoromethyl)sulfonyl]oxy]-2,2':6',2"-terpyridine

A solution of 2,6-di-2-pyridyl-4(1H)-pyridone (498 mg, 2 mmol) in dry pyridine **(**5 mL) was treated slowly at 0 °C with trifluoromethanesulfonic anhydride (594 mg, 2 mmol). The resulting mixture was stirred at 0 °C (30 min), allowed to warm to room temperature (25 °C), and kept at this temperature for 48 h. It was then poured into ice-

water (50 g**)** and stirred for 0.5 h. The light-brown solid was separated, washed with cold water (50 mL), and, after drying, dissolved in hexane (15 mL), and the insoluble portion was filtered off. Concentration of the mother liquor to ca. 5 mL and cooling gave colourless, irregular prisms of the triflate: 0.53 g (70%).

3.2.11 4’-vinyl-[2,2’:6'2’’]terpyridine (VT)

A mixture of 4'-[[(trifluoromethyl)sulfonyl]oxy]-2,2':6',2"-terpyridine (1.91 g, 5 mmol), vinyltributyltin (2.22 g, 7 mmol), Et_3N (3 mL, 22 mmol), and bis(tripheny1phosphine)palladium dichloride (100 mg, 0.14 mmol) in DMF (15 mL) was stirred at 90 "C for 4 h under dry nitrogen. The reaction mixture was then diluted with icewater (100 mL), stirred for 1 h, and filtered. The light-yellow solid was washed several times with water and dried. The crude product was dissolved in diethyl ether (100 mL) and the insoluble material removed by filtration. Evaporation of the ether under reduced pressure resulted in a pale-yellow solid that was recrystallized from hexane to yield 4'-vinylterpyridine 1.1 g (yield = 86%) as colourless, irregular prisms.[76]

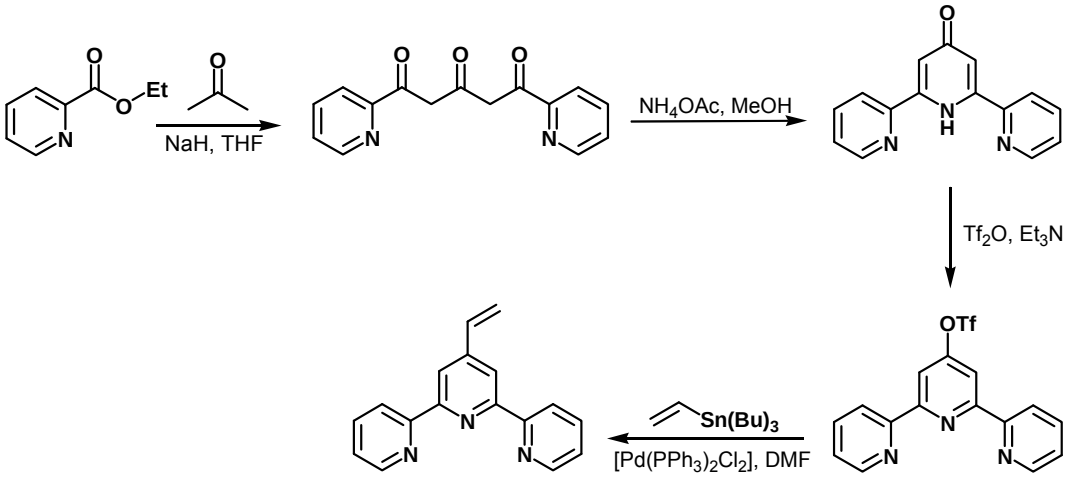

Figure 72. Schematic of the synthesis of 4’-vinylterpyridine.

3.2.12 Preparation of Co-crystals with Resorcinols

Co-crystallization experiments involving TP-based olefins and resorcinols were performed by dissolving 20 mg of the compound and calculated amount of resorcinol derivatives in 1 mL of nitromethane. The solution was allowed to slowly evaporate. After standing at room temperature overnight, the white co-crystals formed. The crystals were separated from the mother liquor by vacuum filtration and air-dried.

3.2.13 Synthesis and Characterization of (5-I-res)·(TPE)

TPE (50.0 mg, 0.15 mmol) and 5-I-res (35.4 mg, 0.15 mmol) was dissolved in 3 ml of nitromethane upon heating. The solution was filtered, and allowed to evaporate slowly at room temperature. White needle like crystals came out of the solution after 12 hours. The crystals (80 mg, yield = 93%) were separated from the mother liquor by vacuum filtration and dried in air. ^{1}H NMR (DMSO, δ/ppm): 9.62 (2H, s), 8.77 (2H, d), 8.65 (4H, d), 8.03 (2H, dt), 7.80 (2H, d), 7.72 (2H, d), 7.53 (4H, m), 7.44 (2H, t), 7.35 (1H, t), 6.55 (2H, d), 6.18 (1H, t).

3.2.14 Synthesis and Characterization of (res)·(4-BrTPE)

4-BrTPE (61.8 mg, 0.15 mmol) and 5-I-res (16.5 mg, 0.15 mmol) was dissolved in 3 ml of nitromethane upon heating. The solution was filtered, and allowed to evaporate slowly at room temperature. White needle like crystals came out of the solution after 2-5 hours. The crystals (65 mg, yield = 83%) were separated from the mother liquor by vacuum filtration and dried in air.

3.2.15 Co-crystals of VT involving Silver templates

VT and Silver salts were dissolved in a 1:1 stoichiometric ratio in a minimum amount of acetonitrile. The solution was filtered and kept at dark for slow evaporation. After 1-3 days, colourless or yellow coloured crystals appeared. The crystals were separated from the mother liquor and air-dried. Co-crystal of $(AgClO_4)\cdot(VT)$ was synthesized by dissolving VT (20 mg, 0.078 mmol), and $AgClO_4$, H_2O (17.5 mg, 0.078 mmol) was dissolved in 2 mL of acetonitrile by sonication. The solution was filtered, protected from light, and allowed to evaporate slowly at room temperature. Light yellow coloured block-like crystals came out of the solution in one day (20 mg, yield = 66 %).

3.2.16 Photoreactivity experiments

The experiments involving the photoreaction of solid co-crystals involved finely grinding the sample and placing a 50 mg portion of the powder between a pair of Pyrex glass plates. The glass plates were then exposed to ultraviolet radiation from a 500 W medium pressure mercury lamp in an ACE Glass photochemistry cabinet for 3-7 days. The course of the photoreaction was checked from time to time by ^1H NMR spectroscopy. The formation of the cyclobutane product was indicated by (1) upfield shift of the pyridyl protons, (2) disappearance of the olefinic bonds and (3) the emergence of the cyclobutane protons.

3.2.17 Characterization of (5-I-res)·(hh-TPC)

The photoreaction of (5-I-res)·(TPE) in the broadband photoreactor was studied from time to time (i.e., every 10 h interval) by ^1H NMR spectroscopy, and the extent of cyclobutane product formation was calculated by comparing the relative intensity of the

olefinic and cyclobutane protons. Quantitative photoconversion was observed after 3-5 days of irradiation depending on the sample size. ^{1}H NMR (DMSO, δ/ppm): δ 9.61 (2H, s), δ 8.52 (4H, d), δ 8.40 (8H, d), δ 7.86 (4H, dt), δ 7.36 (8H, m), δ 7.18 (4H, t), δ 7.06 (2H, t), 6.55 (2H, d), δ 6.18 (1H, t), δ 5.00 (2H, d), δ 4.75 (2H, d).

3.2.18 Isolation and characterization of hh-TPC

hh-TPC was separated from 5-I-res via base-extraction. The powder of (5-I-res)·(hh-TPC) (200 mg) was suspended in 50 mL 4M KOH solution. The suspension was stirred at room temperature for 20 min and then diluted with distilled water (100 mL). The suspension was extracted with dichloromethane (3×50 mL). The organic extracts were combined, washed with water (100 mL), and dried on anhydrous Na_2SO_4. The solvent was evaporated in a rotory-evaporator under reduced pressure leaving hh-TPC as a white crystalline powder. ^{1}H NMR (DMSO, δ/ppm): δ 9.61 (2H, s), δ 8.52 (4H, d), δ 8.40 (8H, d), δ 7.86 (4H, dt), δ 7.36 (8H, m), δ 7.18 (4H, t), δ 7.06 (2H, t), δ 5.00 (2H, d), δ 4.75 (2H, d). ^{13}C NMR (DMSO, δ/ppm): δ 155.7, δ 155.4, δ 152.1, δ 149.7, δ 140.4, δ 137.9, δ 128.9, δ 128.7, δ 126.8, δ 124.9, δ 121.3, δ 121.0, δ 46.7.

3.3 Result and Discussion

In this section, hydrogen-bonded self-assembly and photoreactivity of TPE in solid state will be described. Specifically, the crystal structures of the reactive co-crystals, before and after photoreaction, will be demonstrated and compared to the photostable co-crystals. The metal binding capability of hh-TPC will also be demonstrated. In the following section, the self-assembly and photoreactivity of 4BrTPE and VT in solid state will be described. The crystallographic data for the solid discussed in this chapter is in

Appendix A (Table A10-A12). The list of solids discussed in this chapter are listed in Table 7.

Table 7. Structural formulas of the solids discussed in Chapter 3.

TPE	rctt-hh-TPC	$(AgClO_4)(CH_3CN)$(VT)
(5-I-res)(TPE)	rtcc-hh-TPC	
4(5-I-res)·2(hh-TPC)	$2(ZnCl_2)$·(hh-TPC)	
(4,6-diI-res)·(TPE)	$4(Cu(NO_3)_2)$·2(hh-TPC)	
(4,6-diBr-res)·(TPE)	2(res)·(4-BrTPE)	

3.3.1 Self-assembly and photoreactivity of TPE

Single crystal of TPE, suitable for single crystal X-ray diffraction, was obtained when crystallized from hot hexane upon slow cooling. The single crystal as well as the powder of TPE were UV-irradiated for a week and confirmed photostable by comparing the ^{1}H NMR spectra before and after irradiation. The single crystal structure of TPE (Figure 73) showed the edge-to-face packing of the TPE molecules.

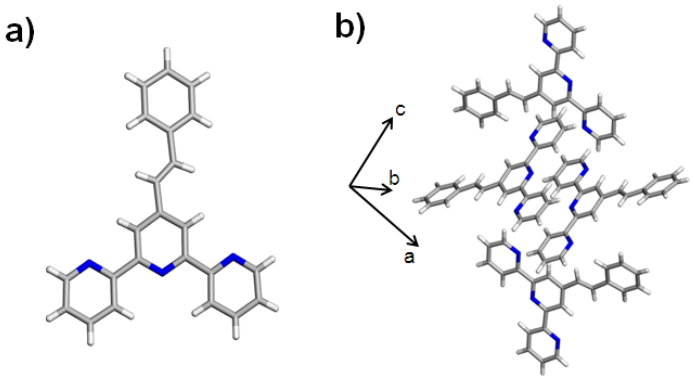

Figure 73. Single-crystal structure of TPE: a) asymmetric unit, and b) unit cell packing.

The nearest olefinic distance was 7.23 Å that explained the lack of photoreactivity of the solid. The TP group formed a *transoid* conformation where the terminal pyridine rings flipped backward. TPE was co-crystallized with a series of resorcinol derivatives and their self-assembly and photoreactivity were studied by ^{1}H NMR spectroscopy. The results of the template screening are listed in Table 8.

Table 8. Co-crystallization and photoreactivity studies involving TPE.

Template	**Stoichiometry (template:reactant)**	**Yield of photoreaction**
resorcinol	1:1	76%
4-chlororesorcinol	1:1	0%
5-methoxyresorcinol	1:1	96%
5-iodoresorcinol	1:1	100%
4,6-dibromoresorcinol	1:1	0%
4,6-diiodoresorcinol	1:1	0%

Co-crystallization of TPE with 5-iodoresorcinol (5-I-res) from nitromethane afforded colourless needles of (5-I-res)·(TPE) upon slow evaporation. The 1:1 stoichiometry of the co-crystal was confirmed using ^{1}H NMR spectroscopy. An X-ray crystal structure analysis of (5-I-res)·(TPE) revealed that the components of the solid, similar to our design, assemble in the solid state *via* O-H···N hydrogen bonds (Figure 74). In contrast to our design, however, the olefin adopts a *transoid* geometry. In this arrangement, the components self-assemble to form a one-dimensional (1D) hydrogen-bonded column with the terminal pyridines forming hydrogen bonds with 5-I-res. The TPE molecules lie stacked head-to-head with a carbon-carbon double bond (C=C) separation of 3.77 Å and 3.94 Å alternatively along the column. The stacked geometry placed the olefins in a suitable position for an intermolecular [2+2] photodimerization.

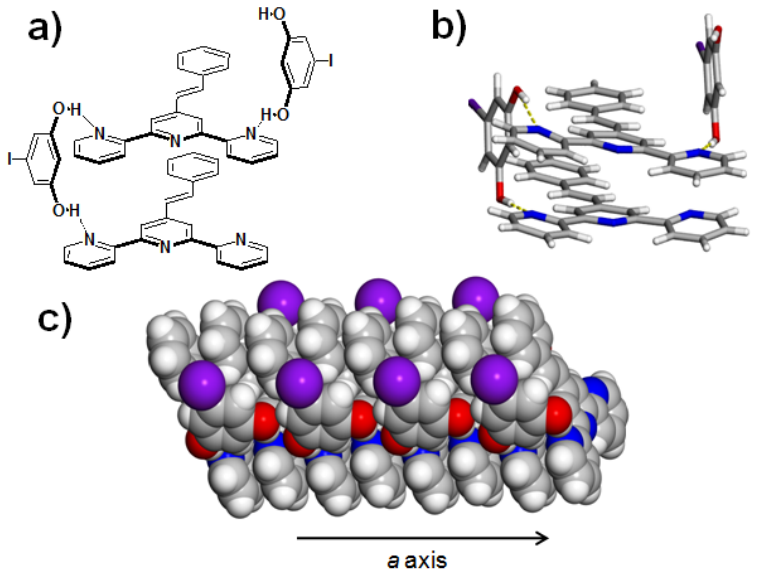

Figure 74. Schematic of a) 1D assembly of (5-I-res)·(TPE) b) the single crystal structure of (5-I-res)·(TPE) and c) the space-filling representation of the 1D assembly along the crystallographic *a*-axis.

A careful inspection in the crystal packing environment of (5-I-res)·(TPE) showed that the 5-I-res molecules on both sides of the column are not on top of each other but rather slipped to avoid steric hindrance between nearest oxygen atoms of two neighbouring 5-I-res molecules. In order to efficiently form hydrogen bonds between the terminal pyridines and resorcinol OHs, the TPE molecules are slipped stacked at an angle of 21° with respect to the ideal perpendicular column-like packing (Figure 75). The packing environment indicates that the formation of similar column-like structure by 4,6-disubstituted resorcinol would lead to the possibility of further steric interactions between the substituents of neighbouring resorcinols on each side of the column. To avoid steric hindrance the 4,6-disubstituted resorcinols would be further slipped and as a result the TPE molecules would be forced to be slip-stacked.

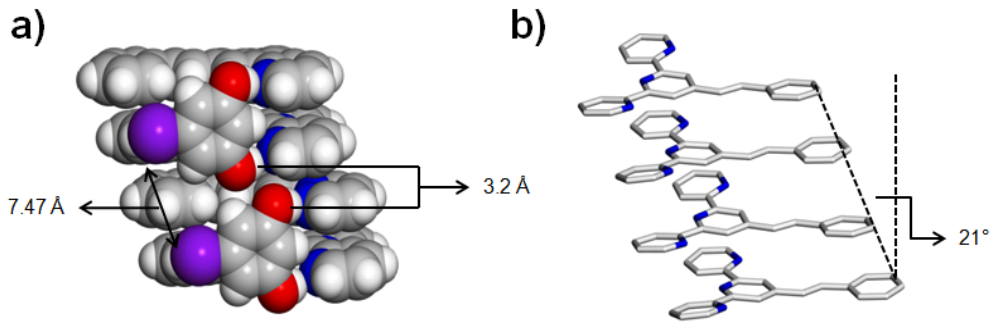

Figure 75. a) Relative positioning of the 5-I-res molecules along the 1D column, and b) slipped-stacking of TPE. (Hydrogen atoms are omitted for clarity)

When a powdered crystalline sample of (5-I-res)·(TPE) was UV-irradiated, TPE reactivity quantitatively to form a cyclobutane product. The formation of a cyclobutane was demonstrated by the disappearance of the olefinic protons (δ = 7.71, 7.55 ppm) and the emergence of signals that correspond to cyclobutane protons (δ = 4.75, 5.00 ppm) (Figure 76). The central pyridine protons of the TP group in TPE (δ = 7.64) shifted

upfield (δ = 7.40) upon TPC formation. All the other pyridine and phenyl protons showed similar trend as expected from the change in hybridization of the carbon atoms from olefin (sp^2) to cyclobutane (sp^3).

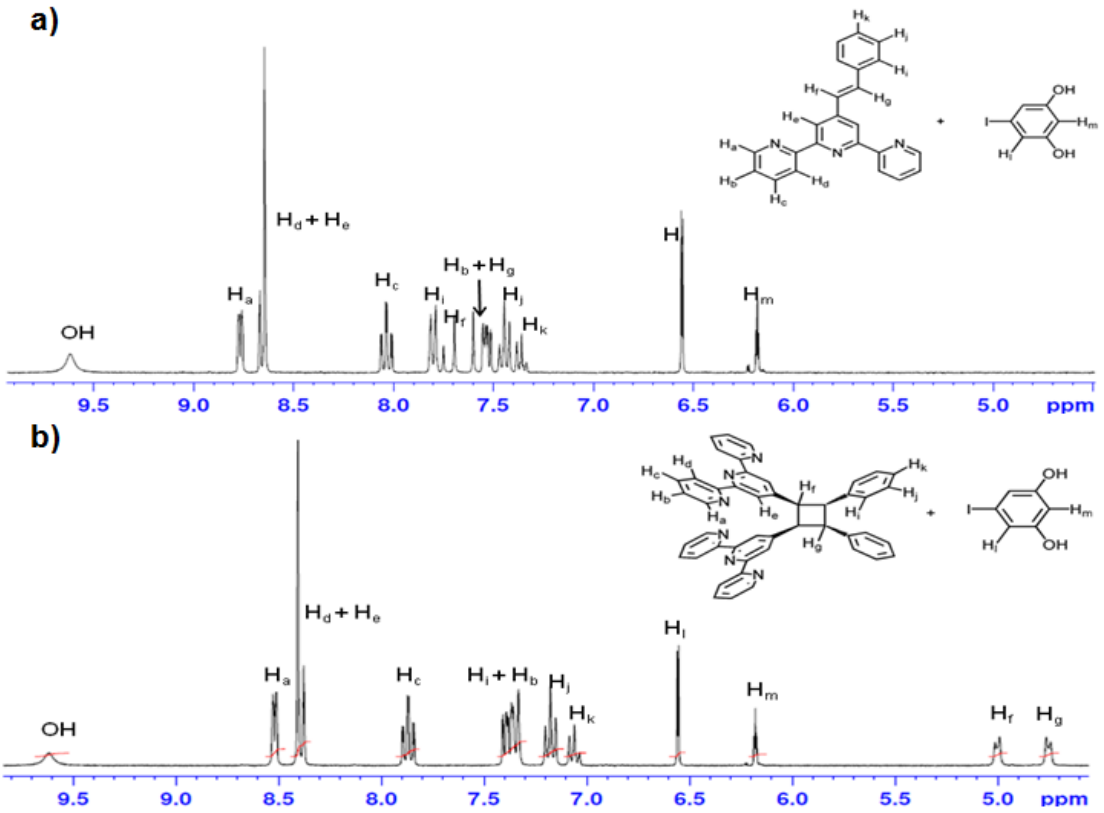

Figure 76. ^{1}H NMR spectra of a) (5-I-res)(TPE), and b) (5-I-res)(TPC).

To determine the stereochemistry of TPC, the photoreacted powder was recrystallized from nitromethane. Diffraction quality single crystals appeared after three days by slow evaporation of the solvent. The crystal structure of the product [(5-I-res)$_4$(hh-TPC)$_2$] showed a six membered discrete assembly formed by two TPC molecules in a head to head geometry (hh-TPC) and four 5-I-res molecules (Figure 77). The stereochemistry of the cyclobutane protons in hh-TPC was found to be *rctt*. The TP

groups on the hh-TPC molecules conformed *transoid* geometry and only the terminal pyridines formed hydrogen bonds with resorcinol OHs. 5-I-res in a *syn-syn* conformation formed hydrogen bonds with terminal pyridines on one end of the TP groups whereas the terminal pyridine on the other end formed hydrogen bond with 5-I-res with anti-anti geometry connecting two different hh-TPC molecules.

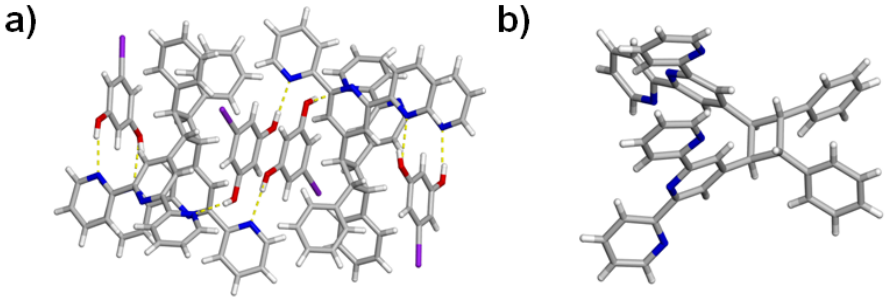

Figure 77. Single crystal structure of $[(5\text{-I-res})_4(\text{hh-TPC})_2]$: a) six component hydrogen-bonded assembly, and b) relative orientation of TP groups in hh-TPC.

The structure analysis of hh-TPC in $[(5\text{-I-res})_4(\text{hh-TPC})_2]$ showed that the TP groups are in a cofacial arrangement where the distance between the central pyridine nitrogen atoms is 5.21 Å and the dihedral angle between the TP groups is only 1.9°. As a means of purification, 5-I-res was separated from the photoproduct by base extraction. X-ray diffraction quality single crystals of TPC were obtained from methanol upon slow evaporation over a period of two days. Moreover, a single-crystal structure determination confirmed that the *rctt*- stereochemistry of hh-TPC retained even after the extraction cycle. The X-ray crystal structure analysis of hh-TPC (Figure 78) showed that the distance between two central pyridine N-atoms of two TP groups increased 6.14 Å. The dihedral angle between two TP groups also increased to 28.5°.

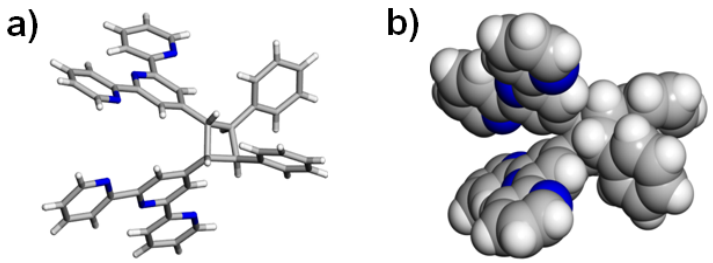

Figure 78. Single crystal structure of hh-TPC: a) capped-stick, and b) space-filling view.

In order to compare the relative disposition of the TP groups in the single crystal structure of hh-TPC with the calculated structure, energy minimization of hh-TPC was carried out. From molecular modeling (Semi empirical/AM1 using Spartan'06 V112 program), we determined that hh-TPC would place two TP groups in close proximity, with the N-atoms of the central pyridine ring being separated by 5.92 Å and splayed at approximately 6.37° (Figure 79b).

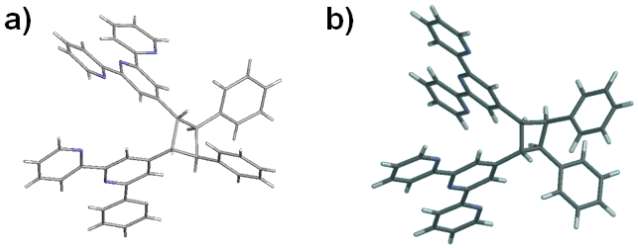

Figure 79. a) Single crystal structure of hh-TPC, and b) energy minimized structure of hh-TPC.

On the other hand, X-ray structure of the photostable co-crystal (4,6-diBr-res)·(TPE) and (4,6-diI-res)·(TPE) (Figure 80) revealed the formation of a similar a 1D Hydrogen-bonded column along the crystallographic *c* axis.

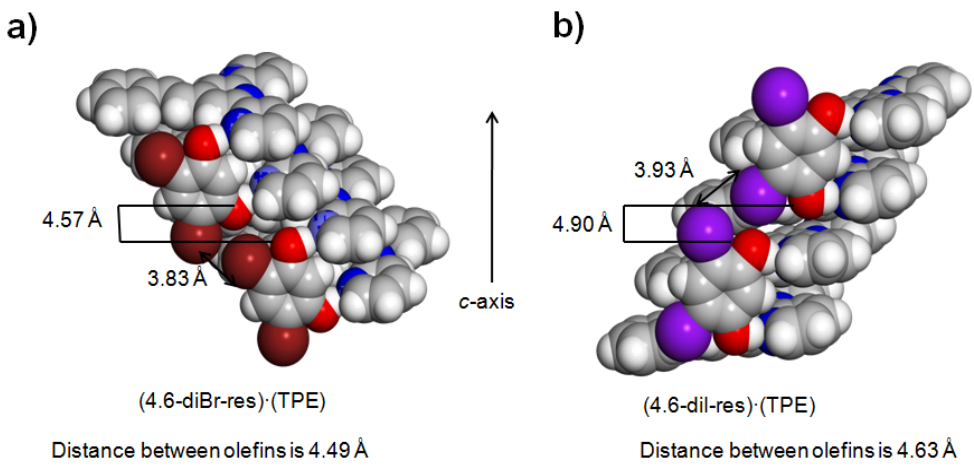

Figure 80. 1D hydrogen-bonded column in the crystal structure of: a) (4,6-diBr-res)·(TPE), and b) (4,6-diI-res)·(TPE).

While single crystal structure analysis of (5-I-res)·(TPE) showed that the olefins are oriented parallel and within a distance of 3.77 Å, the hydrogen-bonding environment in (4,6-diX-res)·(TPE) (X= Br, I) led to different alignment of olefins. In the single crystal structure of both (4,6-diBr-res)·(TPE) and (4,6-diI-res)·(TPE), the olefins are crossed and the distances are 4.49 Å, and 4.63 Å, respectively (Figure 81).

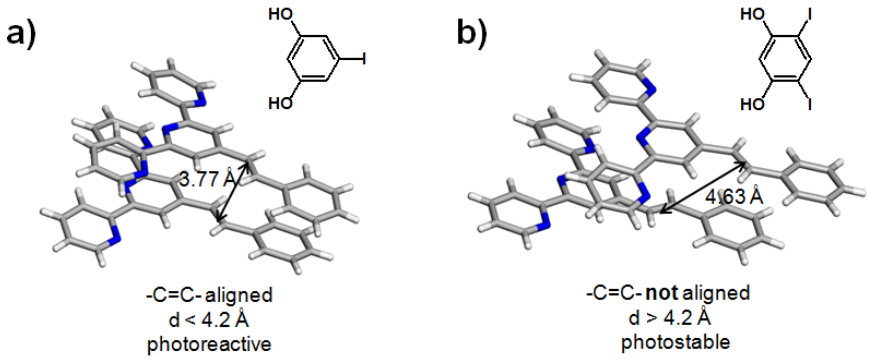

Figure 81. Relative disposition of olefins in the single crystal structure of: a) (5-I-res)·(TPE), and b) (4,6-diI-res)·(TPE)

The stereospecific, quantitative, and gram scale availability allowed to explore the potential application of *rctt*-hh-TPC in the field of coordination chemistry and place two metal ions in close proximity as initially designed. When *rctt*-hh-TPC was reacted with $Cu(acac)_3$ from hot methanol, colourless prisms crystallized out from the solution upon slow evaporation. The single crystal structure analysis showed the isomerization of hh-TPC. The stereochemistry of the cyclobutane changed from *rctt*- to *rtcc*- where the TP groups are not twisted from each other and oriented at an angle of 88° (Figure 82).

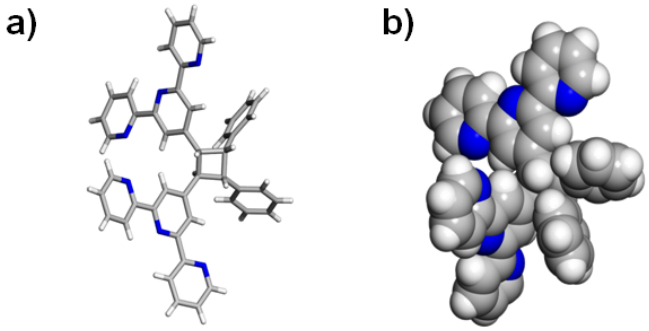

Figure 82. Single crystal structure of *rtcc*-hh-TPC: a) wireframe, and b) space-filling model.

The metal binding studies of *rctt*-hh-TPC revealed that hh-TPC binds metal ions in the form of cofacial complexes; namely, in $[Zn_2(hh\text{-}TPC)_2Cl_4]$ (Zn-TPC) and $[Cu_4(hh\text{-}TPC)_2(NO_3)_8]$ (Cu-TPC). When hh-TPC was crystallized with $ZnCl_2$ or $Cu(NO_3)_2$ from hot methanol solutions of DMF and H_2O (1:1), colourless and green crystals appeared after slow evaporation in approximately five days, respectively. The crystal structure of Zn-TPC (Figure 83) revealed that each TP group of hh-TPC chelates to a zinc chloride molecule. The Zn(II) atom adopts a distorted trigonal bipyramidal geometry with the central pyridine and two coordinating Cl-atoms in the basal plane and the terminal pyridines in the axial sites. The two metal atoms are separated by 7.23 Å.

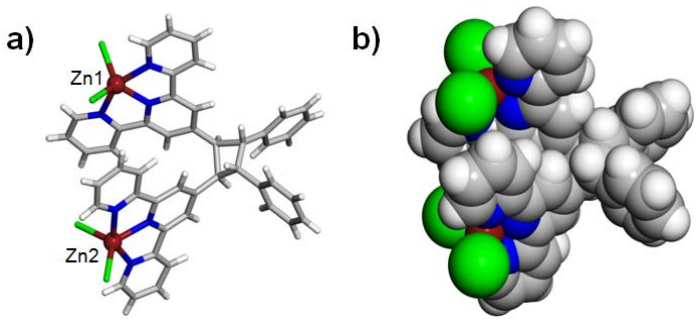

Figure 83. Crystal structures Zn-hhTPC: (a) wireframe representation, and (b) space-filling model.

In the case of Cu-TPC (Figure 84), each Cu(II) atom adopts an octahedral geometry with three N-atoms and a H_2O molecule in the basal plane and O-atoms of two NO_3^- ions in the apical position.

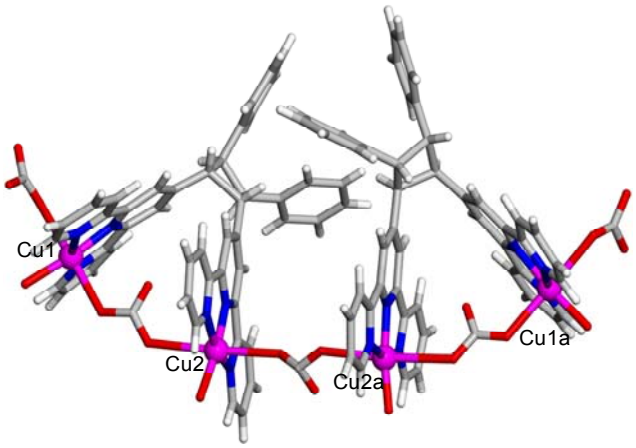

Figure 84. Single crystal structure of symmetry related tetranuclear $[Cu_4(hh\text{-}TPC)_2(NO_3)_8]$

This arrangement led to a discrete tetranuclear complex with a single NO_3^- ion effectively being sandwiched between two metal-bound cofacial complexes. The metal atoms within each cofacial assembly were separated by 6.76 Å (Cu1···Cu2), while the metal ions

between hh-TPC was separated by 6.69 Å (Cu2····Cu2a). The shorter distance between the metal ions in Cu-TPC compared to Zn-TPC was ascribed to the bridging NO_3^- ions.

3.3.2 Self-assembly and photoreactivity of 4-BrTPE

4-BrTPE was synthesized in four steps from 4-bromobenzaldehyde, as described in the experimental section. The self-assembly and reactivity of the olefin was undertaken in solid state to study the effect of functional groups on the styryl end towards the self-assembly process. Additionally, addition of bromo substituent on the styryl end might help to post-synthetically modify the cyclobutane product with cofacially displaced TP groups. When co-crystallized with resorcinol, two different co-crystals were formed, namely, (res)·(4-BrTPE) and 2(res)·(4-BrTPE) (Figure 85) depending on the relative amount of resorcinol used. In both structures, 1D hydrogen-bonded column was observed where the 4-BrTPE molecules were stacked head-to-head. The olefinic double bonds were oriented parallel within a distance of 4.2 Å. The UV-irradiation of the co-crystal led to quantitative formation of cyclobutane product as conformed by the comparing the ^{1}H NMR spectroscopy, before and after UV-irradiation.

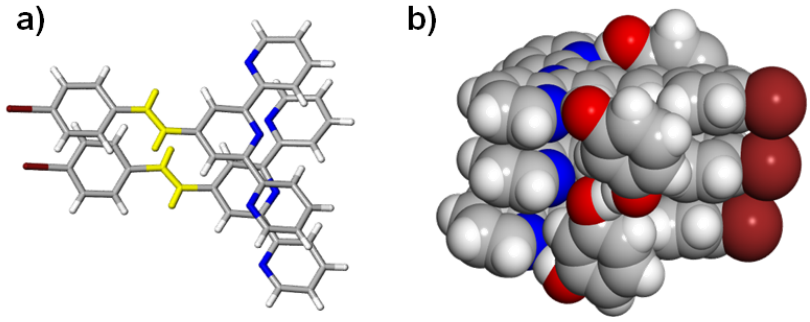

Figure 85. Single crystal structure of 2(res)·(4-BrTPE): a) relative positioning of olefins, and b) space-filling model of the 1D hydrogen-bonded column.

3.3.3 Self-assembly and photoreactivity of VT

The TP-derivatized terminal olefin 4'-Vinyl[2,2':6',2'']terpyridine (VT) (Figure 86a)was synthesized according to a literature procedure in four steps. The molecule, as a pure solid, is photostable. In fact, there was no observable change in the ^{1}H NMR spectra of VT even after prolonged UV-irradiation. This observation was also explained by the single crystal structure of VT (Figure 86b) where the molecules adopted *transoid* geometry, packed in an edge-to-face pattern and the closest distance between the olefins is 8.04 Å.

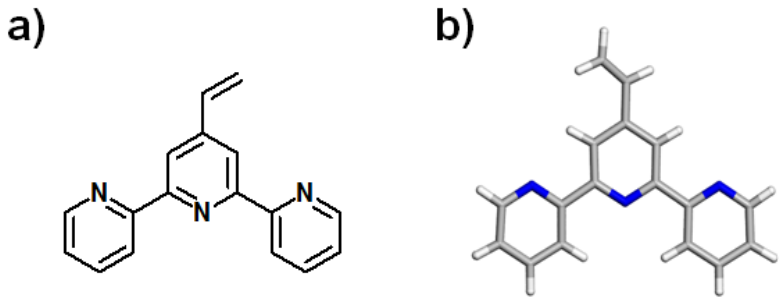

Figure 86. 4'-Vinyl[2,2':6',2'']terpyridine: a) schematic, and b) single crystal structure.

To study the self-assembly and photoreactivity, VT was co-crystallized with resorcinols from nitromethane. The ^{1}H NMR spectra of the co-crystals showed the presence of VT and the resorcinols in 1:1 stoichiometry. However, no photoreaction was observed with any resorcinol-based co-crystals. The use the Ag(I) salts as templates was decided, given the success of their utilization in aligning olefins in solid state. When VT was co-crystallized with $AgClO_4$ in acetonitrile, yellow rod-like crystals appeared after about 12 hours. The crystals were separated from the mother liquor by filtration and air-dried. The crystals became opaque even after a short time of air exposure. The crystals

were powdered and UV-irradiated in high-pressure mercury broadband photoreactor. The ^{1}H NMR spectra of the photoreacted sample show the disappearance of the olefins proton peaks at 7.1, 6.6, and 5.8 ppm with concomitant appearance of the cyclobutane peaks at 4.6, 3.0, and 2.7 ppm. The single crystal structure of [(VT)($AgClO_4$)(CH_3CN)] (Figure 87) shows that terpyridine group adopted *cisoid* geometry to chelate with the Ag(I) ion. The four coordination number of Ag(I) is satisfied by three nitrogen atoms of a VT and one nitrogen atom from the solvent acetonitrile. The ClO_4 counter-anion did not take part in the coordination process. The molecules form a 1D column along crystallographic *c*-axis. In the column, the VT molecules orient in a head-to-tail fashion within an inter-planar distance of 3.33 Å. Given the relative orientation and distance parameters between olefins in [(VT)($AgClO_4$)(CH_3CN)], it was highly unlikely to undergo [2+2]photodimerization in solid state. In fact, when the single crystals of the material, protected by oil surrounding to stop solvent loss, was placed in a broadband UV-reactor no photoreaction was observed even after prolonged UV-irradiation. In contrast, when the material was powdered and then UV-irradiated, upto 94% conversion to the cyclobutane product was observed. It was argued that during the grinding process, the coordinated acetonitrile is lost from the crystal and the molecule undergoes a structure rearrangement to form a reactive assembly where the olefins are placed in suitable geometry to undergo photodimerization in solid state. The assumption was also supported as the single crystals become opaque and lost crystallinity upon standing at room temperature outside the mother liquor.

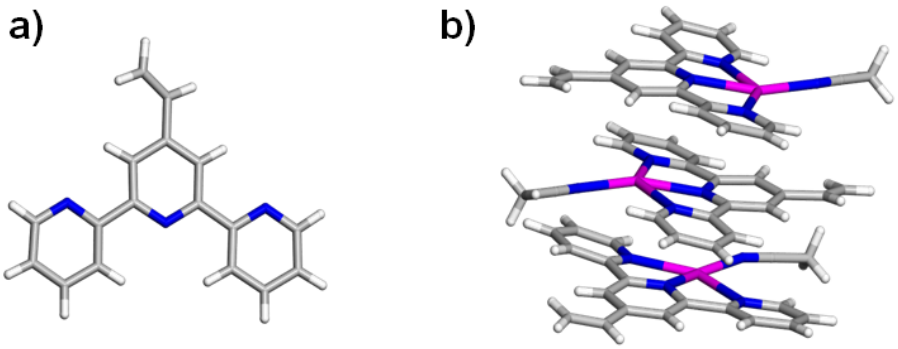

Figure 87. Single crystal structure of: a) VT, and b) (VT)(AgClO4)(CH3CN).

The material was powdered and the PXRD was recorded. The PXRD spectra did not match with the simulated PXRD from the single crystal data. The observation supported the probable formation of a different assembly upon desolvation.

3.4 Conclusion

We have successfully synthesized a cofacial terpyridine *via* template-directed synthesis in solid state. The terpyridine-based olefins, photostable in the pure solid form, were co-crystallized with resorcinols of silver salts to form photoreactive self-assemblies. Upon UV-irradiation, the photodimer was produced stereospecifically, up to quantitative yield, and in gram amounts. Although a discrete, three component, trifurcated hydrogen-bonded assembly was expected, the single crystal structure of the self-assemblies showed a 1D hydrogen-bonded column. The crystal structure analysis of the photoactive and photostable co-crystals clearly showed the differences in the crystal packing responsible for their differences in reactivity. The cofacial photodimer was successfully exploited in coordination chemistry to form dinuclear and tetranuclear cofacial metal-organic complexes. The cofacial terpyridine was successfully utilized to bring two metal ions in close proximity. Finally, a functionalized terpyridine-based olefin as well as a

terpyridine-based terminal olefin was successfully co-crystallized and photodimerized to form photodimers in cofacial arrangement.

CHAPTER 4: FROM THE PERIPHERIES TO THE CORE: STEREOSPECIFIC AND QUANTITATIVE ACCESS TO PYRIDINOPHANES IN SOLID STATE

4.1 Introduction

Macrocycles containing bridged aromatic rings, known as cyclophanes, have been a topic of active research for many years.[77] The rigid aromatic building units, allow the design and synthesis of molecular cavities with defined spatial characteristics, and also serve as binding sites for hosts capable of interacting with their π-electron systems. Thus, several cyclophanes have acted as synthetic receptors in molecular recognition and have been employed as a component to create a cavitand-based nano-sized cage. Although benzene rings have been the most frequently used aromatic subunits (*e.g.,* calixarenes) (Figure 88a), heterocyclic rings are also of equal interest for the construction of cyclophane-type molecular receptors.[78] In terms of nomenclature, cyclophanes with heteroatoms in the aromatic unit are called heterophanes.[77] The presence of heteroatoms provides a means for the incorporation of specific stereoelectronic characteristics within the macrocyclic structure. Heteroatoms modify the physical and chemical properties of an arene without destroying its aromatic character and thus, heterocyclophanes have been utilized to construct molecular and supramolecular architectures with tuned physical and chemical properties. Since many heterocycles, in particular those with nitrogen atoms, play an important role in biochemistry, azacyclophanes are of particular interest to model biological settings. In this context, the self-assembly between specific metal centers and selected pyridine-based ligands have been demonstrated to provide a variety of well-defined discrete supramolecular architectures (*e.g.,* macrocycles, cages, tubes and capsules). Using pyridine as a heterocyclic unit is interesting for the construction of heterocyclophanes because of their potential ability to bind a number of metal cations as

well as hydrogen-bond donor molecules. Cyclophanes involving pyridines, popularly known as pyridinophanes have been shown to be useful for ion complexation, molecular recognition, stabilization of unusual oxidation states and/or coordination environment of metal ions.[79] For example, 3,11,19-trithia-[3.3.3]pyridinophane has shown to form a rare penta-coordinated nickel(II) complex Figure 88b).[80] The constrained environment of the pyridinophane was argued to be responsible for such unusual coordination geometry around the metal ion. Pyridinophanes, integrated on azamacrocycles or N-heterocyclic carbene, have also been exploited to construct supramolecular architectures *via* metal coordination and catalysis.[81]

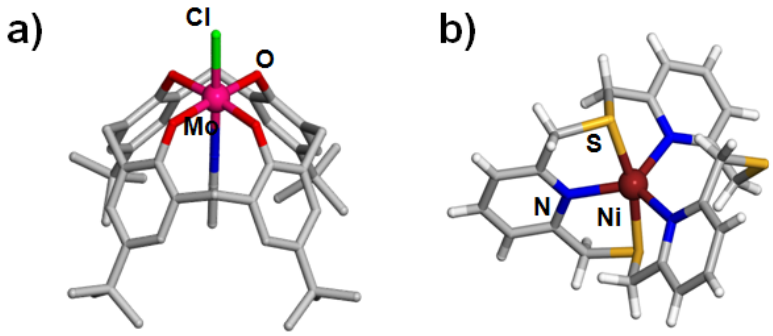

Figure 88. Single crystal structure of the metal-complexes of : a) discrete Mo(V) complex of calixarene, and b) penta-coordinated nickel(II) complex of 3,11,19-trithia-[3.3.3]pyridinophane.

4.1.2 [2.2]Cyclophanes and Pyridinophanes

Driven by the interest in the properties of strained molecules, the challenges inherent in their synthesis, and also in the pursuit of improved understanding of aromaticity, research on the preparation of bridged aromatics with ever shorter bridges has made remarkable progress in the past few decades. [2.2]cyclophanes, where the

aromatic components are preorganized in a forced proximity by dimethylene bridges, are of particular interest since it enforces cofacial overlap of aromatic rings with minimized intramolecular motion and useful for the study of π-π electron delocalization and ring strain. For example, [2.2]paracyclophane, where two benzene rings are covalently connected by two dimethylene bridges at *para* positions (Figure 89), have attracted widespread attention in organic synthesis (*e.g.,* catalysis) and material sciences (*e.g.,* optical devices).[82]

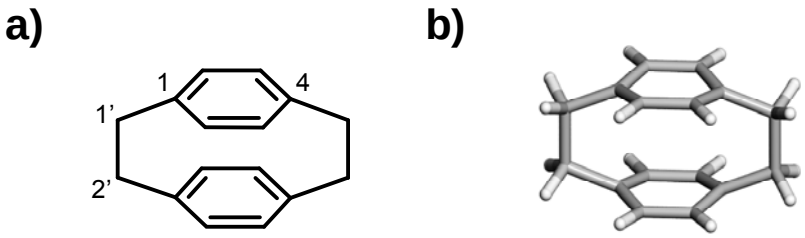

Figure 89. Single crystal structure of [2.2]paracyclophane: a) Schematic, and b) wireframe representation.

[2.2](n,m)Pyridinophanes, where two pyridine rings are connected by two dimethylene bridges, could not only modulate the physical and chemical properties of cyclophanes, but also import additional coordination sites. The designation of [2.2] signifies the number of atoms, occasionally carbon, bridging two pyridine rings, whereas (n,m) signifies the relative positions of the bridge substituents on the pyridines (Figure 89a). Although a few members of the [2.2]pyridinophane family have been synthesized over years, their syntheses often involve multistep synthetic routes, harsh reaction conditions, challenging separation procedures and poor yields, limiting their applications. [2.2](2,6)pyridinophane and [2.2](2,5)pyridinophane have been structurally characterized by single crystal X-ray crystallography.[83] The conformational flexibility in the methylene bridges can lead to two possible conformers of [2.2](2,6)pyridinophane, namely, *syn* and

anti (Figure 90a). In the *syn* conformer, the methylene groups of each aliphatic chain are close to an eclipse conformation, with the pyridine rings stacked face-to-face; whereas in *anti* conformer, the methylene groups form a gauche conformation with the two aromatic rings oriented parallel on the opposite sides of each aliphatic bridge with the nitrogen lone pairs oriented in opposite direction. The single crystal structure of [2.2](2,6) pyridinophane shows that the molecule adopts an *anti* conformation in the solid state (Figure 90b). The *syn* conformation of [2.2](2,6)pyridinophane is higher in energy, and in the solution two conformers (*i.e. syn*, *anti*) rapidly equilibrate, as evidenced by ^{1}H NMR spectroscopy.[84] Thus, the *syn* conformer of [2.2](2,6)pyridinophane could not be isolated and characterized by X-ray crystallography up to date.

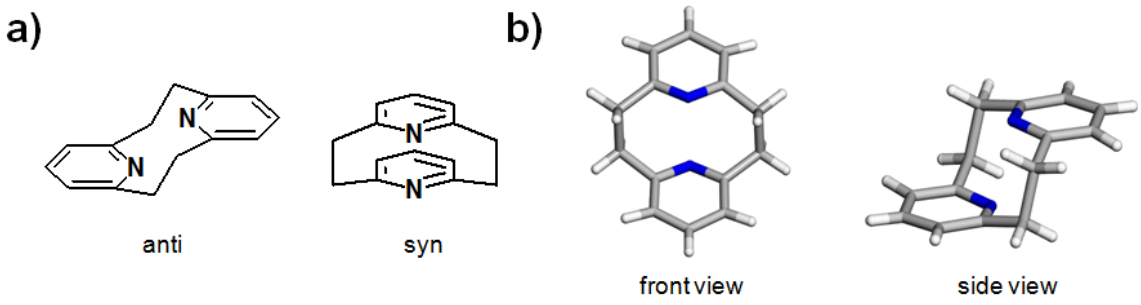

Figure 90. [2.2](2,6)pyridinophane: a) Schematic of the conformations, and b) single crystal structure of the anti conformer.

4.1.3 Paddlanes

In [2.2]metacyclophane, the benzene analogue of [2.2](2,6)pyridinophane,[85] the energy barrier between the two conformers is higher and the *syn* conformer has been shown to be stabilized by engineering the molecular structure (*e.g.,* substituting aromatic rings, metal coordination) (Figure 91a).[86] Nevertheless, the *syn* conformer of the

molecules invariably transforms to *anti* above room temperature. In this context, transformation of the dimethylene bridges of the aromatic decks into cyclobutane rings, termed as a paddlane, has been demonstrated as an efficient method to lock the molecule in the *syn* conformation.[87] Syntheses of paddlane frameworks are also of particular interest to synthetic chemists as an efficient one-pot generation of complex molecules (*i.e.,* a constrained tricyclic system) from simple precursors (Figure 91b).[88]

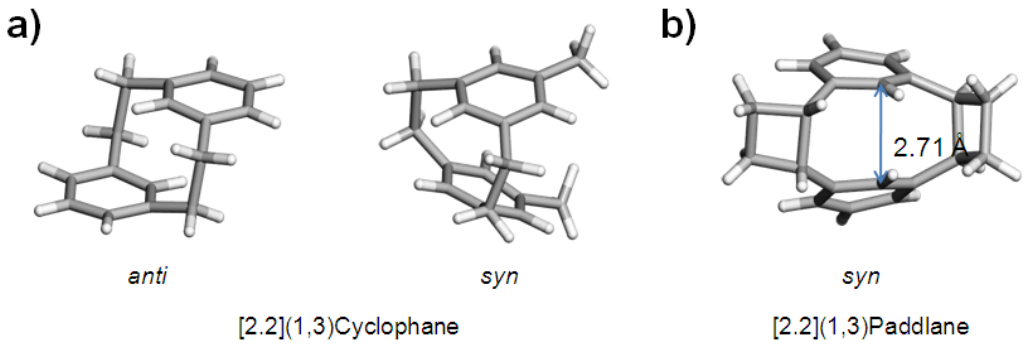

Figure 91. a) Substituent effect on the conformations of[2.2](1,3)cyclophane, and b) cyclobutanes locking the syn conformation within a paddlane framework.

For example, a one-pot synthesis of [2.2](1,3)-paddlane has been achieved by intermolecular double [2+2]photodimerization of 1,3-divinylbenzene in benzene under high dilution condition (~30 mmol) with 5% overall yield. The bridged benzene rings are not parallel to each other within the paddlane framework, but inclined at an angle of 33.6° towards the cyclobutane bridged end. The cause of inclination was argued to be the dimethylene connections between the benzene bridges rather than the cyclobutanes. The inclination led to a short non-bonded contact distance between the carbon atoms of the benzene decks, specifically the carbon atom in between the cyclobutane bridges. In fact, where the centroid to centroid distance of the benzene decks is 3.34 Å, the closest distance of two carbon atoms is only 2.71 Å. Given the sum of van der Waals radius of

two carbon atoms being 3.4 Å, singnificant ring strain, and π-π stacking interaction were said to be responsible for this interesting geometry. Although the cyclobutane rings hinder intramolecular rotations of the benzene rings, the molecule can still exist as three stereoisomers at room temperature. The isomers differ in the mutual orientation of the cyclobutane rings around cyclophane core, designated as *endo-endo*, *exo-exo*, and *endo-exo* (Figure 92).[87] While the *endo-endo* and *exo-exo* isomers equilibrate to each other in solution, the molecular symmetry in *endo-exo* isomer allows it to retain its geometry even after intramolecular rotations.

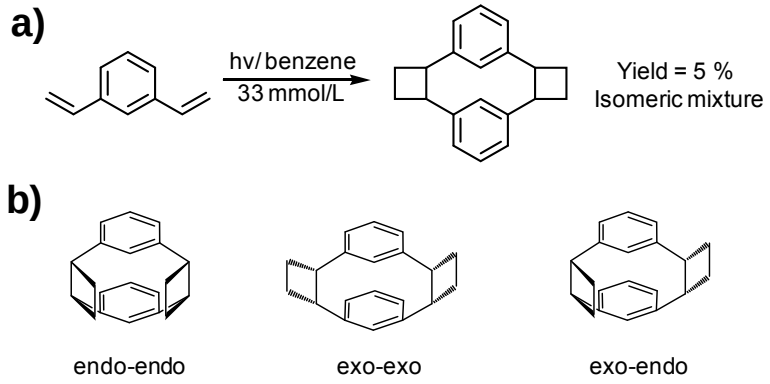

Figure 92. Schematic: a) photochemical synthesis, and b) stereoisomers of [2.2](1,3)paddlane.

4.1.4 Solid state synthesis of [2.2]cyclophanes

Because of strict control over the crystal lattice, the reactions in the solid state proceed, more often than not, with a high degree of selectivity. Thus, the regio- and/or stereochemical outcome of product distribution are often influenced by the crystal packing environment. Formation of a [2.2]paracyclophane moiety within a [2.2](1,4)-paddlane framework has been shown to be achieved stereospecifically and in quantitative

yield by double [2+2]photodimerization of suitable diene molecules in the solid state. In this context, synthesis of [2.2](1,4)-paddlane by double photodimerization of 1,4-divinylbenzene in solution remained unsuccessful, where the reaction stops at the monocyclized intermediate.[88] The stepwise formation of the [2.2](1,4)-paddlane product upon double cyclization in the solid state was ascribed to the crystal lattice that align the unreacted olefins from the monocyclized product in close proximity for further reaction. Specifically, a solid solution of ethyl and propyl α-cyano-4-[2-(4-pyridyl)ethenyl]cinnamate has been shown to afford a highly constrained tricyclic [2.2]paracyclophane in quantitative yield upon intermolecular double [2+2]photodimerization in solid state (Figure 93a).[89] The topochemical behaviour of the reaction, and the stepwise ring closure mechanism were established by single crystal X-ray diffraction. The quantitative photoconversion led to a mixture of three paracyclophane products (*i.e.,* two homodimers and a heterodimer). Recently, a crystalline modification of a coumarin derivative, namely 4-methyl-7-styrylcoumarin has also been recently reported that undergoes intermolecular double [2+2]photodimerization to form a [2.2]paracyclophane within a *para*-paddlane architecture with 72% yield as a mixture of isomeric products (Figure 93b).[90]

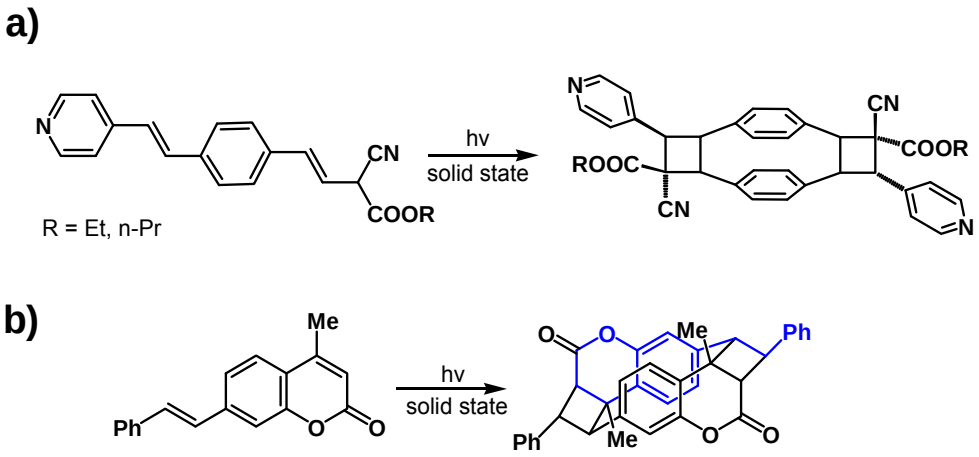

Figure 93. Schematic: a) photochemical generation of [2.2](1,4)-paddlane from the mix crystal of ethyl and propyl α-cyano-4-[2-(4-pyridyl)ethenyl]cinnamate, and b) [2.2](1,4)-paddlane synthesis from 4-methyl-7-styrylcoumarin.

Although the above two examples show how the solid state can be successfully implemented as a synthetic medium for cyclophanes, they were purely based on discovery. There was no design in the synthesis of photoactive material and little to no control over the reaction outcome, yield, and geometry of the product. In order to increase the reliability of the solid state as a medium for organic synthesis, a modular technique for the rational design of photoactive materials with control over the yield and/or product geometry is required.

Recently, the principles of supramolecular chemistry have been successfully implemented by MacGillivray *et. al.* to control bimolecular reactivity in solids. This is done by using molecules that function as linear template to assemble reactant olefins into discrete hydrogen-bonded molecular assemblies for intermolecular [2+2]photodimerization reaction. Template-directed solid-state synthesis of a [2.2]paracyclophane, namely tetrakis(4-pyridyl)-1,2,9,10-diethano[2.2]paracyclophane (4,4'-tppcp) has been obtained stereospecifically, quantitatively, and in gram amounts *via* intermolecular double [2+2]photodimerization of 1,4-bis(4-pyridylethenyl)benzene.[38] In

4,4'-tppcp, the dimethylene bridges of the cyclophane core are fused to pyridine decorated cyclobutane rings (Figure 94). The control over the reaction outcome and product yield has been demonstrated by template-switching strategy. Recently, Brunklaus *et. al.* also synthesized a fluoro derivative of 4,4'-tppcp *via* templated-synthesis in solid state, which demonstrates the modularity of the templated-directed synthetic approach. The molecule, being decorated with pyridines at the exteriors, has also successfully been applied as a ligand in coordination directed self-assemblies.

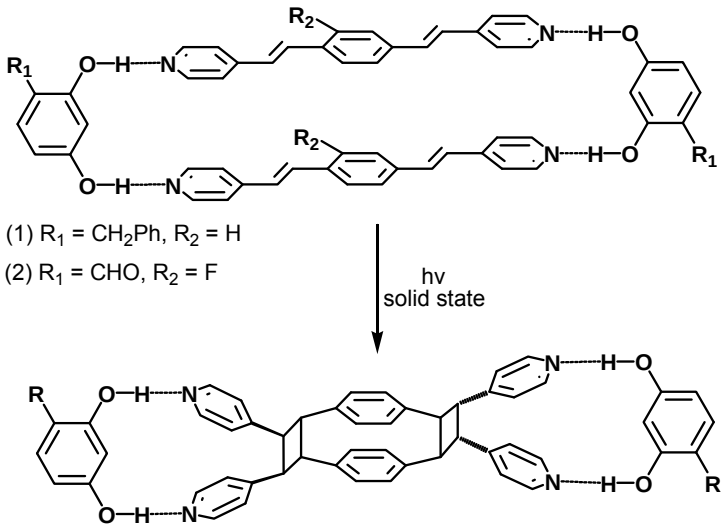

Figure 94. Template-directed synthesis of [2.2]paracyclophanes.

4.1.5 Synthesis of Pyridinophanes

Typical syntheses of [2.2]pyridinophanes often require multiple steps, harsh reactions, challenging separation techniques and low yield. A facile synthesis of pyridinophanes *via* intramolecular [2+2] photocycloaddition in solution has recently been realized where the cyclobutane ring acts as the covalent bridge on one side of the pyridinophane core.[91] Specifically, dioxaoligomethylene tethered vinyl pyridines (Figure

95) have been subjected to intramolecular [2+2] photocycloaddition reaction in an acetonitrile solution that yields the pyridinophane products as a mixture of isomers (*i.e., exo-syn* and *exo-anti*) with moderate yields. Although the product yield has been significantly improved compared to traditional syntheses, the reaction required special treatments such as a UV cut-off filter, inert atmosphere, and high dilution. The synthesis still needs a high dilution method and thus, neither economically efficient nor environment friendly. Structurally more constrained, pyridine analogues of paddlane have not been synthesized thus far.

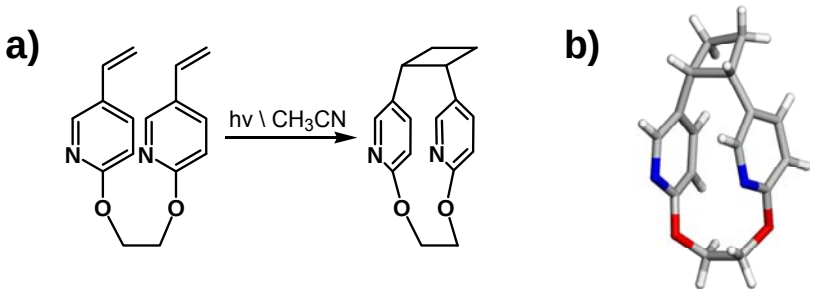

Figure 95. Access to pyridinophane *via* intramolecular [2+2]photodimerization reaction: a) synthesis, and b) the single crystal structure of the *exo-syn* isomer.

The above literature precedences indicate that stereospecific and high yielding syntheses of pyridinophanes have never been achieved up to date. Although intramolecular [2+2]photodimerization reaction in the liquid state improved the yield as indicated in the last example, the occurance of the stereochemistry of choice could not be controlled. Additionally, structural characterics of the olefinic reactants (*i.e.*, dioxaoligomethylene tether) rule out the possibility of synthesizing [2.2]pyridinophanes by this approach. As we have been successful accessing [2.2]cyclophanes stereospecifically and in quantitative yield using our templated synthetic methodology in the solid state, it is of particular interest to explore the possibility of applying the

methodology towards the efficient syntheses of pyridinophanes in the solid state. The study for the construction of [2.2]pyridinophanes (Figure 96) *via* templated solid-state synthesis not only can provide a convenient route to their syntheses, but also test the tolerance of the templated synthetic approach towards changes in reactant shape (*e.g.*, linear vs. bent), as well as increased supramolecular complexity (*e.g.*, additional hydrogen-bond accepting site). Stereospecific, quantitative, and gram scale access, combined with the decoration of the peripheries and core by pyridine rings, could also potentially allow the downstream application of the pyridinophane products in material science (*e.g.*, optical properties). In particular, the utilization of pyridinophanes as novel ligands in coordination-bond directed self-assemblies are envisioned.

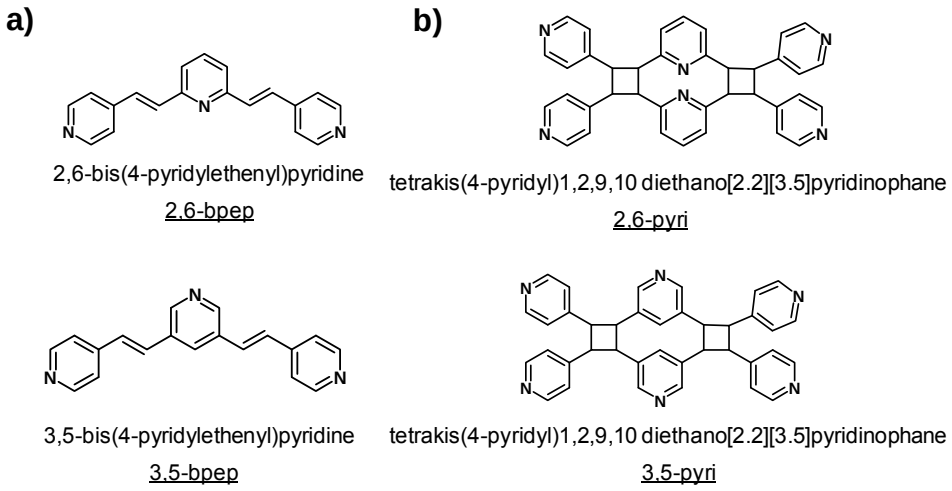

Figure 96. Schematic: a) diolefin precursors, and b) expected pyridinophane products.

4.2 Experimental

All reagents and solvents used were reagent grade and commercially available. Nitromethane, acetonitrile, dichloromethane were purchased from Fisher Scientific Co.

2,6-bis(bromomethyl)pyridine, 3,5-dibromopyridine, 4-vinylpyridine, dichlorobis(triphenylphosphine)palladium(II) were purchased from Sigma-Aldrich Chemical Company. Templates used for co-crystallization experiments (resorcinol, 4-chlororesorcinol, 5-iodoresorcinol, 5-methoxyresorcinol, 4,6-diiodoresorcinol, 4,6-dibromoresorcinol) were either commercially available or synthesized using literature procedures.

Single crystal X-ray diffraction experiments were performed on a Bruker-Nonius Kappa CCD diffractometer using MoKα radiation (λ = 0.7107 Å). The structures were solved using direct methods and refined by full-matrix least-squares based on F2. All non-hydrogen atoms were refined using the anisotropic model. Hydrogen atoms bonded to carbon atoms were placed in idealized positions defined by the hybridization of the belonging carbon atom. The positions of hydrogen atoms bonded to oxygen atoms were calculated so as to establish the best possible hydrogen bonds to a nearest neighbour hydrogen bond acceptor. All crystallographic calculations were performed using the set of crystallographic programs WinGX, along with SHELX-97 locally implemented on a Pentium-based PC.

4.2.1 Synthesis of 3,5-bpep

The synthesis of 3,5-bpep was accomplished by the Heck reaction between 4-vinylpyridine and 3,5-dibromopyridine using K_2CO_3 as base. In a typical experiment, 3,5-dibromopyridine (2 g, 8.47 mmol) and 4-vinylpyridine (2.4 g, 20.33 mmol) was refluxed in 100 mL saturated solution of K_2CO_3 and 1 mL of *tert*-butylamine for three days. The solution was cooled down and extracted with dichloromethane (3×50 mL) and the organic layer was washed with water. The solvent was evaporated in a rotory evaporator and the resultant solid was recrystallized form nitromethane. The resultant yellow solid (1.9 g, 80 %) was dried in air. Single crystals, suitable for X-ray diffraction

were obtained by slow evaporation of an acetonitrile solution. ^{1}H NMR (DMSO-d_6, δ/ppm): δ 8.74 (1H, d), 8.60 (2H, d), 8.44 (1H, t), 7.62 (1H, d), 7.58 (2H, d), 7.49 (1H, d).

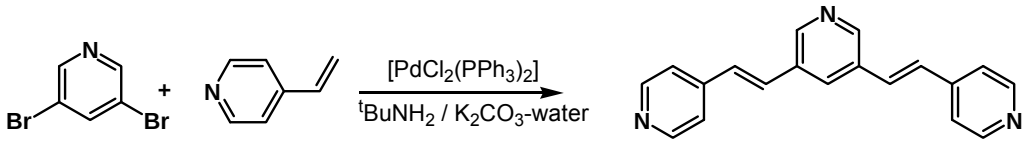

Figure 97. Synthesis of 3,5-bpep.

4.2.2 Synthesis of (5-OMe-res)·(3,5-bpep)

Co-crystals of resorcinol and 3,5-bpep were prepared by mixing solid 3,5-bpep (0.10 g, 11 mmol) and res (0.05 g, 11 mmol) in 3 mL nitromethane. The suspension was heated to dissolve, then left to cool slowly at room temperature. The white crystalline needles of (res)·(3,5-bpep) (0.13 g, 87% yield) was filtered and dried in air. Single crystals of (res)·(3,5-bpep) suitable for the diffraction experiment were prepared by slow evaporation of a solution of (res)·(3,5-bpep) in nitromethane.

4.2.3 3,5-bis(diethylmethylphosphonato)pyridine

3,5-bis(bromomethyl)pyridine (2.0 g, 7.57 mmol) and triethylphosphite (3.0 g, 18.16 mmol) was refluxed for six hours. The solution was cooled down and used for the next step without further purification.

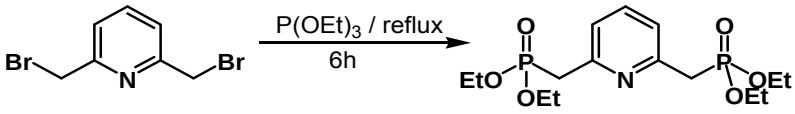

Figure 98. Synthesis of 2,6-bis(diethylmethylphosphonato)pyridine.

4.2.4 Synthesis of 2,6-bpep

Synthesis of 2,6-bpep was carried out *via* HWE reaction between 2,6-bis(diethylmethylphosphonato)pyridine and 4-pyridinecarbaldehyde using ^{t}BuOK as base. In a mixture of 3,5-bis(diethylmethylphosphonato)pyridine (3.0 g, 7.93 mmol) and 4-pyridinecarbaldehyde (1.85 g, 17.44 mmol), ^{t}BuOK (1.95 g, 17.44 mmol) was added slowly with stirring. The resultant brown semi-solid was stirred at room temperature for 2 h. The solution was dumped into 200 mL water and filtered under vacuum. The white solid was washed multiple times with water to wash away free base. The resultant white solid powder (1.34 g, 60%) was dried in air. Single crystals of 2,6-bpep were obtained by slow cooling of an acetonitrile solution of 2,6-bpep. ^{1}H NMR (DMSO-d_6 δ/ppm) δ 8.61 (4H, d), 7.90 (1H, t), 7.77 (2H, d), 7.67 (4H, d), 7.63 (2H, d), 7.57 (2H, d). ^{13}C NMR (DMSO-d_6 δ/ppm) δ 154.0, δ 150.1, δ 143.5, δ 137.8, δ 132.3, δ 130.0, 122.5, δ 121.3.

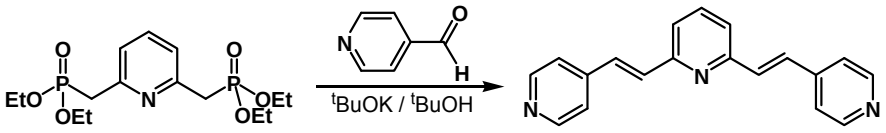

Figure 99. Synthesis of 2,6-bpep.

4.2.5 Synthesis of (res)·(2,6-bpep)

Co-crystals of resorcinol and 2,6-bpep were prepared by mixing solid 2,6-bpep (0.28 g, 11 mmol) and res (0.11 g, 11 mmol) in 15 mL nitromethane. The suspension was heated to dissolve and left to cool slowly at room temperature. The white crystalline precipitate of (res)·(2,6-bpep) (0.39 g, 80% yield) was filtered and dried in air. Single crystals of (res)·(2,6-bpep) suitable for the diffraction experiment were prepared by slow evaporation of a solution of (res)·(2,6-bpep) in nitromethane.

4.2.6 Synthesis of (res)·(2,6-bpep)·(CH_3NO_2)

A photostable polymorphic form of the co-crystals of resorcinol and 2,6-bpep were prepared by mixing solid 2,6-bpep (0.28 g, 11 mmol) and res (0.11 g, 11 mmol) in 15 mL acetonitrile. The suspension was heated to dissolve and left to cool slowly at room temperature. The white crystalline precipitate of (res)·(2,6-bpep) (0.39 g, 80% yield) was filtered and dried in air. Single crystals, suitable for the diffraction experiment, were obtained by slow evaporation of a solution of (res)·(2,6-bpep) in acetonitrile.

4.2.7 Photoreactivity Experiments

The powdered co-crystals were spreaded in between two pyrex glass plates and uv-irradiated in a high-pressure broadband mercury photoreactor. Extent of the photoreaction was studied in regular interval (~10 h) *via* ^{1}H NMR spectroscopy. The photoreaction completed in 2-4 days as confirmed by the complete disappearance of the olefinic protons and appearance of the cyclobutane protons.

4.2.8 Isolation and Characterization of 3,5-pyri

The photoreacted powder of (5-OMe-res)(3,5-bpep) (100 mg) was suspended in 4M KOH (50 mL) solution and the solution was stirred for 1 h at room temperature. The solution was diluted by adding distilled water (100 mL) and extracted with dichloromethane (3×50 mL). The dichloromethane extracts were combined, washed with with distilled water (100 mL), and dried using anhydrous Na_2SO_4. The solvent was evaporated using a rotory-evaporator to get 3,5-pyri as a white solid (67 mg, quantitative). ^{1}H NMR (DMSO-d_6 δ/ppm) δ 8.40 (4H, dd), 7.98 (1H, s), 7.77 (2H, s), 7.30 (4H, dd), 4.90 (1H, d), 4.73 (2H, s), 4.67 (1H, d). ^{13}C NMR (DMSO-d_6 δ/ppm) δ 149.3, δ 149.2, δ 148.8, δ 148.6, δ 147.0, δ 144.3, δ 139.2, δ 133.6, δ 123.4, δ 123.3, δ 47.9, δ 47.4, δ 42.0.

4.2.9 Isolation and Characterization of 2,6-pyri

The photoreacted powder of (res)(2,6-bpep) (50 mg) was suspended in 4M KOH (10 mL) solution and the solution was stirred for 1 h at room temperature. The solution was diluted by adding distilled water (30 mL) and extracted with dichloromethane (3×30 mL). The dichloromethane extracts were combined, washed with with distilled water (50 mL), and dried using anhydrous Na_2SO_4. The solvent was evaporated using a rotory-evaporator to get 3,5-pyri as a white solid (34 mg, quantitative). ^{1}H NMR (DMSO-d_6 δ/ppm) δ 8.40 (4H, dd), 7.98 (1H, s), 7.77 (2H, s), 7.30 (4H, dd), 4.90 (1H, d), 4.73 (2H, s), 4.67 (1H, d). ^{13}C NMR (DMSO-d_6 δ/ppm) δ 156.6, δ 150.2, δ 149.1, δ 136.2, δ 128.8, δ 128.1, δ 123.5, δ 120.4, δ 49.2, δ 42.3.

4.3 Results and Discussion

General and crystallographic parameters for the co-crystals before and after photodimerization are given in Appendix A, Tables A13-A15. In the following section, the co-crystallization, solid-state characterization and photoreactivity of 26-bpep, and 3.5-bpep will be discussed. Solid-state characterization of the pyridinophanes, namely, 2,6-pyri and 3,5-pyri will also be discussed and finally the application of the pyridinophane architecture in coordination bond directed self-assemblies will be shown. Solids discussed in this chapter is shown in Table 9.

Table 9. Structural formulas of the crystalline solids discussed in Chapter 4.

2(5-OMe-res)·2(3,5-bpep)	2,6-bpep
(3,5-pyri)(CH_3NO_2)(H_2O)$_2$	(res)·(2,6-bpep)(photoactive)
(3,5-pyri)·4($Cu(OAc)_2$·solvent	(res)·(2,6-bpep)(photostable)
	(2,6-pyri)($PhCH_3$)$_2$

The retrosynthetic analysis of 3,5-pyri (Figure 100) shows that it can be synthesized from 3,5-bpep *via* template-controlled intermolecular double [2+2]photodimerization reaction in solid state. The 3,5-bpep molecule, in turn, can be accessed by Heck reaction between 3,5-dibromopyridine and 4-vinylpyridine.

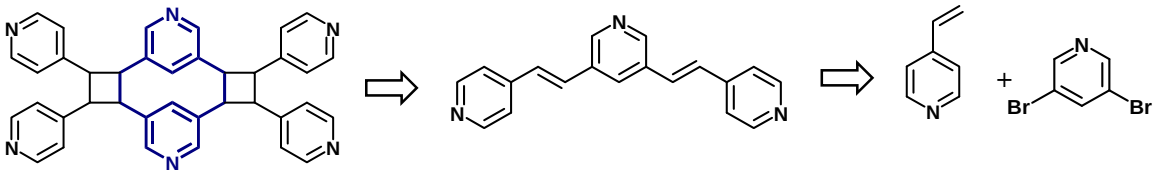

Figure 100. Retrosynthetic analysis for the synthesis of [2.2](3.5)pyridinophane. Pyridinophane unit is highlighted in blue.

The reactivity of the 3,5bpep was studied as a pure solid. Single crystals of the compound were obtained from an acetonitrile solution upon slow evaporation. The material was UV-irradiated in between two pyrex glass plates in a broadband UV reactor for three days. The ^{1}H NMR spectrum of the photoreacted material showed complete disappearance of the olefin peaks at δ 7.56 and δ 7.69 and emergence of the cyclobutane peaks at δ 4.53 and δ 4.31. The peripheral pyridyl protons at δ 8.60 and δ 7.59 are shifted upfield to δ 8.29 and δ 7.07. The aromatic protons of the central pyridine at δ 8.75 and δ 8.45 also shifted upfield to δ 8.12 and δ 8.29, respectively.

In order to study the self-assembly process and the photoreactivity of the co-crystals, 3,5-bpep was co-crystallized with a series of resorcinols. The reactivity studies of the co-crystals are described in Table 9. The components and stoichiometry of the co-crystals were confirmed by ^{1}H NMR spectroscopy. When 3,5bpep was co-crystallized with 5-methoxyresorcinol (5-OMe-res) from nitromethane, colourless crystals of (5-OMe-res)·(3,5-bpep) were obtained in four hours upon slow evaporation. The 1:1 stoichiometry of the components in the solid was determined by the ^{1}H NMR spectroscopy. The material was exposed to UV-irradiation and the course of the [2+2]photocycloaddition reaction was monitored every 10 hours by ^{1}H NMR spectroscopy. The reaction was complete in 48 hours as confirmed by the complete disappearance of the olefinic protons at δ 7.52 and δ 7.64, and emergence of the cyclobutane protons at δ 4.74, δ 4.82 and δ 4.95. The pyridyl *ortho* protons from the

olefin disappeared and an overlapping pair of doublets appeared at δ 8.45-8.49. The pyridyl *meta* protons also from the starting olefin also disappeared and a pair of doublets appeared at δ 7.34 and δ 7.39, respectively. The pattern of the pyridyl protons and the presence of three different types of cyclobutane protons in a 1:2:1 ratio, confirms the formation of the *endo-exo* isomer in quantitative yield (Figure 101). The *exo-endo* configuration of the pyridinophane product was also evident form the presence of three different cylobutane carbon peaks in the ^{13}C NMR spectrum.

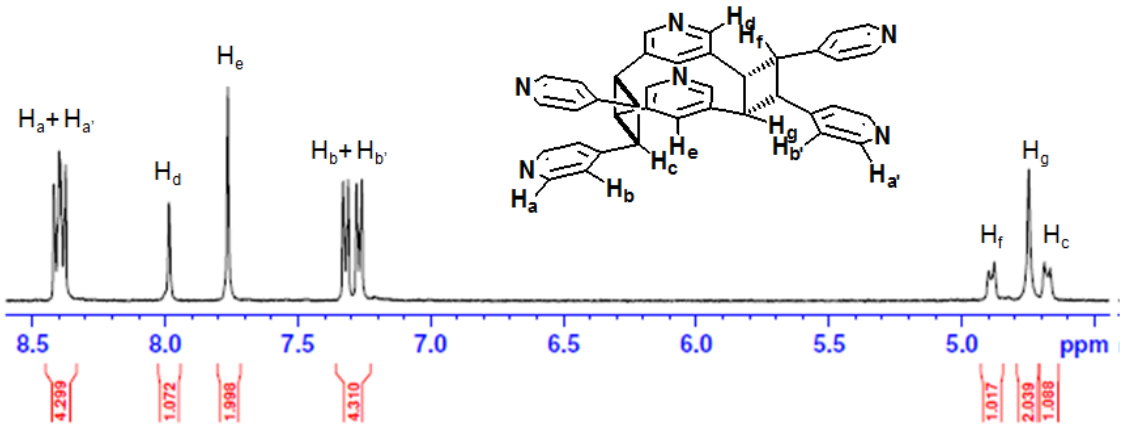

Figure 101. ^{1}H NMR spectrum of the *exo-endo* 3,5-pyri.

The single crystal structure of (5-OMe-res)·(3,5-bpep) showed that a four component discrete assembly [2(5-OMe-res)·2(3,5-bpep)] (Figure 102) formed which involved two 5-OMe-res and two 3,5-bpep molecules. The resorcinol molecules form O-H···N (O···N 2.70, 2.71 Å) hydrogen bonds with the peripheral pyridines with the 3,5-bpep molecules stacked parallel. The central pyridines form a syn orientation where both nitrogen atoms from the stacked 3,5-bpep molecules point at the same direction and did not participate in hydrogen-bonding with resorcinols. The olefins are stacked parallel within a distance of 3.67 Å, and are suitable for photoreaction.

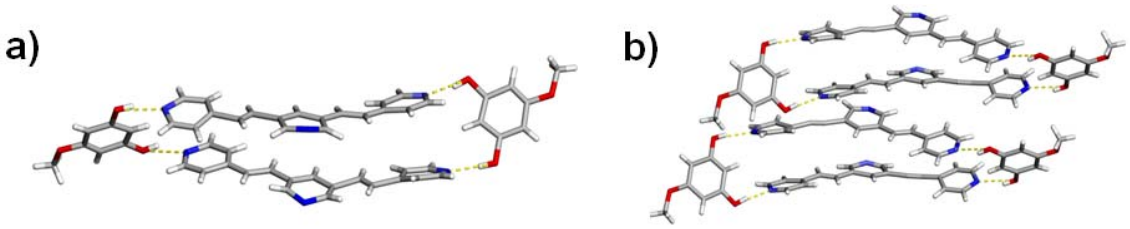

Figure 102. Four component discrete assembly of [2(5-OMe-res)·2(3,5-bpep)]. Solvent molecules are omitted for clarity.

To further confirm the structure, the template molecule was separated from the photoproduct and the single crystal X-ray structure of the pyridinophane was studied. Diffraction quality single crystals of pure 3,5-pyri was obtained by recrystallization from nitromethane. The single crystal structure of the compound [(3,5-pyri)(CH_3NO_2)(H_2O)$_2$] (Figure 103) confirmed the *endo-exo* geometry of the product.

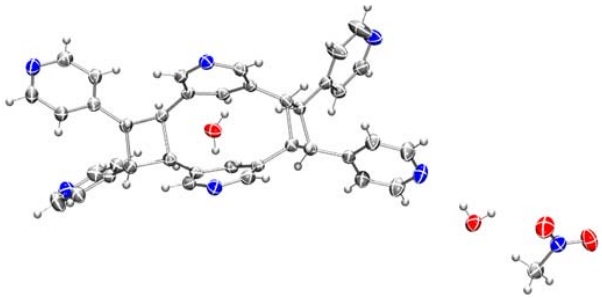

Figure 103. ORTEP drawing of [(3,5-pyri)(CH_3NO_2)(H_2O)$_2$].

The pyridine groups in the pyridinophane core adopted a *syn* conformation, where two pyridine nitrogen atoms point at the same direction within a distance of 4.42 Å and a torsional angle of 37°. Compared to the [2.2](1,3)paddlane, the bridged pyridines in 3,5-pyri were also inclined towards the cyclobutane bridged end. The higher degree of inclination of pyridinophanes compared to that of [2.2](1,3)paddlane can be ascribed to

the addition of functionality (*i.e.,* pyridines) at the peripheries, the substitution of a C-H with a nitrogen atom in the aromatic bridge, and the crystal packing environment. As a result, the centroid to centroid distance between aromatic bridges increased from 2.95 Å to 3.41 Å. Analogous to the paddlane, the 3,5-pyri also had longer C-C bonds (*i.e.,* 1.61 Å) in the inner part of the cyclobutanes. In contrast to [2.2](1,3)paddlane, the outer cyclobutane C-C bonds of 3,5-pyri were also of higher length (*i.e.,* 1.58 Å) probably due to the increased steric crowding by the peripheral pyridine rings. The peripheral *exo* pyridine rings and the pyridines in the pyridinophane core involve in hydrogen bonding (N···O distance 2.86 Å and 2.89 Å) with water molecules present in the structure whereas the *endo* peripheral pyridines don't take part in hydrogen bonding. Four 3,5-pyri and four water molecules for a eight member loop that extend in three dimension to form a hydrogen-bonded 2D net (Figure 104).

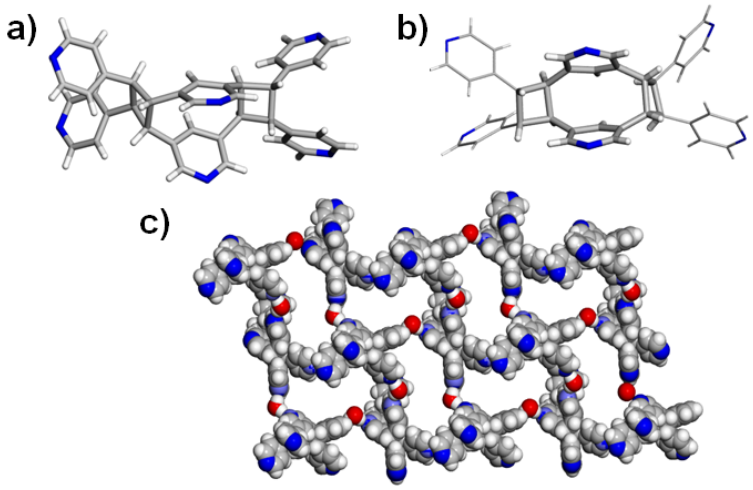

Figure 104. Single crystal structure of [(3,5-pyri)(CH_3NO_2)(H_2O)$_2$]: a) wireframe representation, b) *exo-endo* geometry, and c) hydrogen-bonded 2D net.

3,5-Pyri was crystallized with $Cu(OAc)_2$ from methanol/water solution, light blue crystals appeared after one week upon slow evaporation of the solvent. The single crystal

structure of (3,5-pyri)·4(Cu(OAc)$_2$·solvent (Figure 105) shows that the three out of four peripheral pyridine rings and out of two central pyridines form coordination bonds with Cu. There are two different Cu ions in terms of coordination environment. The octahedral geometry of the Cu ions involve four peripheral pyridines of four neighbouring 3,5-pyri molecules in the basal plane and two water molecules on the axial sites. In the other type of Cu site, the basal plane is satisfied by water and acetate ligands whereas the axial sites are satisfied by two pyridine rings, one from a central pyridine of a 3,5-pyri and a peripheral pyridine of a neighbouring 3,5-pyri. Each 3,5-pyri ligand coordinated with four different Cu atoms, where three out of four peripheral pyridine and one out of two central pyridine participated in forming coordination bonds. Overall, the coordination environments led to a 3D metal-organic framework where 3,5-pyri ligands act as afour connecting nodes. Two types of Cu(II) ions present in the structure acted as four and two connecting nodes, respectively. The 2D grid-like structure along *ac* plane created rhombohedral voids with dimension of 22.02, and 12.04 Å. The extension of the grid structure along *c* axis also created rhombohedral voids with dimension of 7.53, and 15.81 Å.

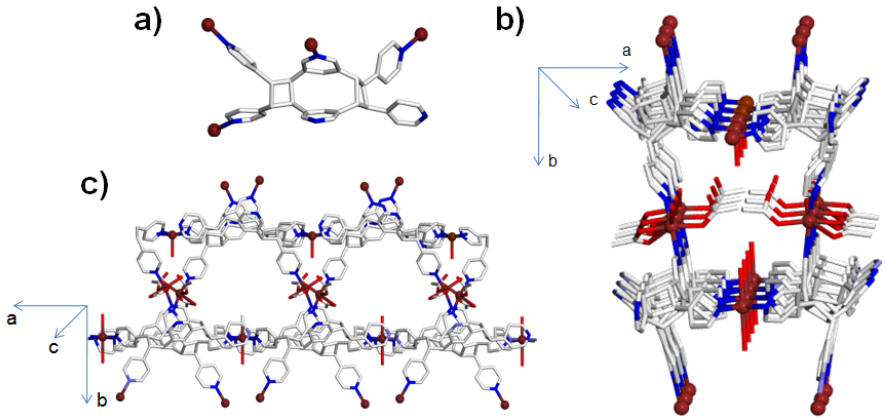

Figure 105. Single crystal structure of (3,5-pyri)·4(Cu(OAc)$_2$·solvent a) 3,5-pyri with coordination environment, b) side view, and c) front view.

The related diolefin 2,6-bis(4-pyridylethenyl)pyridine (2,6-bpep) was synthesized by Horner-Wadsworth-Emmon (HWE) reaction between 4-pyridinecarboxyaldehyde and 2,6-bis(diethylphosphonato)pyridine. Single crystal structure of 2,6-bpep, suitable for single crystal X-ray diffraction, was obtained from nitromethane by slow evaporation. The single crystal structure of 2,6-bpep showed that one olefinic group is stacked with another olefinic group of a neighbouring 2,6-bpep molecule. One olefin from two neighbouring molecules stacks in a head-to-tail geometry within a distance of 4.00 Å (Figure 106).

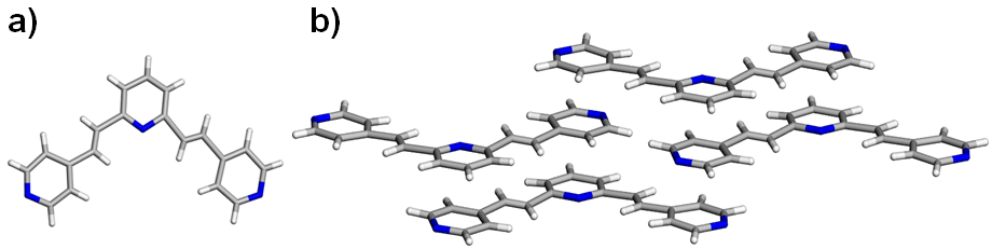

Figure 106. Single crystal structure of 2,6-bpep: a) asymmetric unit, and b) solid state packing.

In order to study the photoreactivity of 2,6-bpep in the form of co-crystals, 2,6-bpep was co-crystallized with a series of resorcinol molecules with different steric and electronic environment incorporated in their structures in terms of substituents. Co-crystallization between 2,6-bpep and resorcinol was expected to form a four component discrete assembly constituted of two 2,6-bpep and two resorcinol molecules. Two resorcinol molecules, one on each side of a pair of stacked 2,6-bpep, would form two O-H···N hydrogen bonds with the peripheral pyridyl groups (Figure 107).

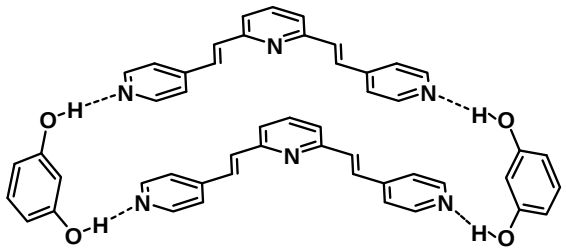

Figure 107. Schematic of the expected four component discrete assembly of 2(res)·2(2,6-bpep)

When 2,6-bpep was co-crystallized with resorcinol in nitromethane, a white crystalline solid separated from the solution upon slow evaporation of the solvent. The 1:1 stoichiometry of the two components in the solid was confirmed by ^{1}H NMR spectroscopy. The material was UV-irradiated in between two glass plates in a medium pressure broadband UV-photoreactor, and the extent of the reaction was monitored every ten hours by comparing the ^{1}H NMR spectra of the material, before and after UV-irradiation. The white powder tuned into yellow over time and the reaction was complete in three days. The quantitative formation of cyclobutane product was confirmed by the complete disappearance of the olefinic protons at δ 7.77 and δ 7.63, and emergence of the cyclobutane protons at δ 5.15 and δ 5.35. The pyridyl *ortho* protons of 2,6-bpep at δ 8.62 disappeared and a doublet appeared at δ 8.45. The pyridyl *meta* protons of 2,6-bpep at δ 7.65 also disappeared and a doublet appeared at δ 7.25. The pattern of the pyridyl protons and the presence of two different types of cyclobutane protons in a 1:1 ratio, conforms the formation of the *exo-exo* or *endo-endo* isomer of pyridinophane in quantitative yield. A ^{13}C NMR spectrum of the photoreacted material showed only two peaks in the cyclobutane region (δ 49.2, δ 42.3), that also shows the formation of a symmetrical pyridinophane (*i.e.*, *exo-exo*, and *endo-endo*). A single crystal X-ray analysis of (res)·(2,6-bpep) (Figure 108) showed the formation of 1D hydrogen-bonded chain consisting of res anf 2,6-bpep molecules. The 2,6-bpep molecules were stacked within

olefinic distance of 3.85 Å, where the double bonds conformed an *endo-endo* geometry. A resorcinol molecule formed hydrogen bond with terminal pyridines on on side of the stacked 2,6-bpep molecules, whereas on the other side only one terminal pyridine formed hydrogen bond with resorcinol. The central pyridines and one terminal pyridine of the stacked pair of 2,6-bpep molecules did not take part in hydrogen bonding. The resorcinol molecules hydrogen bonded with each other to generate an infinite 1D molecular chain.

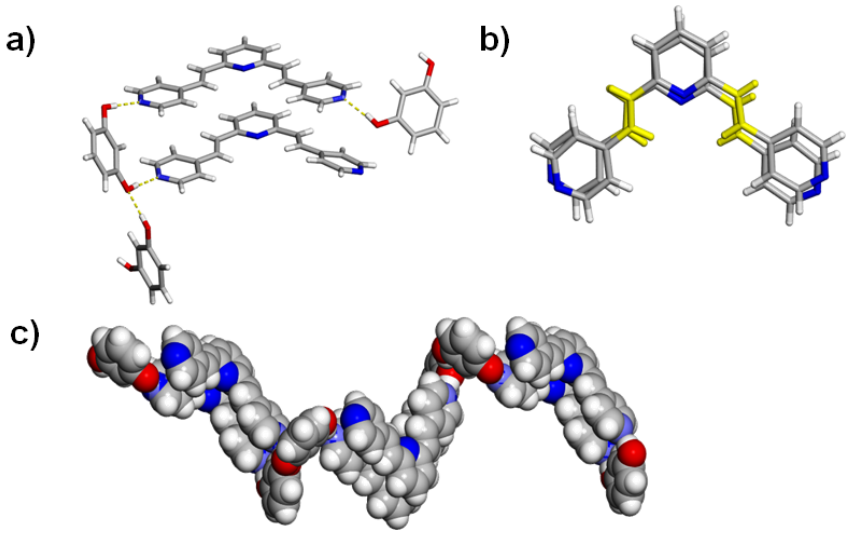

Figure 108. Single crystal structure of (res)·(2,6-bpep): a) repeating unit in 1D chain, b) relative positioning of the olefins, and b) space-filling model of the 1D hydrogen-bonded chain.

When the co-crystallization experiment of 2,6-bpep with resorcinol was repeated using acetonitrile as solvent, a white crystalline precipitate of (res)·(2,6-bpep) was formed by slow evaporation of the solvent. The 1:1 stoichiometry of the components in the co-crystal was confirmed by ^{1}H NMR spectroscopy. When the powder was UV-irradiated, no photodimerization reaction was observed even after prolonged (ca. 72 hours) irradiation. The crystal structure of the co-crystal shows a polymorphic form of (res)·(2,6-bpep) (Figure 109) obtained from nitromethane. The structure formed a 1D column of

2,6-bpep along the crystallographic *a*-axis with the central pyridine nitrogens of the neighbouring 2,6-bpep molecules pointed at the same direction. The resorcinols align vertically on both sides of the column forming hydrogen-bonds (O-H···N 2.74-2.76 Å) with the peripheral pyridine nitrogen atoms. The neighbouring 2,6-bpep molecules stack offset with the nearest C=C bonds being crossed and at distances of 3.87 Å, and 4.32 Å.

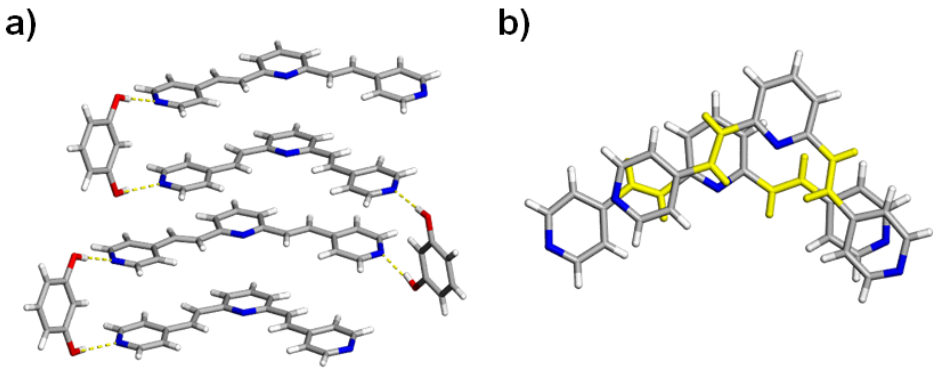

Figure 109. (res)·(2,6-bpep): a) wireframe representation of the hydrogen-bonded packing motif and, b) relative positioning of the olefins of neighbouring 2,6-bpep molecules.

The template was isolated from the photoreacted material by base extraction. The purified material was crystallized from toluene by slow evaporation. The single crystal structure of (2,6-pyri)·2($PhCH_3$) showed that the expected formation of the 2,6-pyri in an *endo-endo* geometry (Figure 110).

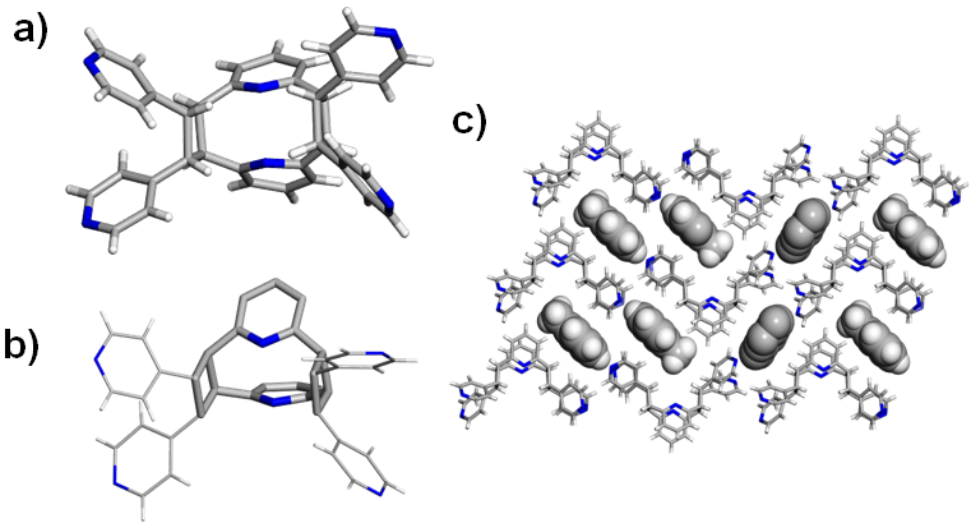

Figure 110. Single crystal structure of 2,6-pyri: a) capped-stick view, and b) highlight of the *endo-endo* geometry of the pyridinophane core, and c) channel structure with the toluene molecules.

The inclination angle between the pyridine bridges increased to 43° compared to only 37° in 3,5-pyri. The increased angle can be ascribed to the less steric hindrance between the nitrogen lone pairs compared to C-H bonds. As a result, centroid to centroid distance between the pyridine rings slightly increased to 3.43 Å, whereas the non-bonded distance between nitrogen atoms of bridged pyridines was only 2.55 Å (sum of van der Waals radius is 3.1 Å). Due to increased steric crowding of the peripheral pyridines combined with the *endo-endo* stereochemistry of cyclobutanes, the C-C bonds were of higher length (*i.e.,* 1.58-1.61 Å).

4.4 Conclusion

In summary, the template-controlled solid-state synthesis has been successfully used to synthesize complex [2.2]pyridinophanes. The template-switching strategy has been demonstrated to influence the desired reaction outcome, as well as the product

geometry. Both the [2.2](3,5)pyridinophane and [2.2](2,6)pyridinophane have been synthesized within the paddlane framework stereospecifically, quantitatively, and in gram amounts. Being decorated with pyridine moieties at the peripheries, as well as the core, led to the unprecedented downstream application of the materials in metal-organic frameworks. Given the *syn* conformation of the pyridine rings within the paddlane frameworks combined with the constrained but well-defined structure of the newly synthesized pyridinophanes, these compounds are also of interest to study optical properties and catalysis.

CHAPTER 5: CRYSTAL ENGINEERING THE CHROMIC PROPERIES OF SALICYLIDENEANILINE

5.1 Introduction

Crystal engineering, defined as the understanding of intermolecular interactions in the context of crystal packing for designing of new solids with desired physical and chemical properties, in one of the important fields in recent chemistry and physics.[12-13] Understanding the structure of new organic compounds in the solid state is critical to engineer their physical and/or chemical properties. Co-crystallization of two or more molecules with complementary functionalities leads to multicomponent molecular assemblies (or more familiarly called co-crystals) where the molecular components are held together by noncovalent interactions (*e.g.,* hydrogen bond). Co-crystallization of two or more molecular components allows them to be incorporated in the same crystal reliably while retaining their own chemical characteristics. Thus, co-crystallization can be exploited to combine physical and/or chemical properties of interests from different molecular components in a single crystalline material in the form of co-crystal.

5.1.1 Thermochromism of Salicylideneanilines

Thermochromism[92,92b] (reversible colour change of substances with variation in temperature) has been observed in various substances (organic[93], inorganic[94], metal-organic[95] and macromolecular compounds) in both solution and the solid state with potential applications as switches and sensors. A variety of mechanisms (*e.g.,* change in coordination geometry in transition-metal complexes, tautomeric equilibrium[96]) are known to be responsible for the thermochromic property. N-salicylidene-anilines (SAs) belong to a special class of organic compounds that exhibit thermochromism in crystals.[97]

Thermochromism of SA crystals is due to a temperature-induced shift of tautomeric equilibrium *via* intramolecular hydrogen transfer between the enol and *cis*-keto forms (Figure 111a).[98] The *cis*-keto form has an absorption band in visible region whereas the enol form does not. The dynamic ratio of the two forms at different temperature leads to the appearance of different colours. Thermochromic SA crystals are generally orange in colour and fluorescent at room temperature. As an example, *N*-(5-chloro-2-hydroxybenzylidene)-aniline has been shown to be thermochromic; while orange at 298 K, it appears greenish-yellow at 80 K (Figure 111b).[92a]

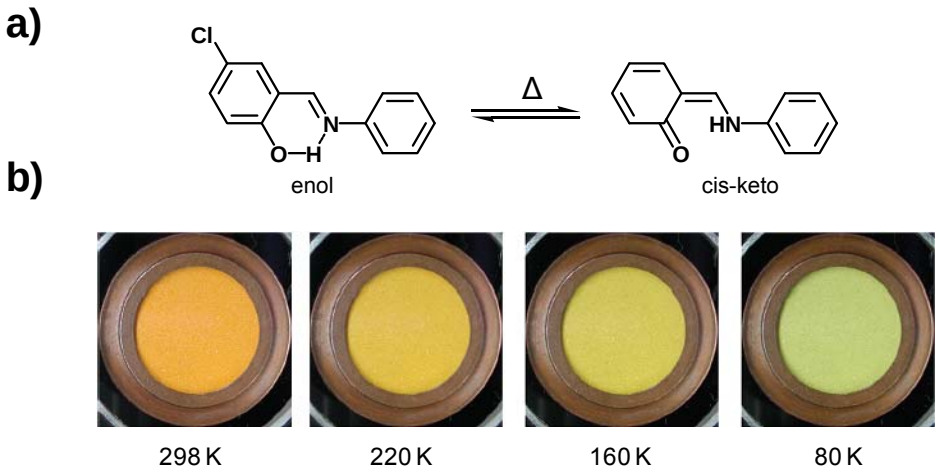

Figure 111. *N*-(5-chloro-2-hydroxybenzylidene)-aniline: a) schematic, and b) photographs of the crystalline solid at different temperatures.

5.1.2. Photochromism of Salicylidineanilines

Photochromism is defined as the reversible photo-colouration of a single chemical species between two states having distinguishably different absorption spectra in the visible region, which are brought about by the action of electromagnetic radiation in at least one direction. Reversible photochemical reactions have potential applications for

photo-electronic devices such as optical memories, switches, sensors, and displays. SAs are an important class of photochromic compounds that show photochromism in the single crystalline form as well as in inclusion compounds. Photochromic SA crystals are generally pale yellow in colour and not fluorescent at room temperature. When photochromic SA crystals are irradiated with UV light (~365 nm), they turn red; when they are left in the dark, or irradiated with visible light (~560 nm), they revert to the original colour.[99] It has been demonstrated that the photo-induced coloured species is the trans-keto form and that the photochromism is caused by the intramolecular hydrogen transfer between the enol and cis-keto form followed by isomerization into the *trans*-keto form (Figure 112).[100] Photochromic SAs have demonstrated remarkable chemical stability, and fatigue resistance (*i.e.,* loss of activity upon prolonged irradiation).[101]

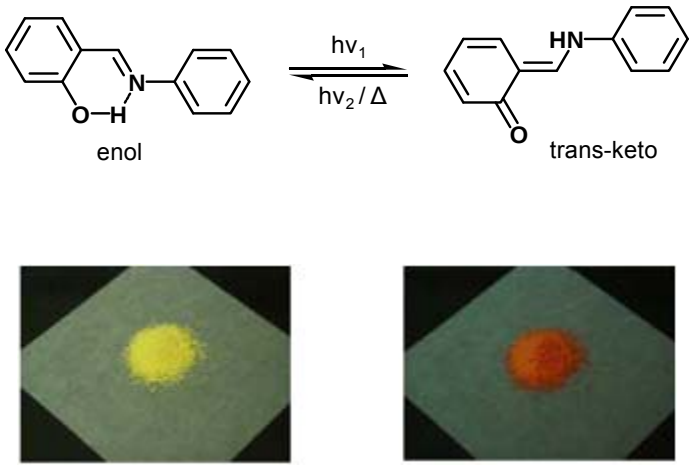

Figure 112. Photochromism of SA: a) mechanism, and b) photographs of SA, before (left) and after (right) uv-irradiation (365 nm).

5.1.3. Crystal Engineering Salicylidenenaniline

Chromic properties in the crystalline state, combined with easy syntheses, make SAs ideal candidates of crystal engineering in order to fine-tune their properties for practical applications. To determine the structure-chromic property relationship of SAs, numerous derivatives have been synthesized over the last several decades. The crystallographic studies of SA derivatives show that, planar SA molecules with a dihedral angle $\varphi < 25°$ (Figure 113) stack face-to-face within short inter-planar distance (ca. 3.5 Å), termed as close-packed structure. The π-π stacking arrangement of the planar molecules in the crystal resist large molecular motion required for isomerization from the enol to the *trans*-keto form in order to show the photochromic property. On the other hand, nonplanar SAs (*i.e.,* $\varphi > 25°$) preclude close contacts in the "open structure" crystal lattice, with sufficient space to undergo isomerization to generate photocoloured *trans*-keto form. Thus, the crystal packing environment plays a guiding role in determining chromic properties of SA derivatives. Thermochromism and photochromism had long been regarded as mutually exclusive properties in SAs.[102] In fact, it has only recently been demonstrated that SAs are generally thermochromic whether they are photochromic or not.[92a]

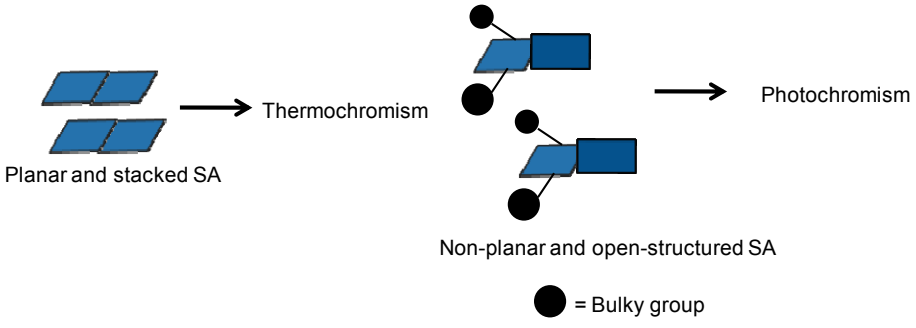

Figure 113. Effect of molecular geometry and packing environment of SA derivatives on chromic property.

The φ angle of SAs has been intentionally increased by introducing bulky substituents (*e.g.,* isopropyl) on the aniline moiety to induce the SA derivative to adopt an open structure for photochromism. In particular, the planar 3,5-dichloro-N-salicylidene-aniline has been shown to be thermochromic, whereas 3,5-dichloro-N-salicylidene-2,6-diisopropylaniline is photochromic (Figure 114).

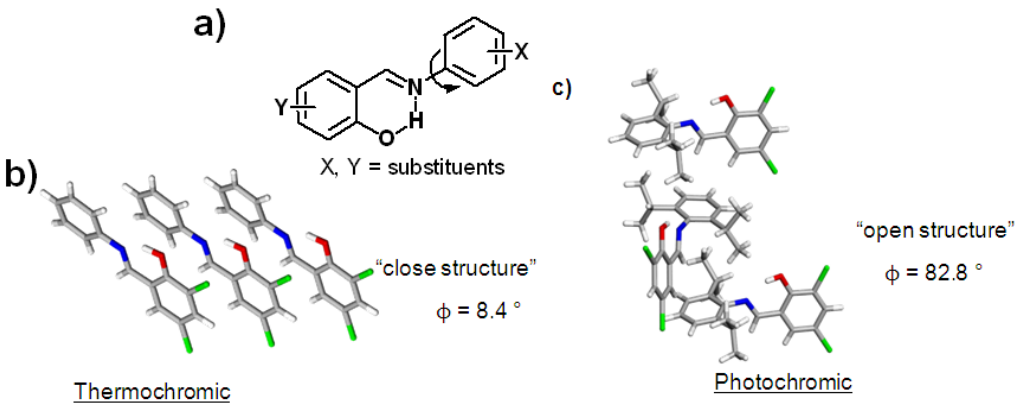

Figure 114. SA derivatives: a) dihedral angle, b) crystal packing in 3,5-dichlorosalicylideneaniline, and c) packing in 3,5-dichloro-2,6-diisopropylsalicylideneaniline.

In this context, 3,5-difluoro-N-salicylidene-2,6-dimethylaniline is photochromic whereas the isostructural 3,5-dichloro and 3,5-dibromo derivatives have been shown to be photo-inactive.[103] Despite similar "close-packed structures," differences in chromic properties of the three derivatives has been attributed to the availability of "reaction room" (*i.e.,* open space for isomerization to take place) in the crystal. Assuming that the phenomenon of thermochromism and/or photochromism is a monotonic function of the molecular geometry (*e.g.,* φ angle), there have been studies to explore whether certain geometries can be allotted to SAs based on their responses to heat and light.[103] In general, no apparent correlation could be established between the substituent characteristics (*i.e.,*

steric, electronic) and chromic property of SAs.[104] The chromic property of a particular SA is also dependent on the polymorphic forms. Several SAs have been demonstrated to form more than one polymorphic form with different chromic properties. Another unique way to modify the chromic behavior of SAs is by inclusion in rigid matrices such as polymers,[105] zeolites,[106] cyclodextrins,[107] and bile acids[108]. The environment of the host matrices have been shown not only to provide enough space for photo-induced isomerization of included SAs, but also slow down the thermo-induced reverse reaction. Although crystallographic studies are crucial to correlate the structure with chromic properties, precise structural informations of SAs within these matrices could not be obtained with high precision even by employing the most reliable single-crystal X-ray diffraction methods. [105] Recently, thermo to photo switching of the chromic properties of a SA derivative *via* inclusion in a porous coordination network has been demonstrated and structurally characterized by single crystal X-ray diffraction.[109] Nevertheless, the crystallinity of the host framework was highly dependent on the co-included solvent molecules while the photo-colouration and photo-decolouration steps had to be conducted at low temperature (120 K).

5.1.4. Crystal Engineering of SA *via* Co-crystallization

MacGillivray et. al. have shown that small organic molecules acting as a linear template (*e.g.*, resorcinol) can preorganize an otherwise photostable solid (*e.g.*, 4,4'-bpe) into a suitable geometry for undergoing photoreaction in solid state. The preorganization of reactant molecules was achieved by formation of a hydrogen-bonded discrete assembly between the template and the molecular recognition group (*i.e.*, pyridine) impregnated on the reactant molecules. The modular technique not only allowed efficient access to molecular targets with different levels of complexity but also allowed the use of various organic molecules as template with different structures and functionalities. Thus,

it is potentially possible to functionalize organic molecules that show interesting physical and/or chemical properties in the solid state in a fashion that also act as a linear template. The utilization of such a template molecule in the preorganization of pyridine derivatized olefins could lead a multicomponent hydrogen-bonded solid where the individual properties of the template molecules are combined with the photoactivity property of the olefin-based molecular component. We envisioned that co-crystallization of functionalized SA molecules with molecules of complementary functionalities would lead to the formation of multi-component molecular assemblies, sustained by noncovalent forces. The substitution of the salicylidene moiety could allow control on the thermo and/or photochromic behaviour of SA derivatives in the solid state whereas the aniline ring can be derivatized into the resorcinol moiety to act as a linear template in preorganizing pyridine-derivatized olefins in the solid state (Figure 115). This approach would potentially be able to form new solids, able to respond to multiple physichemical stimulations (*e.g.*, heat, light).

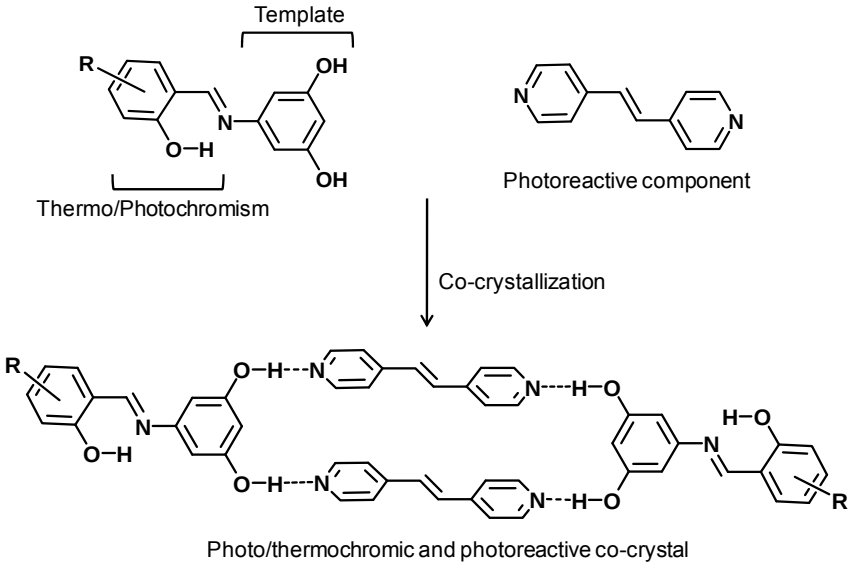

Figure 115. Schematic of the targeted synthesis of photo/thermochromic and photoreactive co-crystal.

We envisaged that SA derivatives, namely N-5-chloro-salicylidene-3,5-dihydroxyaniline (CSDHA), and N-3,5-ditertbutyl-salicylidene-3,5-dihydroxyaniline (CSDHA) (Figure 116a), with a resorcinol moiety integrated into their structures, could act as a linear template in our template-directed solid state approach. The molecules would retain their individual thermo and/or photochromic behaviour in the co-crystal while incorporating additional property of photoreactivity arising from the preorganization of olefinic reactants acting as a second component of the co-crystalline solid. We also explore the possibility to engineer the chromic properties of SA derivatives namely salicylidene-4-hydroxyaniline (SHA), and 5-chlorosalicylidene-4-hydroxyaniline (CSHA) incorporated into hydrogen-bonded multicomponent molecular assemblies (Figure 116b).

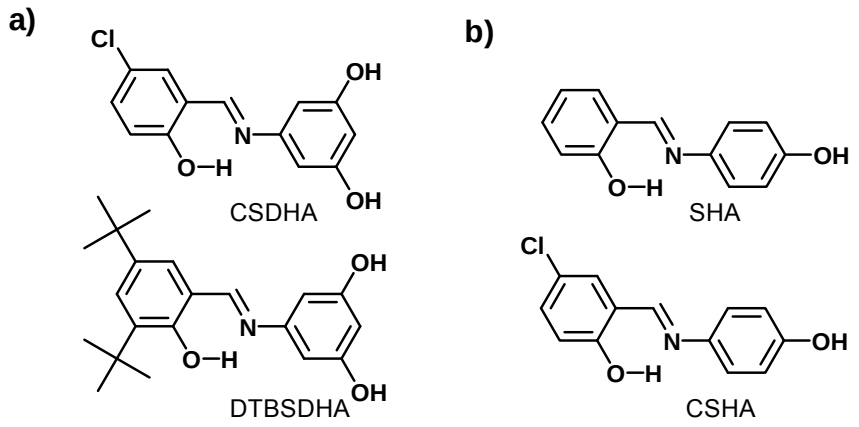

Figure 116. Schematic: a) CSDHA, DTBSDHA, and b) SHA, CSHA.

5.2. Experimental

All reagents and solvents used were reagent grade and commercially available. ethanol, nitromethane, ammonium hydroxide were purchased from Fisher Scientific Co.

Pyrazine, 2,2'-dipyridyl, 4,4'-dipyridyl, 4,4'bpe, 1,2-bis(4-pyridyl)acetylene (4,4'-bpa), salicylaldehyde, 5-chlorosalicylaldehyde, 4-aminophenol and phluoroglucinol were purchased from Sigma-Aldrich Chemical Company. 1,2-bis(4-pyridyl)acetylene was synthesized using standard literature procedures[110].

Single crystal X-ray diffraction experiments were performed on a Bruker-Nonius Kappa CCD diffractometer using MoKα radiation (λ = 0.7107 Å). The structures were solved using direct methods and refined by full-matrix least-squares based on F2. All non-hydrogen atoms were refined using the anisotropic model. Hydrogen atoms bonded to carbon atoms were placed in idealized positions defined by the hybridization of the belonging carbon atom. The positions of hydrogen atoms bonded to oxygen atoms were calculated so as to establish the best possible hydrogen bonds to a nearest neighbour hydrogen bond acceptor. All crystallographic calculations were performed using the set of crystallographic programs WinGX, along with SHELX-97 locally implemented on a Pentium-based PC.

5.2.1 Synthesis of SHA

Synthesis of SHA was achieved by condensing 4-aminophenol and salicylaldehyde (Figure 5). 4-Aminophenol (2 g, 18.34 mmol) and salicylaldehyde (2.24 g, 18.34 mmol) was refluxed in 40 mL of absolute ethanol for 2 hours. The solvent was evaporated at reduced pressure. The orange solid was recrystallized from nitromethane to yield 3.5 g (yield = 90%) of SHA as crystalline orange solid. ^{1}H NMR (DMSO-d_6, δ/ppm): 13.15 (1H, s), 9.75 (1H, s), 8.92 (1H, d), 7.79 (1H, d), 7.48 (1H, dd), 7.29 (1H, t), 7.02 (1H, d), 6.82 (1H, d), 6.80 (2H, d).

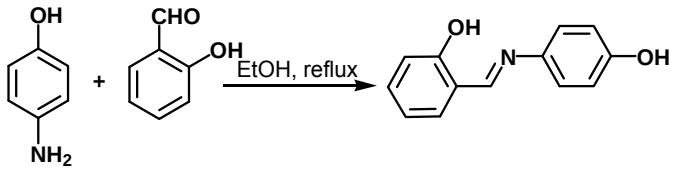

Figure 117. Schematic of the synthesis of SHA.

5.2.2 Synthesis of CSHA

Synthesis of CSHA was achieved by condensing 4-aminophenol and 5-chlorosalicylaldehyde (Figure 5). 4-Aminophenol (2 g, 18.34 mmol) and 5-chlorosalicylaldehyde (2.33 g, 18.34 mmol) was refluxed in 40 mL of absolute ethanol for 2 hours. The solvent was evaporated at reduced pressure. The orange solid was recrystallized from nitromethane to yield 3.2 g (yield = 98%) of CSHA as crystalline orange solid. ^{1}H NMR (DMSO-d_6, δ/ppm): 13.34 (1H, s), 9.80 (1H, s), 8.92 (1H, s), 7.70 (1H, d), 7.42 (1H, d,), 7.35 (2H, d), 7.01 (1H, d), 6.92 (2H, d).

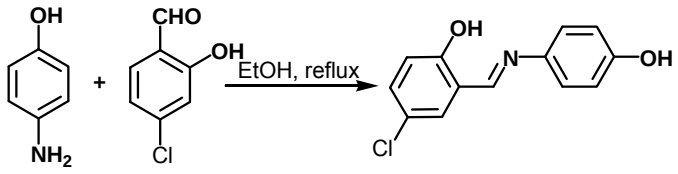

Figure 118. Synthesis of CSHA.

5.2.3 Synthesis of CSDHA

Synthesis of CSDHA was achieved by amination of phluoroglucinol to form 5-aminoresorcinol followed by condensation with 5-chlorosalicylaldehyde (Figure 6). Phluoroglucinol (4 g, 31.74 mmol) was dissolved in 150 ml of concentrated ammonium

hydroxide and stirred at room temperature for 16 hours. The solvent was evaporated at reduced pressure and the resulting solid was recrystallized from boiling nitromethane (50 mL) to yield 5-aminoresorcinol (1.8 g, Yield = 45%) and used immediately without further purification. 5-Aminoresorcinol (2 g, 16 mmol) and 5-chlorosalicylaldehyde (2.5 g, 16 mmol) was refluxed in absolute ethanol (75 mL) for 2 hours. The solvent was evaporated at reduced pressure and the resultant orange solid was recrystallized twice from minimum amount of nitromethane to yield pure CSDHA as orange solid (3.5 g, 83% yield). ^{1}H NMR (DMSO-d_6, δ/ppm): 13.23 (1H, s), 9.56 (1H, s), 8.89 (1H, s), 8.67 (4H, d), 7.81 (1H, s), 7.51 (1H, dd), 7.04 (1H, d), 6.28 (3H, m).

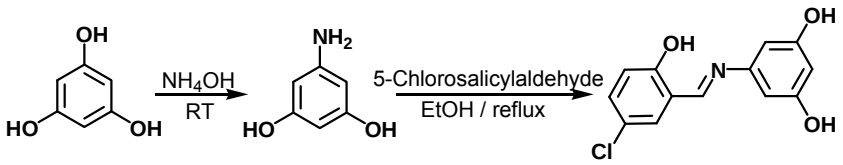

Figure 119. Synthesis of CSDHA.

5.2.4 Synthesis of DTBSDHA

Synthesis of DTBSDHA was achieved by condensing 5-aminoresorcinol with 3,5-ditertbutylsalicylaldehyde. 5-Aminoresorcinol (2 g, 16 mmol) and 3,5-ditertbutylsalicylaldehyde (3.74 g, 16 mmol) was refluxed in absolute ethanol (75 mL) for 2 hours. The solvent was evaporated at reduced pressure and the resultant orange solid was recrystallized twice from minimum amount of nitromethane to yield pure DTBSDHA as orange solid (4.50 g, 82% yield). ^{1}H NMR (DMSO-d_6, δ/ppm): 14.50 (1H, s), 9.50 (2H, s), 8.85 (1H, s), 7.49 (1H, d), 7.37 (1H, d), 6.24 (2H, d), 6.19 (1H, t), 1.40 (9H, s), 1.28 (9H, s).

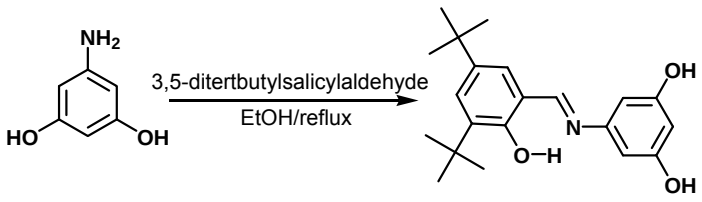

Figure 120. Synthesis of DTBSDHA.

5.2.5 Preparation of co-crystals involving SHA and dipyridyls

Co-crystallization experiments involving SHA were performed by dissolving 50 mg of the compound in 2 mL of nitromethane and adding 16 mg (pyrazine, 4,4'-dipyridyl, 2,2'-dipyridyl) or 18 mg (4,4'-bpe, 4,4'-bpa) of the pyridine based co-crystal former. The solution was heated to boiling and left to cool slowly to room temperature. After standing at room temperature for 5-30 min, the yellow co-crystals that formed were isolated by vacuum filtration, washed with a small amount of nitromethane and air dried. Yields: 65.0 mg (92.72%) for 2(SHA)·(pyrazine), 96.4 mg (97.47%) for 2(SHA)·(4,4'-dipyridyl), 77 mg (90.59%) for 2(mpa)·(2,2'-dipyridyl), 74.4 mg (97.51%) for 2(SHA)·(4,4'-bpe), 70.3 mg (93.48%) for 2(SHA)·(4,4'-bpeth), 81.2 mg (93.87%) for 2(SHA)·(4,4'-bpace).

5.2.6 Thermochromism Experiments

Finely ground samples of the pure SAs and co-crystals were taken in a sealed vial and placed in a dry ice-acetone bath (220 K) and liquid nitrogen bath for 15 min and the colour change of the sample was compared with that of at room temperature (298 K).

5.2.7 Photochromism Experiments

The finely ground powder as well as the single crystals of the materials were placed on watch glasses and irradiated with 365 nm high pressure mercury lamp (96 W) for 60 min.

5.2.8 Photoreactivity Experiments

The experiments involving the photoreaction of solid co-crystals involved finely grinding the sample and placing a 50 mg portion of the obtained crystalline powder between a pair of Pyrex glass plates. The glass plates were then exposed to ultraviolet radiation from a 500 W high pressure mercury lamp in an ACE Glass photochemistry cabinet for 2-3 days.

5.3. Results and Discussion

The thermochromic property of CSDHA as a pure solid and within the co-crystal with 4,4'-bpe will be discussed and rationalized from the simgle crystal structure and packing environment. The photoreactivity of the cocrystals will also be described. The design and synthesis of a photochromic SA, namely DTBSDHA will also be described. Photochromic property of DTBSDHA as a pure solid and within co-crystal along with the photoreactivity of the photoactive component within the co-crystals will be described and explained by the molecular geometry and crystal packing environment. Furthermore, two structurally related thermochromic SAs (*i.e.,* SHA, and CSHA) will be discussed and the change in their chromic properties upon co-crystallization will be rationalized based on their crystal structure. The crystallographic data for the crystals discussed in this chapter

is given in Appendix A (Table A16). Solids discussed in this chapter are given in Table 10.

Table 10. Solids discussed in chapter 5.

(CSDHA)·(4,4'-bpe)	(SHA)·(pyrazine)
(DTBDHA)·(4,4'-bpe)	(SHA)·(4,4'-bpa)
(SHA)·2(4,4'-dp)	(CSHA)·(4,4'-bpe)

When CSDHA was co-crystallized with 4,4'-bpe from nitromethane, orange crystals appeared after slow evaporation of the solution. ^{1}H NMR spectroscopy of the crystals shows the presence of both components in a 1:1 stoichiometric ratio. The colour change of the solid (CSDHA)·(4,4'-bpe) from orange (298 K) to yellow (220 K) shows the CSDHA retained the thermochromic property even after the co-crystal formation (Figure 121).

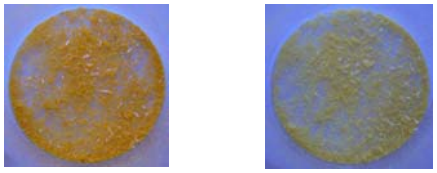

Figure 121. Photographs of (CSDHA)·(4,4'-bpe) at different temperatures.

The co-crystals were UV-irradiated in a broadband medium pressure mercury photoreactor in order to explore the photoreactivity of the co-crystal. The ^{1}H NMR spectroscopy shows the disappearance of the olefin peak at 7.58 ppm and emergence of the cyclobutane peak at 4.7 ppm. The pyridyl protons were also shifted upfield from 8.7

ppm and 8.4 ppm to 7.7 ppm and 7.3 ppm, respectively. The observation is consistent with the formation of 4,4'-tpcb, stereospecifically and in quantitatively yield. The co-crystal even after the photoreaction maintained the thermochromic property Based on the hydrogen bond formation between resorcinol moieties and 4,4'-bpe, and the hydrogen bonding geometries of SA molecules, it can be envisioned that the hydrogen-bond between CSDHA and 4,4'-bpe would lead to a four component discrete assembly where the 4,4'-bpe molecules will be stacked within 4.2 Å and the OHs of the resorcinol moiety in CSDHA molecules would form hydrogen bonds with pyridines on both sides of the stacked 4,4'-bpe molecules (Figure 122).

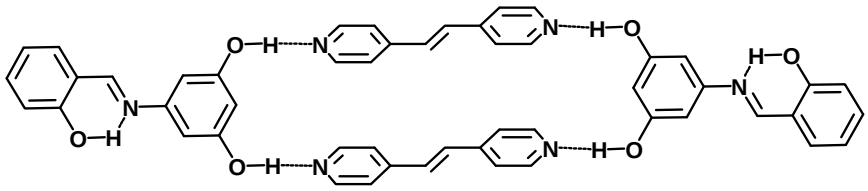

Figure 122. Schematic of the expected self-assembly of 2(CSDHA)·2(4,4'-bpe).

The crystal structure of (CSDHA)·(4,4'-bpe) showed that two CSDHA and two 4,4'-bpe molecules formed a four component, hydrogen-bonded discrete assembly 2(CSDHA)·2(4,4'-bpe), as initially expected. The salicylidene –OH group formed intramolecular hydrogen-bond with the imine nitrogen whereas the resorcinol –OH groups were involved in forming hydrogen-bonds with pyridine moiety of 4,4'-bpe molecules. The 4,4'-bpe molecules were stacked at a distance of 3.75 Å, within the discrete assembly (Figure 123). The 4,4'-bpe molecules of the neighbouring assemblies were far apart with the nearest olefinic distance being 8.30 Å.

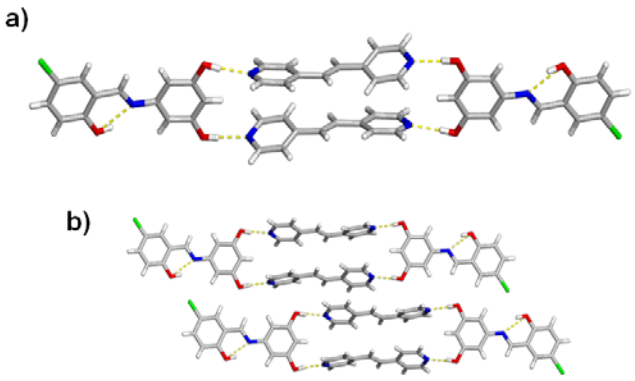

Figure 123. Single crystal structure of 2(CSDHA)·(4,4'-bpe): a) four component discrete assembly, and b) packing of neighbouring assemblies.

A further study of the crystal structure of 2(CSDHA)·(4,4'-bpe) revealed that the CSDHA molecules from the neighbouring assemblies were also stacked in a head-to-tail geometry with an interplanar distance of 3.32 Å (Figure 124). The dihedral angle (*i.e.*, Φ) between the salicylidene and the resorcinol moiety was only 4.4°. The planarity and the close-packed arrangemt of the CSDHA molecules explained the thermochromic behavior of the co-crystal.

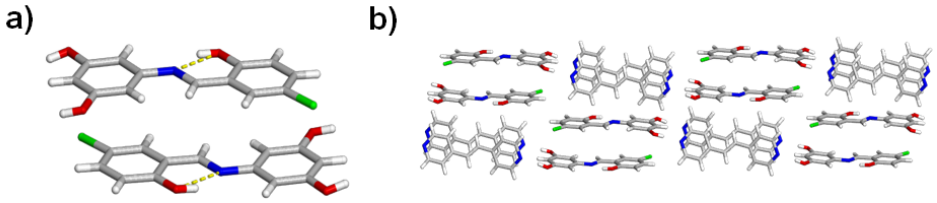

Figure 124. Crystal packing of CSDHA within 2(CSDHA)·2(4,4'-bpe): a) head-to-tail arrangement, and b) neighbouring assemblies.

The ditertbutyl-substituted salicylideneaniline (*i.e.*, DTBDHA) was observed to be photochromic as both powder and single crystalline form. The pale yellow crystalline

blades turned to bright red upon exposure to uv-light (365 nm). The photocolor was both thermally and photochemically reversible. We envisioned that co-crystallization of DTBDHA with 4,4'-bpe could lead to a bimolecular co-crystal where the resorcinol moiety of DTBDHA would act as a template to align the 4,4'-bpe molecules in close proximity for undergoing photoreaction. The salicylidene moiety of DTBDHA would still retain the photochromic character within the co-crystal, thus leading to the formation of a crystal where two different properties are integrated in two different molecular units connected by non-covalent interactions (*i.e.*, hydrogen-bonds). When DTBDHA was co-crystallized with 4,4'-bpe from nitromethane as a solvent, pale yellow coloured co-crystals of (DTBDHA)·(4,4'-bpe) appeared upon slow evaporation of the solvent. The presence of both molecular components in a 1:1 stoichiometric ration within the co-crystal was confirmed by ^{1}H NMR spectroscopy. The crystals when irradiated with uv-light (365 nm), turned into bright-red even after very short period of irradiation (*e.g.*, 1-2 min). When exposed to visible light, the photocolour disappeared in seconds (Figure 125). The photocolour also disappeared slowly (*e.g.*, 4-6 h) when kept in dark at room temperature. When the powder of the material was uv-irradiated (broadband high pressure mercury), no colour change was observed even after very long period of irradiation (*ca.* 10 h). The observation can be explained by the reversible nature of the photochromism and the presence of both 365 nm and 560 nm light in the spectrum of the broadband photoreactor.

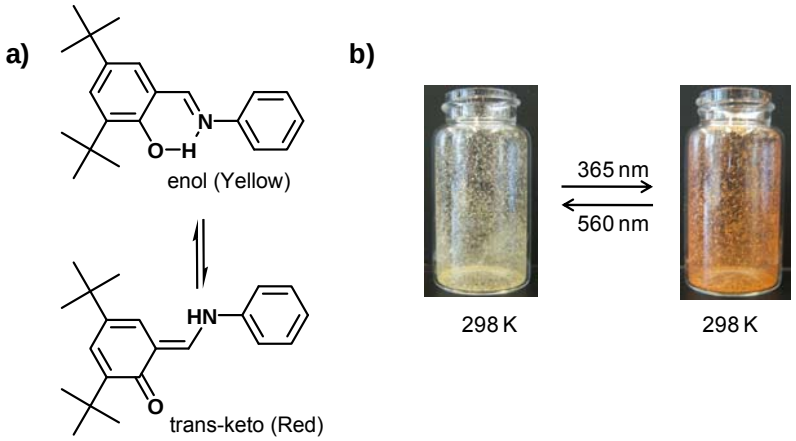

Figure 125. Photochromism of (DTBDHA)(4,4'-bpe): a) mechanism, and b) photographs before and after uv-irradiation.

However, the ^{1}H NMR spectrum of the co-crystal after broadband uv-irradiation showed the formation of cyclobutane ring. Thus, it was concluded that DTBDHA was able to align 4,4'-bpe in suitable orientation to undergo [2+2]photodimerization in solid state. To rationalize the photochromism and photoreactivity of (DTBDHA)·(4,4'-bpe) from their molecular packing environment, the co-crystal was studied by single crystal x-ray diffraction. The single crystal structure of (DTBDHA)·(4,4'-bpe) showed the expected formation of a four component discrete assembly consisting of two DTBDHA, and two 4,4'-bpe molecules held together by four O-H···N hydrogen bonds (Figure 126). The resorcinol moiety of DTBDHA formed intermolecular O-H···N hydrogen-bonds with pyridine ring of 4,4'-bpe molecules where the salicylidene –OH groups formed intramolecular hydrogen bond with imine nitrogen. The 4,4'-bpe molecules were stacked parallel at a distance of 3.90 Å, satisfying the geometric criteria for [2+2]photodimerization in solid state. As the nearest distance of olefins in between neighbouring assemblies was 5.06 Å, higher than the upper limit of olefinc distance to undergo photoreaction in solid state, cyclobutane is expected to form by photodimerization within assembly.

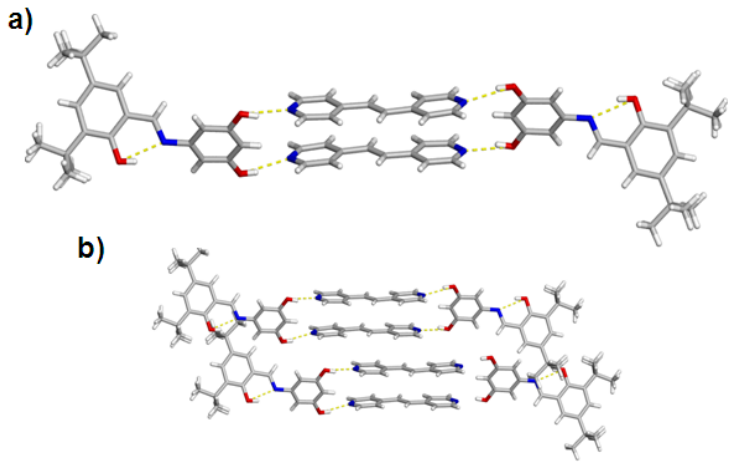

Figure 126. Single crystal structure of (DTBDHA)·(4,4'-bpe): a) four-component hydrogen-bonded discrete assembly, and b) packing environment of neighbouring assemblies.

The DTBDHA molecules were non-planar within the co-crystal as commonly observed in the crystal structures of the photochromic salicylidenenanilines. The resorcinol moiety twisted from the plane of the salicylidene with a dihedral angle (*i.e.*, ϕ) of 47.9 °. The two tert-butyl groups acted as space opener in between the DTBDHA molecules to avoid close-packed arrangement in the crystal where the nearest distance between the salicylidene rings was 7.13 Å apart (Figure 127).

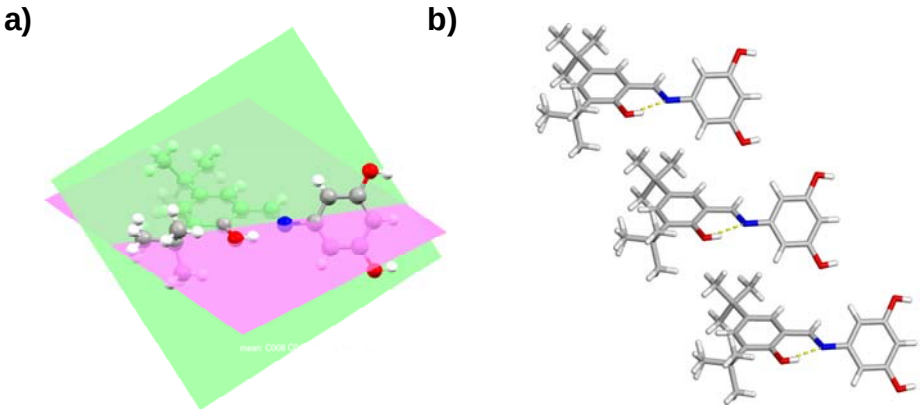

Figure 127. DTBDHA molecules within 2(DTBDHA)·2(4,4'-bpe): a) dihedral angle, and b) packing arrangement.

In this section of this chapter, change of chromic behavior of SA derivarives within hydrogen-bonded co-crystals will be descrived. As observed before, SA molecules included in various matrices (e.g., polymer, deoxycholic acid, metal-organic frameworks) lead to changes in their chromic properties. SA molecules, regardless of their chromic behavior as a pure solid form, turn to photochromic when included in various matrices. The thermo-to-photo stwitching of SA derivatives upon inclusion was explained by the isolation of SA molecules in the inclusion compound avoiding the close-packed environment. We envisioned that co-crystallization of appropriate SA derivatives would lead to changes in crystal packing environment of pure SA derivatives and could lead to changes in chromic properties. We envisioned that isolation co-crystallization of SHA with pyridyls would result in the formation of co-crystals with 2:1 (SHA: dipyridyl) stoichiometry where the 4-OH groups would involve in forming intermolecular O-H···N hydrogen bonds with pyridyl nitrogens. In particular, when SHA was co-crystallized with 4,4'-dipyridyl from nitromethane, bright yellow co-crystal formed upon slow cooling of the solution (Figure 128). The ^{1}H NMR spectra of the resultant co-crystals showed the 2:1 (SHA: 4,4'-dipyridyl) stoichiometry of the components.

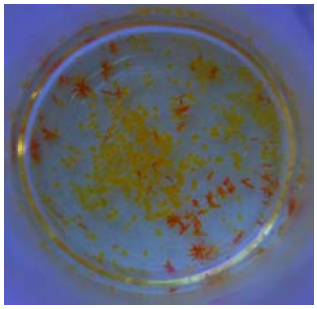

Figure 128. Photograph of SHA as a pure solid (orange) and the co-crystal 2(SHA)·(4,4'-dipyridyl) (yellow).

When, the yellow crystals of 2(SHA)·(4,4'-dipyridyl) were UV-irradiated (365 nm), the colour changed to red. The thermal stability of the red form was high. The red colour was persistent in the dark for days at room temperature and stored in an oven (46 °C) for prolonged time (4 h) without any visible decolouration or chemical decomposition. On the contrary, when the sample was irradiated with visible light (560 nm), the red colour disappeared and the sample regained the original yellow colour (Figure 129). The observation is consistent with other photochromic SAs with the notable exception that the co-crystals show unprecedented high thermal stability.

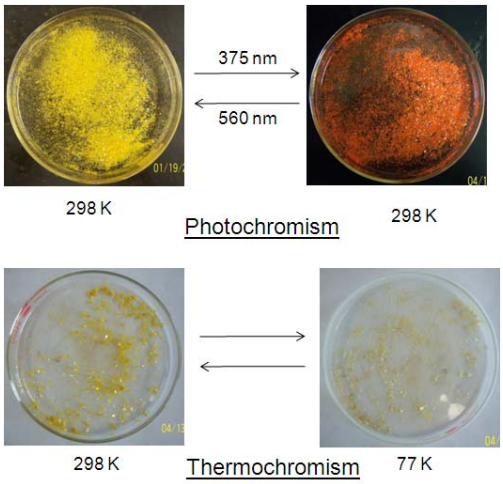

Figure 129. Photographs of the reversible photochromism and thermochromism shown by 2(SHA)·(4,4'-dipyridyl).

N-salicylidene-4-hydroxyaniline (SHA) has been reported to show thermochromism as a pure solid.[111] The single crystal structure of SHA as a pure solid (Figure 130) had two crystallographically independent molecules in the asymmetric unit. The molecules are essentially planar with φ angle of 9.7° for one molecule and 12.3° for the other. The molecules stack head to head, as well as head to tail in the crystal with a short contact distance of 3.7 Å, thus, forming a close-packed structure. While there are

intramolecular hydrogen bonds between the *ortho*-hydroxy group and the imine nitrogen in the salicylidene moiety, the independent molecules are connected by intermolecular hydrogen bonds between the hydroxyl groups in the aniline moiety.

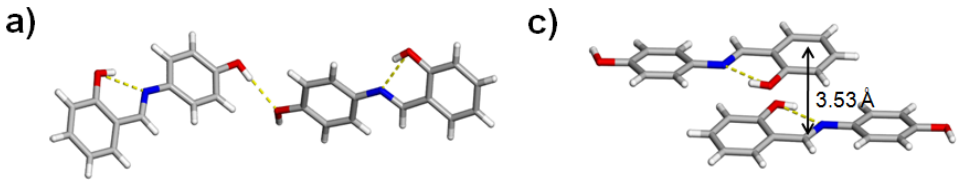

Figure 130. Single crystal structure of SHA: a) asymmetric unit with intra and intermolecular hydrogen bonds, and c) close-stacked arrangement of SHA molecules in the crystal lattice.

The single crystal structure of 2(SHA)·(4,4'-dipyridyl) revealed that the 4-OH groups of the SHA molecules were involved in hydrogen bonding with the pyridyl nitrogens, as expected (Figure 131). The SHA molecules are essentially planar with a φ nearly zero. The observation contradicts the fact that photochromic SAs have high φ (*i.e.,* φ > 25°). Athough planar, SHA molecules aren't involved in close-packed stacking interactions in the co-crystal with the shortest distance between two parallel SHA molecules being 5.88 Å. The above structural criteria conform to the formation of "open structure" reported for other photochromic SAs.

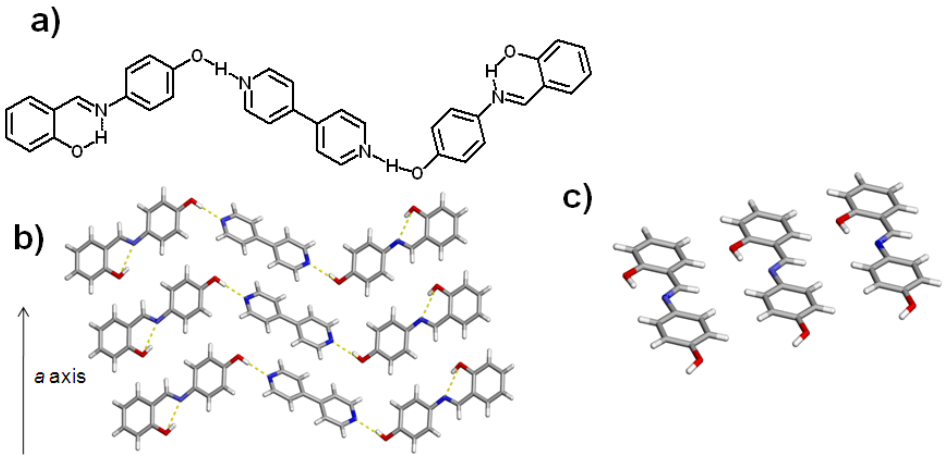

Figure 131. Single crystal structure of 2(SHA)·(4,4'-dipyridyl): a) schematic, b) crystal packing along crystallographic *a*-axis, and c) relative positioning of SHA molecules in the crystal.

Thus, the change from close-packed structure to an open structure *via* co-crystal formation prompted the change in chromic properties of SHA. In order to examine the modularity of the process, SHA was co-crystallized with other dipyridyls with different size and geometry. The chromic property of the resultant co-crystals is shown in Table 11.

Table 11. Results of co-crystallization and chromic properties involving SHA.

Salicylideneaniline (sha)	Cocrystal Former	Chromic Property
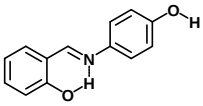 Thermochromic		Thermochromic
	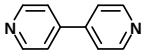	Photochromic and Thermochromic
	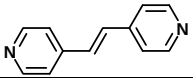	Thermochromic
	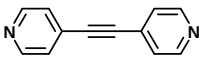	Photochromic and Thermochromic
	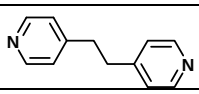	Thermochromic

Results in Table 11 show that the photochromic property of the co-crystals is dependent on the position of nitrogen on the pyridyl ring as well as the length of the dipyridyl compounds. Surprisingly, co-crystallization of SHA with 4,4'-dp, 4,4'-bpe, and 4,4'-bpa lead to hydrogen-bonded co-crystals that show photochromism. This is the first observation of the thermo-to-photo switching phenomena of SA within an organic-based co-crystal. The single crystalline nature of the co-crystals also allowed the structural study of the

When SHA was co-crystallized with pyrazine in a 2:1 (SHA: pyrazine) stoichiometric ratio using nitromethane as solvent, yellow coloured crystal crystals appeared upon slow evaporation of the solvent at room temperature. The presence of both components in a 1:1 stoichiometry within the co-crystal was confirmed by ^{1}H NMR spectroscopy. The uv-irradiation (365 nm) of the co-crystals in both single crystal and powder form did not induce any photocolour at room temperature even after a long irradiation time (16 h). The single crystal structure analysis of (pyrazine)·(SHA) showed the formation of a three component hydrogen-bonded discrete assembly consisting of two SHA and a pyrazine molecule. The salicylidene –OH group was engaged in intramolecular hydrogen bonding with the imine nitrogen atom, whereas the phenol –OH group formed intermolecular hydrogen-bond with pyrazine nitrogen atoms (Figure 132).

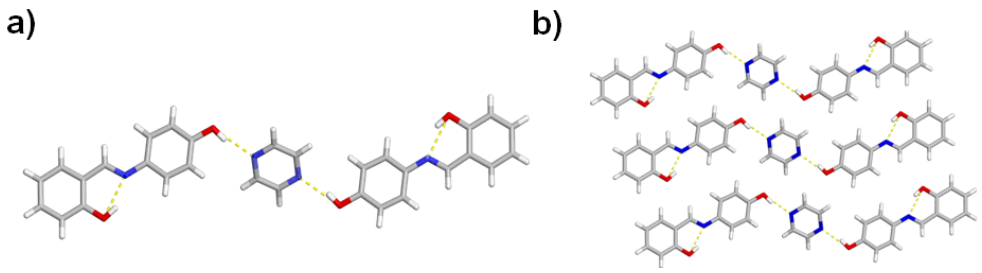

Figure 132. Single crystal structure of (pyrazine)·2(SHA): a) three component discrete hydrogen-bonded assembly, and b) crystal packing environment along crystallographic *a* axis.

The SHA molecules with the co-crystal were essentially planar (Φ= 5.3°) with the nearest SHA molecules 6.14 Å apart from each other. The relative geometry and orientation of SHA molecules within (pyrazine)·2(SHA) were similar to that of SHA molecules in photochromic (4,4'-DP)·2(SHA). A further detailed crystallographic study of (pyrazine)·2(SHA) was needed in order to explain the non-photochromic behaviour of the co-crystal. The crystal packing of (4,4'-DP)·2(SHA) showed that a pyrazine molecule was stacked over the salicylidene moiety of the SHA molecule within a distance of 3.36 Å. The close-packed environment around the salicylidene moiety could lead to a restricted movement of the ring, explaining the non-photochrmic behaviour.

When SHA was co-crystallized with 4,4'-bpa using nitromethane as solvent, light yellow crystals came out of the solution upon slow evaporation of the solvent. The ^{1}H NMR spectroscopy confirmed the presence of both components in a 1:1 stoichiometry. The light yellow co-crystals, when uv-irradiated (12 h, 365 nm) in both single crystal as well as powder form, turned to bright red. The single crystal structure of (4,4'-bpa)·2(SHA) (Figure 133) showed the formation of a three component hydrogen-bonded assembly as previously observed for other dipyridyls. The phenol –OHs were involved in forming intermolecular hydrogen-bond with pyridine rings of 4,4'-bpa whereas the salicylidene –OHs were engaged in the intramolecular hydrogen-bond formation process. The SHA

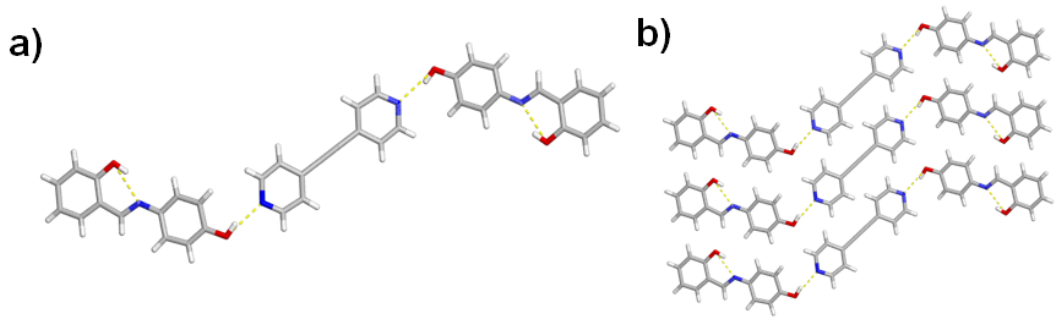

Figure 133. Single crystal structure of (4,4'-bpa)·2(SHA): a) three component hydrogen-bonded discrete assembly, and b) crystal packing environment along the crystallographic *a* axis.

molecules within the co-crystal were essentially planar (Φ = 0.9°), where the nearest distance between the SHA molecules were 5.95 Å, forming a open structure as previously observed in (4,4'-dp)·2(SHA).

Thus, the correlation of the single crystal structure with the chromic behaviour of the SHA within hydrogen-bonded co-crystals revealed that the chromicity of SHA is highly dependent on the crystal packing environment around the SHA molecules. The formation an open structure is the necessary condition for showing photochromic property. The dihedral angle is shown to be less-important for guiding the chromic property for a certain crystal environment.

A related solid, namely N-5-chlorosalicylidene-4-hydroxyaniline, (CSHA) where a hydrogen atom at the benzylidene moiety is replaced by a chlorine atom, was also examined to understand the effect of crystal packing on the chromic property in the crystalline state. CSHA has been demonstrated to be thermochromic in the crystalline state and there are no polymorphic variations reported up to date.[98] The single crystal structure of CSHA (Figure 134) showed similar intra and intermolecular hydrogen-bonded netwrok structure as seen in case of SHA. On the contrary, the intermolecular hydrogen bonding between nonplanar (Φ = 30.5°) CSHA molecules led to the formation

of a 1D chain. Based on the angle criteria, CSHA should be photochromic but there are no reports with this behaviour. A detailed study of the crystal packing showed that the salicylidene moiety of the CSHA molecules were close-stacked within a distance of 3.52 Å. Thus, the photoinactivity of CSHA can be explained by the lack of enough space in the crystal to allow large molecular movement required for photo-induced isomerization.

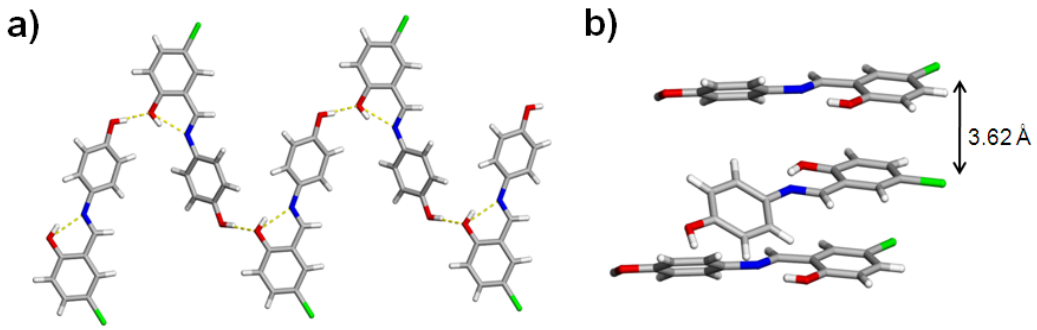

Figure 134. Single crystal structure of CSHA: a) hydrogen-bonded 1D chain, and b) relative close-stacked arrangement.

CSHA was co-crystallized with bipyridyl derivatives and their chromic properties were studied in order to correlate with the results obtained for that of SHA. When CSHA was co-crystallized with 4,4'-bpe, orange co-crystals were obtained. The ^{1}H NMR study showed the co-crystals contained CSHA and 4,4'-bpe in a 2:1 stoichiometry, similar to the co-crystals obtained from SHA. When irradiated with UV-light (350 nm), no change in colour was observed both at low temperature (220 K) and room temperature, ever after a prolonged period of irradiation (6 h). On the contrary, the co-crystals retained the thermochromic property of the pure crystalline CSHA. In fact, the orange crystals turned yellow at 220 K. Thus, change in molecular structure (i.e, replacement of hydrogen with a chlorine atom) drastically affected the chromic properties of the co-crystals. To investigate the whether the crystal packing environment of CSHA in the co-crystal

corresponds to the expected close packed structure as of in the pure crystalline form, (4,4'-bpe)·2(CSHA) was studied by single crystal X-ray diffraction. The single crystal structure of 2(4,4'-bpe)·(CSHA) (Figure 135) showed the formation of a three component hydrogen-bonded strand as observed in (4,4'-dp)·2(SHA). The OH group on the aniline moiety formed O-H···N hydrogen bonds (O···N distance 2.73 Å, and 2.75 Å) with the pyridines. The OH group on the salicylidene moiety formed intramolecular hydrogen bonds with the imine nitrogen as generally observed in SA molecules. Unlike SHA, the CSHA molecules in (4,4'-bpe)·2(CSHA) are not planar. The angle of twist of the aniline moiety with respect to the salicylidene part is 36.4°. Thus, with respect to the angle criteria discussed above the co-crystal should be photochromic. In order to explain the photoinactivity of the co-crystal, further studies on the crystal packing environment were carried out. In the crystal, the planar salicylidene part of the nearest CSHA molecules was close-packed within 3.67 Å. Thus, the photo-inactivity of the co-crystal can be explained by the lack of enough space in the co-crystal for photoisomerization of CSHA molecules.

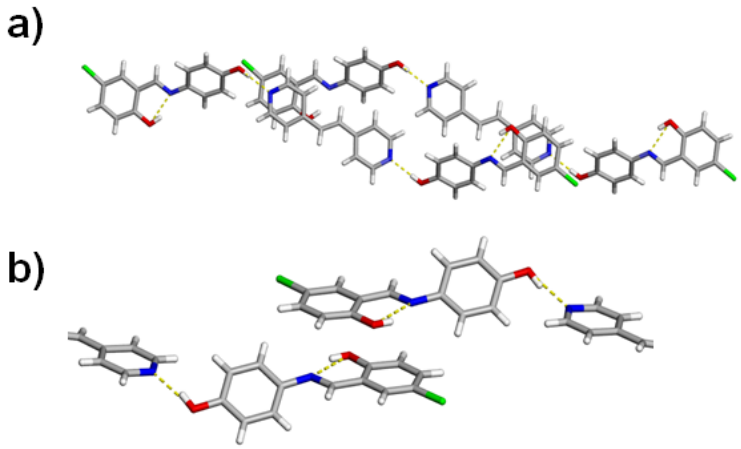

Figure 135. Single crystal structure of (4,4'-bpe)·(CSHA): a) three component hydrogen-bonded discrete stands, and b) relative orientation of neighbouring CSHA molecules.

5.4. Conclusion

In this chapter, crystal engineering of the chromic properties of salicylideneanilnes *via* co-crystallization has been demonstrated. Bicomponent co-crystals has also been synthesized that are able to show multiple properties in the single crystalline form. Specifically, SA molecules, first engineered to show thermo or photochromism has also been derivatized to act as a linear template to preorganize olefins for photoreaction in the solid state. Thus, the newly formed co-crystalline solids are able to show both photoreactivity (irreversible) and thermo/photochromic properties (reversible). The study also shows that co-crystallization of salicylideneaniline derivatives with co-crystal formers having complementary functional groups lead to bicomponent co-crystal with chromic properties, different from the parent compound. The change in chromic properties in the co-crystals is due to the change in the crystal packing environment and relative dispositions of SA molecules. This study also shows that the planarity of the SA molecules is not the sole criteria of determining the chromic characters, but the crystal packing environment (*i.e.,* close or open structure).

CHAPTER 6: CONCLUSION

The use of supramolecular chemistry and noncovalent interactions to guide reactions in solids has been attracting much attention in recent years. There are several fascinating examples appeared in the literatures recently where supramolecular forces play an important role in deciding the reaction pathway and product outcome. Reactions in solid state or more frequently in multicomponent molecular assemblies has been demonstrated as a general way to synthesize molecular targets efficiently, synthetically challenging otherwise. The results in this dissertation show the generality and synthetic viability of template-directed solid state synthesis in a multi-component molecular solid for rational design and efficient supramolecular construction of synthetically challenging molecular targets of different levels of complexity.

The molecular recognition unit in our templated synthetic approach (i.e. pyridine) has been modified *via* substitution at hydrogen bonding site (i.e. ortho) as well as the reaction site (i.e. meta). The results show that even with increased structural complexity, the reactants were successfully preorganized in solid state for reaction and provided targeted products stereospecifically and in quantitative yield. Even by increasing the steric bulk at the hydrogen bonding site, *via* switching to more constrained hydrogen bonding environment (*e.g.,* 2-pyridyl), templated synthesis and template-switching strategy has demonstrated remarkable control over the formation of required assembly and reaction. Crystallization condition, concentration of template, and the hydrogen bonding strength of the molecular recognition unit have been shown to play important role in deciding the outcome of an assembly. During the study, there were a few interesting reactions observed where the olefins reacted in a rare SCSC fashion within a multicomponent solid with potential applications in material science. A reactive metal-organic solid was also discovered where the monoolefin is behaving as a potential dioefin to undergo photopolymerization in solid state to form a stereoregular polymer with

cyclobutane rings at the main chain. The SCSC reaction allowed the characterization of the product *via* single crytal X-ray diffraction. In general, this is the first systematic study on the synthetic viability of templated solid state synthesis.

The application of templated synthesis in solid state for the construction of a conformationally flexible and supramolecularly complex, cofacial terpyridine has been demonstrated to be an important moiety in the biomimetic catalysts. But, the challenges involved in their synthesis, largely outweigh their important contribution in material science. As the templated solid state synthetic approach frequently lead to the synthesis of molecular targets stereospecifically and in quantitative yield, the application of templated synthesis towards the synthesis of cofacial aromatics was conceived. Terpyridine was chosen as the molecular recognition unit as well as the aromatic surface given the presence of three pyridines as potential hydrogen-bonding site for preorganizing olefins in solid state as well as various applications of terpyridine units in coordination directed self-assemblies. Nevertheless, this was the first study towards the hydrogen-bonded self-assemblies involving terpyridine and also reactivity of terpyridine-based olefins in general. The results show that we have been successful to synthesize a cofacial terpyridine (*i.e.,* hh-TPC) *via* template-controlled [2+2]photodimerization stereospecifically and in quantitative yield where the terpyridine units are cofacially displaced by a cyclobutane ring. The metal-coordination of hh-TPC showed that metal ions can be placed in close proximity, as initially designed.

Efficient supramolecular synthesis of [2.2]pyridinophanes in paddlane framework has been demonstrated. [2.2]Pyridinophanes, a constrained bridged heteroaromatics, are of particular interest for their aromaticity, ring strain, optical properties and applications in material sciences. The synthesis of [2.2]pyridinophane involve multiple steps, harsh reaction condition, challenging separation procedures and low yield. The isolation of the syn- geometry, where the aromatic rings are stacked on each other are of limited success. Pyridine-derivatized diolefins with a pyridine linker in the middle was selected as a

potential reactant that could lead to the formation of [2.2]pyridinophanes within a paddlane framework *via* templated [2+2]photodimerization reaction in solid state. The result show that the pyridinophanes were synthesized stereospecifically, quantitatively and in gram amounts. The paddlane unit automatically fixed the relative orientation so the bridged pyridines in the syn geometry. The pyridinophanes were also successfully applied in the field of coordination-driven self-assembles to form metal-organic frameworks.

Apart from chemical properties (*e.g.,* reactivity), some physical properties (*e.g.,* optical) have also been demonstrated to be dependent on the crystal packing environment. Control over the chromic properties of salicylideneanilines *via* crystal engineering has been demonstrated. Thermochromism or photochromism with photoreactivity properties of two different molecular components has successfully been combined *via* co-crystallization. Given the two components of the co-crystals can independently respond to different physical stimulations (*e,g*, temp, light) and show different properties such as photoreactivity and thermochromism, co-crystallization has been shown as a modular method of combining properties in a single crystal. Various potential applications (*e.g.*, optical switch, optical data storage) in material science are envisioned.

Co-crystallization of functionalized SA derivatives with co-crystal formers having complementary recognition unit, has been demonstrated. The effect of crystal packing environment on the crystal packing environment has been studied. The results showed that a thermochromic SA molecule became photochromic in a bicomponent molecular crystal. The modularity of the technique was also studied by co-crystallization studies with related co-crystal formers of different size and geometries.

In summary, the results in this dissertation show that template-controlled solid state synthesis can provide unprecedented control in solid state synthesis. The efficient synthesis of complex molecular targets, synthetically challenging *via* conventional

synthetic routes, has shown the generality and synthetic applicability of reactions conducted in co-crystals. Stereospecific, quantitative and gram scale synthesis of molecular targets also allow the downstream applications of molecular targets in synthetic chemistry as well as material science. Not only reactivity, co-crystallization can be exploited as a general technique to modify physical properties of a pure molecular solid. Consequently, reactions in co-crystals hold great potential in design, synthesis, and applications of molecular targets with different levels of complexity, and are expected to be considered and appreciated as an efficient mainstream organic synthetic strategy in near future.

REFERENCES

1. (a) Nicolaou, K. C.; Sorensen, E. J., *Classics in Organic Synthesis*. Wiley-VCH: New York, 1996; Vol. Vol 1; (b) Nicolaou, K. C.; Sorensen, E. J., *Classics in Organic Syntesis II*. Wiley-VCH: New York, 2003; Vol. 2.

2. Nicolaou, K. C.; Vourloumis, D.; Winssinger, N.; Baran, P. S. *Angew. Chem. Int. Ed.* **2000,** *39*, 44.

3. Corey, E. J. *Chem. Soc. Rev.* **1988,** *17*, 111.

4. Corey, E. J. *Angew. Chem. Int. Ed. Eng.* **1991,** *30*, 455.

5. Stryer, L., *Biochemistry*. M.H. Freeman and Co.: New York, 1988.

6. Lehn, J. M., *Supramolecular Chemistry*. VCH: New York, 1995; Vol. 1.

7. Braga, D. *Chem. Commun.* **2003**, 2751.

8. Steed, J. W.; Atwood, J. L., *Supramolecular Chemistry*. Wiley: New York, 2009.

9. Desiraju, G. R. *Angew. Chem. Int. Ed. Engl.* **1995,** *34*, 2311.

10. Desiraju, G. R. *Acc. Chem. Res.* **2002,** *65*, 565.

11. (a) Metrangolo, P.; Resnati, G. *Chem. Eur. J.* **2001,** *7*, 2511; (b) Metrangolo, P.; Neukirch, H.; Pilati, T.; Resnati, G. *Acc. Chem. Res.* **2005,** *38*, 386.

12. Desiraju, G. R. *Angew. Chem. Int. Ed.* **2007,** *46*, 8342.

13. Desiraju, G. R. *Chem. Commun.* **1997**, 1475.

14. M. C. Etter, T. W. P. *J. Am. Chem. Soc.* **1988,** *110*, 5896.

15. (a) Desiraju, G. R. *Chem. Commun.* **2003,** *5*, 466; (b) Dunitz, J. D. *CrystEngComm* **2003,** *5*, 506.

16. Sarma, J. A. R. P.; F. H. A., Vanessa J. Hoy, Judith A. K. Howard, Ram Thaimattam,; Kumar Biradhad, Desiraju, G. D. *Chem. Commun.* **1997**, 101.

17. BS, S. *Ars. Pharm.* **2009,** *50*, 99.

18. Bernstein, J., *Polymorphism in Molecular Crystals*. Clarendon Press: Oxford, 2002.

19. Behr, J. P., *The Lock and Key Principle. The State of the Art-100 Years on*. Wiley: New York, 1994.

20. Lehn, J. M. *proc. Nat. Acad. Sci. USA* **2002,** *99*, 4763.

21. Lindoy, L. F.; Atkinson, I. *Science* **2002,** *295*, 2418.

22. Chapman, R. G.; Sherman, J. C. *Tetrahedron* **1997,** *53*, 15911.

23. Gerbeleu, N. V.; Aroin, V. B.; Burgess, J., *Template Synthesis in Macrocyclic Chemistry*. Wiley: Chichester, 1999.

24. Raymo, F. M.; Stoddart, J. F. *Chem. Rev.* **1999,** *99*, 1643.

25. Kelly, T. R.; Zhao, C.; Bridger, G. J. *J. Am. Chem. Soc.* **1989,** *111*, 3744.

26. Bassani, D. M.; Darcos, V.; Mahony, S.; Desvergne, J. P. *J. Am. Chem. Soc.* **2000,** *122*, 8795.

27. Garibay, M. A. G. *Acc. Chem. Res.* **2003,** *36*, 491.

28. Tanaka, K.; Kaupp, G., *Solvent-free Organic Synthesis*. 2 ed.; Wiley: New York, 2009.

29. Ramamurthy, V.; Venkatesan, K. *Chem. Rev.* **1987,** *87*, 433.

30. Khuong, T. A. V.; Nunez, J. E.; Godinez, C. E.; Garcia-Garibay, M. A. *Acc. Chem. Res.* **2006,** *39*, 413.

31. Klebe, G. *Struct. Chem.* **1990,** *1*, 597.

32. Khan, M.; Brunklaus, G.; Enkelmann, V.; Spiess, H. W. *J. Am. Chem. Soc.* **2008,** *130*, 1741.

33. Lauher, J. W.; Fowler, F. W.; Goroff, N. S. *Acc. Chem. Res.* **2008,** *41*, 1215.

34. Schmidt, G. M. J. *Pure Appl. Chem.* **1971,** *27*, 647.

35. Coates, G. W.; Dunn, A. R.; Henling, L. M.; Ziller, J. W.; Lobkovsky, E. B.; Grubbs, R. H. *J. Am. Chem. Soc.* **1998,** *120*, 3641.

36. Desiraju, G. R.; Sharma, C. V. K. M. *Chem. Commun.* **1991**, 1239.

37. Feldman, K. S.; Campbell, R. F. *J. Org. Chem.* **1995,** *60*, 1924.

38. MacGillivray, L. R. *Acc. Chem. Res.* **2008,** *41*, 280.

39. MacGillivray, L. R.; Reid, J. L.; Ripmeester, J. A. *J. Am. Chem. Soc.* **2000,** *122*, 7817.

40. Friscic, T. M., L. R. *Chem. Commun.* **2003**, 1306.

41. Gao, X. F., T.; MacGillivray, L. R. *Angew. Chem., Int. Ed.* **2004,** *43*, 232.

42. Papaefstathiou, G. S. K., A. J.; MacGillivray, L. R. *Chem. Commun.* **2001**, 2462.

43. Friscic , T. M., L. R. *Chem. COmmun.* **2005**, 5748.

44. Praetorius, P. K., F. *Ber.* **1910,** *43*, 2744.

45. Lewis, F. D., Oxman, J. D., Huffman, J. C. *J. Am. Chem. Soc.* **1984,** *106*, 466.

46. Papaefstathiou, G. S. Z., Z.; Geng, L.; MacGillivray, L. R. *J. Am. Chem. Soc.* **2004,** *126*, 9158.

47. Chu, Q.; Swenson, D. C.; MacGillivray, L. R. *Angew. Chem. Int. Ed.* **2005,** *44*, 2569.

48. Han, Y. F.; Lin, Y. J.; Jia, W. G.; Wang, G. L.; Jin, G. X. *Chem. Commun.* **2008**, 1807.

49. Stein, A. M., B. J.; Schoroden, R. C. *Adv. Mater.* **2000,** *12*, 1403.

50. (a) Rowsell, J. L. C. Y., O. M. *Angew. Chem. Int. Ed.* **2005,** *44*, 4670; (b) Millward, A. R.; Yaghi, O. M. *J. Am. Chem. Soc.* **2005,** *127*, 17998.

51. (a) et.al., L. R. M. *Acc. Chem. Res.* **2008,** *41*, 280; (b) Vittal, J. J. *Coord. Chem. Rev.* **2007,** *251*, 1781; (c) Wang, X., Y.; Wang, Z. M.; Gao, S. *Chem. Commun.* **2007**, 1127.

52. Mal, K. N., Fujiwara, M., Tanaka, Y. *Nature* **2003,** *421*, 350.

53. Michaelides, A., Skoulika, S., Siskos, M., *Chem. Commun.* **2004**, 2418.

54. Toh, L. N., Nagarathinam, M., Vittal, J. J., *Angew. Chem. Int. Ed.* **2005,** *44*, 2237.

55. Papaefstathiou, G. S.; Georgiev, I. G.; Friščić, T.; MacGillivray, L. R. *Chem. Commun.* **2005**, 2974.

56. Nagarathinam, M.; Vittal, J. J. *Angew. Chem. Int. Ed.* **2006,** *45*, 4443.

57. Michaelides, A., Skoulika, S., Siskos, G. M., *CrystEngComm* **2008,** *10*, 817.

58. (a) Papaefstathiou, G. S., MacGillivray, L. R., *Angew. Chem. Int. Ed.* **2002,** *41*, 2070; (b) Papaefstathiou, G. S., Milios, C., MacGillivray, L. R. *Microporous Mesoporous Mater.* **2004,** *71*, 11.

59. Blake, A. J., Champness, N. R., Chung, S. S. M., Li, W. S., Schroder, M., *Chem. Commun.* **1997**, 1675.

60. Sarma, J. A. R. P.; Desiraju, G. R. *Pro. Indian Aead. Sci.* **1986,** *96*, 599.

61. Hasegawa, M. *Chem. Rev.* **1983,** *83*, 507.

62. Maekawa, Y.; Lim, P.; Saigo, K.; Hasegawa, M. *Macromolecules* **1991,** *24*, 5752.

63. Hasegawa, M.; Kinbara, K.; Adegawa, Y.; Saigo, K. *J. Am. Chem. Soc.* **1993,** *120*, 3820.

64. Toh, N. L.; Nagarathinam, M.; Vittal, J. J. *Angew. Chem. Int. Ed.* **2005,** *44*, 2237.

65. Collman, J. P.; Wagenknecht, P. S.; Hutchison, J. E. *Angew. Chem. Int. Ed.* **1994,** *33*, 1537.

66. (a) Fukuzumi, S. *Bull. Chem. Soc. Jpn.* **2006,** *79*, 177; (b) Collman, J. P.; Hutchison, J. E.; Ennis, M. S.; Lopez, M. A.; Guilardt, R. *J. Am. Chem. Soc.* **1992,** *114*, 8074.

67. (a) Chang, C. J.; Loh, Z. H.; Shi, C.; Anson, F. C.; Ancera, D. G. *J. Am. Chem. Soc.* **2004,** *126*, 10013; (b) Chang, C. J.; Baker, E. A.; Pistorio, B. J.; Deng, Y.; Loh, Z. H.; Miller, S. E.; Carpenter, S. D.; Nocera, D. G. *Inorg. Chem.* **2002,** *41*, 3102.

68. Collman, J. P.; Wang, Z.; Straumansc, A. *J. Org. Chem.* **1998,** *63*, 2424.

69. Crowley, J. D.; Steele, I. M.; Bosnich, B. *Eur. J. Inorg. Chem.* **2005**, 3907.

70. Schubert, U. S.; Eschbaumer, C. *Angew. Chem. Int. Ed.* **2002,** *41*, 2892.

71. (a) Eryazici, I.; Moorefield, C. N.; Newkome, G. R. *Chem. Rev.* **2008,** *108*, 1834; (b) Flamigni, L.; Collin, J. P.; Sauvage, J. P. *Acc. Chem. Res.* **2008,** *41*, 857; (c) Constable, E. C. *Chem. Soc. Rev.* **2007,** *36*, 246.

72. CCDC v 1.12, search date March 10, 2010.

73. The olefinic carbon atoms are only 18.2% of the total non-hydrogen atoms in cinnamic acid.

74. Renaud, F.; Piguet, C.; Bernardinelli, G.; Hopfgartnerc, G.; Bünzli, J. C. G. *Chem. Commun.* **1999**, 457.

75. Kadjane, P.; Charbonnière, L.; Camerel, F.; Lainé, P. P.; Ziessel, R. *J. Fluoresc.* **2008,** *18*, 119.

76. Potts, K. T.; Konwar, D. *J. Org. Chem.* **1991,** *51*, 4815.

77. Gleiter, R.; Hopf, H., *Modern Cyclophane Chemistry*. Wiley: New York, 2005.

78. Furstner, A.; Alcarazo, M.; Krause, H.; Lehmann, C. W. *J. Am. Chem. Soc.* **2007,** *129*, 12676.

79. Vedernikov, A. N.; Huffman, J. C.; Caulton, K. G. *Inorg. Chem.* **2002,** *41*, 6867.

80. Vetrichelvan, M.; Lai, Y. H.; Mok, K. F. *Eur. J. Inorg. Chem.* **2004**, 2086.

81. Baker, M. V.; Brown, D. H.; Haque, R. A.; Simpson, P. V.; Skelton, B. W.; White, A. H.; Williams, C. C. *Organometallics* **2009,** *28*, 3793.

82. Bartholomew, G. P.; Bazan, G. C. *Acc. Chem. Res.* **2001,** *34*, 30.

83. (a) Pahor, N. B.; Calligaris, M.; Randaccio, L. *J. Chem. Soc. Perkin Trans 2* **1978**, 38; (b) Staab, H. A.; Hasselbach, H. J.; Krieger, C. *Liebigs Ann* **1986**, 751

84. N.B.Pahor; M.Calligaris; L.Randaccio *J. Chem. Soc. Perkin Trans 2* **1978**, 38.

85. Y.Kai; N.Yasuoka; N.Kasai *Acta Crystallogr.,Sect.B:Struct.Crystallogr.Cryst.Chem.* **1977,** *33*, 754.

86. (a) Koray, A. R.; Zahn, T.; Ziegler, M. L. *J. Organomet. Chem.* **1985,** *53*, 291; (b) Schulz, J.; Nieger, M.; Vogtle, F. *J. Chem. Soc. Perkin Trans 2* **1992**, 2095.

87. Nishimura, J.; Horikoshi, Y.; Wada, Y.; Takahashi, H.; Sato, M. *J. Am. Chem. Soc.* **1991,** *113*, 3485.

88. Nakamura, Y.; Hayashida, Y.; Wada, Y.; Nishimura, J. *Tetrahedron* **1997,** *53*, 4593.

89. Maekawa, Y.; Kato, S.; Hasegawa, M. *J. Am. Chem. Soc.* **1991,** *113*, 3867.

90. Moorthy, J. N.; Venkatakrishnan, P. *Cryst Grow&Design* **2007,** *7*, 713.

91. Funaki, T.; Inokuma, S.; Ide, H.; Yonekura, T.; Nakamura, Y.; Nishimura, J. *Tett. Lett.* **2004,** *45*, 2393.

92. (a) Harada, J.; Fujiwara, T.; Ogawa, K. *J. Am. Chem. Soc.* **2007,** *129*, 16216; (b) Nassau, K., *The Physics and Chemistry of Color*. 2nd ed.; John Wiley and Sons: New York, 2001.

93. Day, J. H. *Chem. Rev.* **1963,** *63*, 65.

94. Day, J. H. *Chem. Rev.* **1968,** *68*, 649.

95. Bloomquist, D. R.; Willett, R. D. *Coord. Chem. Rev.* **1982,** *47*, 125.

96. Willett, R. D.; Haugen, J. A.; Lebsack, J.; Morrey, J. *Inorg. Chem.* **1974,** *13*, 2510.

97. Hadjoudis, E.; Mavridis, I. M. *Chem. Soc. Rev.* **2004,** *33*, 579.

98. Ogawa, K.; Kasahara, Y.; Ohtani, Y.; Harada, J. *J. Am. Chem. Soc.* **1998,** *120*, 7107.

99. Goto, T.; Tashiro, Y. *J. Fluoresc.* **1997,** *72*, 931.

100. Kawato, T.; Koyama, H.; Nanatomi, H.; Isshiki, M. *J. Photochem.* **1885,** *28*, 103.

101. Arod, F.; Pattison, P.; Schenk, K. J.; Chapuis, G. *Cryst Grow&Design* **2007,** *7*, 1679.

102. Cohen, M. D.; Schmidt, G. M. J. **1662,** *66*, 2442.

103. Fukuda, H.; Amimoto, K.; Koyama, H.; Kawato, T. *Org. Biomol. Chem.* **2003,** *1*, 1578.

104. Ohshima, A.; Momotake, A.; Arai, T. *Bull. Chem. Soc. Jpn.* **2006,** *79*, 305.

105. Yin, M.; Haramoto, Y.; Nanasawa, M. *Plymer Journal* **1995,** *27*, 136.

106. Casades, I.; Alvaro, M.; Garcia, H.; Pillai, M. N. *Eur. J. Org. Chem.* **2002,** *13*, 2074.

107. Pistolis, G.; Gegiou, D.; Hadjoudis, E. *J. Photoch. Photobio. A* **1996,** *93*, 179.

108. Koyama, H.; Kawato, T.; Kanatomi, H.; Matsushita, H.; Yonetani, K. *Chem. Commun.* **1994**, 579.

109. Haneda, T.; Kawano, M.; Kojima, T.; Fujita, M. *Angew. Chem. Int. Ed.* **2007,** *46*, 6643.

110. Ogawa, K.; Fujiwara, T.; Harada, J. *Mol. Crys.t Liq. Cryr.* **2000,** *344*, 169.

111. Coe, B. J.; Harriesa, J. L.; Harrisab, J. A.; Brunschwigb, B. S.; Colesc, S. J.; Lightc, M. E.; Hursthouse, M. B. *Dalton Trans* **2004**, 2935.

APPENDIX A: TABLES OF CRYSTALLOGRAPHIC DATA

Table A1. Relevant Crystallographic parameters for the crystals of (5-CN-res)·2(MPyPE), 2(4,6-diBr-res)·2(MPyPE), (4,6-ditBu-res)·(MPyPCB) .

Compound	(5-CN-res)·2(MPyPE)	2(4,6-diBr-res)·2(MPyPE)	(4,6-ditBu-res)·(MPyPCB)
T / K	293(2)	293(2)	293(2)
λ / Å	0.71073	0.71073	0.71073
Crystal system	triclinic	triclinic	monoclinic
Space group	P -1	P -1	P $2_1/n$
a / Å	10.6786(12)	9.7863(11)	17.9642(18)
b / Å	11.9236(13)	11.6713(13)	10.2297(11)
c / Å	12.5180(13)	14.0433(15)	19.161(2)
α / °	98.948(8)	68.523(5)	90
β / °	111.329(8)	88.140(5)	92.040(5)
γ / °	96.431(8)	81.855(5)	90
V / Å^3	1441.8(3)	1477.3(3)	2351.2(4)
Z	2	2	4
ρ_{calc} / g cm^{-3}	1.211	1.48	1.157
μ / mm^{-1}	0.076	2.77	0.263
2θ range / °	2.96 – 25.54	1.56 – 27.41	1.00 – 27.88
collected reflections	13250	12471	73288
unique reflections	5081	6659	16837
parameters	366	309	411
S	0.954	1.113	1.108
R	0.0817	0.0632	0.0987
wR^2	0.1591	0.1232	0.1878
$\rho_{min, max}$ / e Å^{-3}	0.185, -0.176	0.688, -0.691	0.595, -0.489

Table A2. Relevant crystallographic parameters for the crystals of CPyPE, CPyPCB, and (AgOTf)·(CPyPE).

Compound	CPyPE	CPyPCB	(AgOTf)·(CPyPE)
T / K	200(2)	200(2)	293(2)
λ / Å	0.71073	0.71073	0.71073
Crystal system	orthorhombic	monoclinic	monoclinic
Space group	P bcn	P 2_1/n	P 2_1/n
a / Å	11.9968(13)	11.5063(13)	12.2102(13)
b / Å	11.8022(13)	11.5202(13)	16.8970(18)
c / Å	15.1168(16)	16.1176(17)	13.4755(14)
α / °	90.00	90.00	90.00
β / °	90.00	96.141(5)	104.658(5)
γ / °	90.00	90.00	90.00
V / Å^3	2140.4(4)	2124.2(4)	2689.7(5)
Z	8	4	4
ρ_{calc} / g cm^{-3}	1.339	1.436	1.690
μ / mm^{-1}	0.319	0.326	1.077
2θ range / °	2.96 – 25.54	2.07 – 27.82	5.83 – 25.00
collected reflections	59702	43894	35890
unique reflections	10217	10020	9681
parameters	137	309	353
S	1.109	0.973	1.119
R	0.0671	0.0811	0.0577
wR^2	0.1345	0.2280	0.1577
$\rho_{min, max}$ / e Å^{-3}	0.256, -0.219	2.397, -0.576	1.223, -0.813

Table A3. Relevant crystallographic parameters for the crystals of (AgOTf)(CPyPCB), (res)(MPyPyE), (4,6-diBr-res)(MPyPyCB).

Compound	(AgOTf)(CPyPCB)	(res)(MPyPyE)	(4,6-diBr-res)(MPyPyCB)
T / K	200(2)	200(2)	293(2)
λ / Å	0.71073	0.71073	0.71073
Crystal system	monoclinic	triclinic	monoclinic
Space group	P 2_1/n	P -1	P $2_1/n$
a / Å	12.0745(13)	8.4806(9)	8.9323(10)
b / Å	17.1717(18)	10.4111(11)	11.7224(13)
c / Å	13.3767(14)	10.8853(12)	17.0405(18)
α / °	90.00	69.166(5)	90.00
β / °	107.172(5)	72.543(5)	90.404(5)
γ / °	90.00	68.332(6)	90.00
V / Å^3	1563.8(3)	818.89(15)	1784.2(3)
Z	4	1	2
ρ_{calc} / g cm^{-3}	1.388	1.096	1.229
μ / mm^{-1}	0.255	0.073	2.301
2θ range / °	1.73 – 27.49	2.04 – 25.69	2.11 – 25.41
collected reflections	37930	12273	19595
unique reflections	9646	2946	6504
parameters	209	219	226
S	1.13	1.099	1.101
R	0.0885	0.0809	0.0752
wR^2	0.2690	0.1894	0.2106
$\rho_{min, max}$ / e Å^{-3}	1.696, -0.571	0.354, -0.247	1.037, -0.501

Table A4. Relevant crystallographic parameters for the crystals of (res)·(CPyPyE), (4,6-ditBu-res)·(CPyPyE), (res)·(MPyMPyE).

Compound	(res)·(CPyPyE)	(4,6-ditBu-res)·(CPyPyE)	(res)·(MPyMPyE)
T / K	200(2)	190(2)	293(2)
λ / Å	0.71073	0.71073	0.71073
Crystal system	monoclinic	triclinic	triclinic
Space group	P 2_1/n	P -1	P -1
a / Å	12.9868(14)	8.6860(10)	9.6817(11)
b / Å	10.1008(11)	10.7123(12)	10.0629(11)
c / Å	13.1740(14)	14.2805(15)	10.4142(11)
α / °	90.00	102.328(5)	71.703(5)
β / °	99.395(5)	104.252(5)	64.205(5)
γ / °	90.00	98.120(5)	72.772(5)
V / Å^3	3278.3(6)	1231.53	852.09(16)
Z	4	2	1
ρ_{calc} / g cm^{-3}	1.664	1.685	1.249
μ / mm^{-1}	2.114	1.176	0.081
2θ range / °	1.59 – 27.49	1.52 – 27.88	2.17 – 25.40
collected reflections	27667	53820	34789
unique reflections	7513	17201	5866
parameters	380	316	219
S	1.102	1.133	0.955
R	0.0415	0.0395	0.0606
wR^2	0.1196	0.1026	0.1667
$\rho_{min, max}$ / e Å^{-3}	1.715, -1.413	0.608, -1.232	0.548, -0.220

Table A5. Relevant crystallographic parameters for the crystals of (46-diBr-res)·(3M2Py4CPE), (AgClO3)·(4C3PyPE), (AgClO3)·(4C3PyPCB).

Compound	(46-diBr-res)·(3M2Py4CPE)	(AgClO3)·(4C3PyPE)	(AgClO3)·(4C3PyPCB)
T / K	200(2)	190(2)	190(2)
λ / Å	0.71073	0.71073	0.71073
Crystal system	monoclinic	triclinic	triclinic
Space group	P 2_1/n	P -1	P -1
a / Å	16.0614(17)	8.6860(10)	11.1347(12)
b / Å	11.7944(13)	10.7123(12)	13.4490(14)
c / Å	17.5408(18)	14.2805(15)	17.6811(19)
α / °	90.00	102.328(5)	103.313(5)
β / °	115.192(5)	104.252(5)	101.100(5)
γ / °	90.00	98.120(5)	96.489(5)
V / Å^3	2649.9(5)	1231.53	2493.8(5)
Z	2	2	2
ρ_{calc} / g cm^{-3}	1.623	1.685	1.414
μ / mm^{-1}	0.896	1.176	1.098
2θ range / °	1.99 – 26.02	1.52 – 27.88	1.21 – 25.35
collected reflections	37930	53820	38024
unique reflections	7141	17201	8887
parameters	209	316	641
S	1.131	1.133	1.834
R	0.0562	0.0395	10.58
wR^2	0.1487	0.1026	0.3278
$\rho_{min, max}$ / e Å^{-3}	0.958, -0.859	0.608, -1.232	2.884, -5.640

Table A6. Relevant crystallographic parameters for the crystals of (46-diI-res)·2(MPy4CPE), (5-OMe-res)·2(MPy4CPE), (46-ditBu-res)(4Py4CpCB).

Compound	(46-diI-res)·2(MPy4CPE)	(5-OMe-res)·2(MPy4CPE)	(46-ditBu-res)(4Py4CpCB)
T / K	200(2)	190(2)	190(2)
λ / Å	0.71073	0.71073	0.71073
Crystal system	triclinic	triclinic	triclinic
Space group	P -1	P -1	P -1
a / Å	9.9185(11)	10.4636(11)	17.9642(18)
b / Å	11.7876(13)	12.9499(14)	10.2297(11)
c / Å	14.7888(16)	12.9734(14)	19.161(2)
α / °	112.414(5)	114.026(5)	90.00
β / °	91.301(5)	105.548(5)	92.040(5)
γ / °	96.813(5)	93.174(5)	90.00
V / Å^3	1582.8(3)	1519.6(3)	3519.0(6)
Z	2	2	4
ρ_{calc} / g cm^{-3}	1.723	1.249	1.157
μ / mm^{-1}	2.190	0.249	0.070
2θ range / °	1.99 – 26.02	1.75 – 27.43	1.53 – 27.92
collected reflections	37930	29107	73288
unique reflections	7141	6949	16837
parameters	209	383	411
S	1.131	1.002	1.108
R	0.0562	0.0480	0.0592
wR^2	0.1487	0.1293	0.1514
$\rho_{min, max}$ / e Å^{-3}	0.958, -0.859	0.359, -0.294	0.595, -0.489

Table A7. Relevant crystallographic parameters for the crystals of (4C3PyPyE), (res)·(4C3PyPyE), (4-hex-res)·(4C3PyPyE).

Compound	(4C3PyPyE)	(res) (4C3PyPyE)	(4-hex-res) (4C3PyPyE)
T / K	200(2)	190(2)	190(2)
λ / Å	0.71073	0.71073	0.71073
Crystal system	monoclinic	monoclinic	monoclinic
Space group	P 2_1/n	P 2_1/c	C2/c
a / Å	10.1524(11)	12.9868(14)	30.668(4)
b / Å	9.9763(11)	10.1008(11)	16.0231(17)
c / Å	10.9504(12)	13.1740(14)	14.3391(15)
α / °	90.00	90.00	90.00
β / °	112.218(5)	115.192(5)	105.026(5)
γ / °	90.00	90.00	90.00
V / Å^3	1026.74(19)	1563.8(3)	6805.3(13)
Z	4	4	8
ρ_{calc} / g cm^{-3}	1.403	1.388	1.585
μ / mm^{-1}	0.335	0.255	0.252
2θ range / °	2.33 – 27.98	1.73 – 27.49	2.42 – 25.35
collected reflections	28621	43199	34425
unique reflections	4912	7161	12356
parameters	137	383	386
S	1.131	1.102	0.994
R	0.0343	0.0829	0.0683
wR^2	0.0943	0.2448	0.1828
$\rho_{min, max}$ / e Å^{-3}	0.279, -0.206	1.669, -0.452	0.705, -0.349

Table A8. Relevant crystallographic parameters for the crystals of (4-dodec-res)·2(4C3PyPyE), (res)·2(4C3PyPyE), (res)·(4C3PyPyCB).

Compound	(4-dodec-res)·2(4C3PyPyE)	(res)·2(4C3PyPyE)	(res)·(4C3PyPyCB)
T / K	200(2)	200(2)	190(2)
λ / Å	0.71073	0.71073	0.71073
Crystal system	triclinic	triclinic	triclinic
Space group	P -1	P -1	P -1
a / Å	7.6184(9)	7.4406(8)	7.7071(9)
b / Å	10.5652(12)	12.3956(13)	9.3152(10)
c / Å	23.889(3)	14.6487(16)	19.2319(19)
α / °	84.300(5)	92.700(5)	77.687(5)
β / °	86.404(5)	103.158(5)	80.060(5)
γ / °	82.277(5)	95.463(5)	71.854(5)
V / Å^3	1893.6(4)	1306.3(2)	1273.5(2)
Z	2	2	2
ρ_{calc} / g cm^{-3}	1.719	1.382	1.6
μ / mm^{-1}	0.243	0.285	0.270
2θ range / °	1.72 – 27.85	1.65 – 27.90	1.09 – 25.35
collected reflections	42805	22138	27327
unique reflections	8829	6104	4677
parameters	455	335	344
S	1.084	1.040	1.294
R	0.0549	0.0919	0.0442
wR^2	0.1241	0.2516	0.1077
$\rho_{min, max}$ / e Å^{-3}	0.604, -0.511	2.496, -0.857	0.286, -0.288

Table A9. Relevant crystallographic parameters for the crystals of (5-OMe-res)·2(2CPy4CPE), (res)·2(2CPy4CPE), (4,6-diI-res)·(26CPyPyCB).

Compound	(5-OMe-res)·2(2CPy4CPE)	(res)·2(2CPy4CPE)	(4,6-diI-res)·(26CPyPyCB)
T / K	200(2)	200(2)	200(2)
λ / Å	0.71073	0.71073	0.71073
Crystal system	triclinic	triclinic	triclinic
Space group	P -1	P -1	P -1
a / Å	7.6184(9)	7.4406(8)	9.0917(10)
b / Å	10.5652(12)	12.3956(13)	10.7274(12)
c / Å	23.889(3)	14.6487(16)	21.789(3)
α / °	84.300(5)	92.700(5)	87.628(5)
β / °	86.404(5)	103.158(5)	88.951(5)
γ / °	82.277(5)	95.463(5)	68.771(5)
V / Å^3	1893.6(4)	1306.3(2)	1979.2(4)
Z	2	2	2
ρ_{calc} / g cm^{-3}	1.719	1.382	3.926
μ / mm^{-1}	0.243	0.285	6.910
2θ range / °	1.72 – 27.85	1.65 – 27.90	1.87 – 27.91
collected reflections	42805	22138	34937
unique reflections	8829	6104	9347
parameters	455	335	470
S	1.084	1.040	1.068
R	0.0549	0.0919	0.0303
wR^2	0.1241	0.2516	0.0841
$\rho_{min, max}$ / e Å^{-3}	0.604, -0.511	2.496, -0.857	1.205, -0.954

Table A10. Relevant crystallographic parameters for the crystals of TPE, (5-I-res)·(TPE), (5-I-res)·(hh-TPC).

Compound	TPE	(5-I-res)·(TPE)	(5-I-res)·(hh-TPC)
T / K	200(2)	200(2)	200(2)
λ / Å	0.71073	0.71073	0.71073
Crystal system	monoclinic	triclinic	monoclinic
Space group	P 2_1/c	P -1	P 2_1/n
a / Å	14.2711(15)	7.5310(9)	17.8364(19)
b / Å	8.1049(9)	13.2092(14)	13.0324(14)
c / Å	15.0547(16)	25.014(3)	21.830(3)
α / °	90.00	91.805(5)	90.00
β / °	93.885(5)	91.456(5)	99.141(5)
γ / °	90.00	95.530(5)	90.00
V / Å^3	1737.3(3)	2474.5(5)	5010.0(10)
Z	4	4	5
ρ_{calc} / g cm^{-3}	1.611	1.598	1.511
μ / mm^{-1}	0.097	1.329	0.852
2θ range / °	1.43 – 25.38	1.55 – 25.77	1.37 – 25.41
collected reflections	42805	27518	47743
unique reflections	8829	8974	16607
parameters	236	633	640
S	1.332	1.063	1.03
R	0.0931	0.0709	0.0775
wR^2	0.3079	0.1733	0.1772
$\rho_{min, max}$ / e Å^{-3}	1.050, -0.406	0.944, -0.840	0.722, -0.933

Table A11. Relevant crystallographic parameters for the crystals of hh-TPC , (4,6-diBr-res)·(TPE), (4,6-diI-res)·(TPE)**.**

Compound	hh-TPC	(4,6-diBr-res)·(TPE)	(4,6-diI-res)·(TPE)
T / K	150(2)	290(2)	290(2)
λ / Å	0.71073	0.71073	0.71073
Crystal system	triclinic	monoclinic	monoclinic
Space group	P -1	P 2_1/c	P 2_1/c
a / Å	15.7403(17)	11.1330(12)	11.1705(12)
b / Å	16.4372(17)	25.475(3)	25.888(3)
c / Å	18.0283(19)	8.9929(10)	9.2658(10)
α / °	101.809(5)	90.00	90.00
β / °	115.044(5)	94.544(5)	95.121(5)
γ / °	91.270(5)	90.00	90.00
V / Å^3	4105.2(8)	2542.5(5)	2668.8(5)
Z	3	4	4
ρ_{calc} / g cm^{-3}	1.175	1.822	1.735
μ / mm^{-1}	0.077	2.506	2.388
2θ range / °	1.28 – 25.40	2.52 – 25.35	1.57 – 25.41
collected reflections	59286	37736	20224
unique reflections	18314	9289	9588
parameters	975	328	326
S	1.616	1.041	1.546
R	0.1510	0.0499	0.0624
wR^2	0.4346	0.0997	0.1242
$\rho_{min, max}$ / e Å^{-3}	1.909, -0.548	0.316, -0.400	1.391, -0.961

Table A12. Relevant crystallographic parameters for the crystals of (rtcc-hh-TPC), (Zn-TPC), (Cu-TPC).

Compound	rtcc-hh-TPC	(Zn-TPC)	(Cu-TPC)
T / K	150(2)	150(2)	150(2)
λ / Å	0.71073	0.71073	0.71073
Crystal system	monoclinic	triclinic	monoclinic
Space group	C2/c	P -1	C2/c
a / Å	46.215(5)	13.4654(14)	30.119(4)
b / Å	7.6608(9)	14.1770(15)	20.405(3)
c / Å	22.195(3)	18.8934(19)	16.2840(17)
α / °	90.00	72.059(5)	90.00
β / °	114.240(5)	73.500(5)	100.895(5)
γ / °	90.00	64.793(5)	90.00
V / Å^3	7165.2(15)	3055.3(5)	9827(2)
Z	6	2	4
ρ_{calc} / g cm^{-3}	1.208	1.423	1.457
μ / mm^{-1}	0.077	1.018	0.941
2θ range / °	1.84 – 25.31	1.00 – 25.35	1.00 – 27.88
collected reflections	47748	42275	94841
unique reflections	13055	11105	23477
parameters	470	528	636
S	1.069	0.941	1.083
R	0.0802	0.0716	0.088
wR^2	0.1767	0.1905	0.2543
$\rho_{min, max}$ / e Å^{-3}	0.840, -0.459	1.148, -0.614	1.117, -0.968

Table A13. Relevant crystallographic parameters for the crystals of 2(res)·(4BrTPE), and (VT)($AgClO_4$)CH_3CN).

Compound	2(res)·(4BrTPE)	(VT)($AgClO_4$)CH_3CN)
T / K	200(2)	293 (2)
λ / Å	0.71073	0.71073
Crystal system	triclinic	triclinic
Space group	P -1	P -1
a / Å	15.7167(17)	16.0333(17)
b / Å	16.3749(17)	19.052(2)
c / Å	19.851(2)	13.2449(14)
α / °	85.512(5)	91.805(5)
β / °	69.566(5)	90.00
γ / °	73.066(5)	90.00
V / Å^3	4578.2(8)	90.00
Z	8	8
ρ_{calc} / g cm^{-3}	0.264	1.532
μ / mm^{-1}	0.233	1.153
2θ range / °	1.10 – 25.34	1.66 – 25.32
collected reflections	62969	87111
unique reflections	15976	14712
parameters	1167	263
S	1.048	1.104
R	0.1197	0.0521
wR^2	0.3045	0.1627
$\rho_{min, max}$ / e Å^{-3}	0.738, -0.715	1.125, -1.408

Table A14. Relevant crystallographic parameters for the crystals of (5-OMe-res)(35bpep), (35pyri)(CH_3NO_2)(H2O)2, and (Cu-35pyri).

Compound	(5-OMe-res)(35bpep)	(35pyri)(CH_3NO_2)(H_2O)$_2$	(Cu-35pyri)
T / K	190(2)	190(2)	190(2)
λ / Å	0.71073	0.71073	0.71073
Crystal system	monoclinic	monoclinic	monoclinic
Space group	P 2	P 2_1/c	P 2/c
a / Å	7.6837(9)	11.4524(12)	15.8075
b / Å	10.8168(12)	21.408(3)	22.9630
c / Å	29.472(3)	14.5337(16)	30.6660
α / ^{o}	90.00	90.00	90
β / ^{o}	92.065(5)	106.791(5)	95.56
γ / ^{o}	90.00	90.00	90
V / Å^3	2447.9(5)	3411.3(7)	2351.2(4)
Z	2	4	4
ρ_{calc} / g cm^{-3}	0.482	1.111	1.157
μ / mm^{-1}	0.033	0.067	0.263
2θ range / ^{o}	1.38 – 25.37	1.75 – 25.35	1.00 – 27.88
collected reflections	26476	69523	71660
unique reflections	8841	12471	33044
parameters	600	468	411
S	1.987	1.563	1.108
R	0.02037	0.0908	0.0987
wR^2	0.5126	0.1112	0.1878
$\rho_{min, max}$ / e Å^{-3}	1.296, -0.860	0.508, -0.427	0.595, -0.489

Table A15. Relevant crystallographic parameters for the crystals of (26bpep), and (res)·(26bpep)·(CH_3NO_2).

Compound	(26bpep)	(res)·(26bpep)·(CH_3NO_2)
T / K	190(2)	293(2)
λ / Å	0.71073	0.71073
Crystal system	triclinic	triclinic
Space group	P -1	P -1
a / Å	5.8930(17)	8.2035(9)
b / Å	11.392(4)	10.2049(11)
c / Å	22.228(8)	28.657(3)
α / °	102.843(14)	85.145(5)
β / °	96.25(2)	81.772(5)
γ / °	90.55(2)	71.974(5)
V / Å^3	1445.4(8)	2255.7(4)
Z	1	2
ρ_{calc} / g cm^{-3}	1.010	1.164
μ / mm^{-1}	0.069	0.075
2θ range / °	1.83 – 25.53	1.44 – 25.34
collected reflections	8104	25047
unique reflections	3167	8013
parameters	388	578
S	1.620	1.018
R	0.2604	0.01044
wR^2	0.5375	0.2624
$\rho_{min, max}$ / e Å^{-3}	0.735, -0.504	0.508, -0.427

Table A16. Relevant crystallographic parameters for the crystals of (res)(26bpep)(photoactive), (26pyri)$(PhCH_3)_2$.

Compound	(res)(26bpep)(photoactive)	(26pyri)$(PhCH_3)_2$
T / K	293(2)	190(2)
λ / Å	0.71073	0.71073
Crystal system	monoclinic	triclinic
Space group	$P2_1/n$	P -1
a / Å	14.9185(16)	8.8525(10)
b / Å	10.3365(11)	9.9758(11)
c / Å	27.124(3)	22.694(3)
α / °	90.00	102.379(5)
β / °	95.552(5)	93.083(5)
γ / °	90.00	105.494(5)
V / Å^3	4163.0(8)	1873.2(4)
Z	4	2
ρ_{calc} / g cm^{-3}	1.262	1.012
μ / mm^{-1}	0.082	0.061
2θ range / °	2.76 – 25.00	1.85 – 25.37
collected reflections	13250	25047
unique reflections	5081	8013
parameters	545	499
S	1.042	1.079
R	0.0444	0.0768
wR^2	0.1197	0.2338
$\rho_{min, max}$ / e Å^{-3}	0.172, -0.169	0.400, -0.281

Table A17. Relevant crystallographic parameters for the crystals of (4,4'-bpe)(csha), (4,4'-bpe)·(csdha), (4,4'-bpe)·(tbsdha).

Compound	(4,4'-bpe)·(csdha)	(4,4'-bpe)·(tbsdha)	(44bp)·(sha)
T / K	190(2)	190(2)	293(2)
λ / Å	0.71073	0.71073	0.71073
Crystal system	triclinic	triclinic	monoclinic
Space group	P-1	P-1	$Pbc2_1$
a / Å	8.8309	7.8499	5.8872
b / Å	10.1401	10.4537	13.1634
c / Å	12.9855	19.317	38.7950
α / °	69.528	95.164	90.00
β / °	84.802	95.974	90.00
γ / °	78.828	109.492	90.00
V / Å^3	1068.4	1473.0	3006.44
Z	1	1	2
ρ_{calc} / g cm^{-3}	1.279	1.158	1.392
μ / mm^{-1}	0.086	0.075	0.456
2θ range / °	1.67-25.43	1.07-25.41	1.69 – 25.00
collected reflections	12952	33895	10695
unique reflections	3577	5813	5650
parameters	292	352	441
S	1.021	1.073	1.123
R	0.0611	0.0557	0.0876
wR^2	0.1624	0.1468	0.1269
$\rho_{min, max}$ / e Å^{-3}	0.360, -0.297	0.431, -0.329	0.465, -0.343

Table A18. Relevant crystallographic parameters for the crystals of (pyrazine)·(sha), (4,4'-bpa)·(sha), and (4,4'-bpe)·(csha).

Compound	(pyrazine)·(sha)	(4,4'-bpa)·(sha)	(4,4'-bpe)·(csha)
T / K	190(2)	190(2)	190(2)
λ / Å	0.71073	0.71073	0.71073
Crystal system	monoclinic	monoclinic	triclinic
Space group	$P2_1/n$	$P2_1/c$	P1
a / Å	13.1000	18.928	6.1390(7)
b / Å	6.1452	5.956	11.0486(12)
c / Å	15.7803	13.515	12.4060(13)
α / °	90.00	90.00	77.210(5)
β / °	91.211	100.40	84.727(5)
γ / °	90.00	90.00	80.671(5)
V / Å^3	1270.1	1498.5	808.36(15)
Z	2	1	2
ρ_{calc} / g cm^{-3}	1.325	1.278	1.392
μ / mm^{-1}	0.09	0.086	0.250
2θ range / °	2.00-24.99	1.09-25.32	1.69 – 25.00
collected reflections	18360	15443	10695
unique reflections	5953	5289	8922
parameters	174	93	434
S	0.894	1.465	1.159
R	0.0535	0.1793	0.0447
wR^2	0.1448	0.4620	0.1269
$\rho_{min, max}$ / e Å^{-3}	0.319, -0.263	0.665, -0.562	0.465, -0.343